AD-A094 418 AIR FORCE INST OF TECH WRIGHT-PATTERSON AFB OH SCHOO--ETC F/G 20/6
A THEORETICAL AND EXPERIMENTAL STUDY ON THE APPLICATION OF STIM--ETC(U)
DEC 80 D C SLATER
UNCLASSIFIED AFIT/GEP/PH/80-9 NL

AD A094418

LEVEL II

DTIC
ELECTE
FEB 3 1981
D

DEPARTMENT OF THE AIR FORCE
AIR UNIVERSITY (ATC)

AIR FORCE INSTITUTE OF TECHNOLOGY

Wright-Patterson Air Force Base, Ohio

81 2 02 018

AFIT/GEP/PH/80-9

14 JAN 1981

APPROVED FOR PUBLIC RELEASE AFR 190-17.

FREDRIC C. LYNCH, Major, USAF
Director of Public Affairs
Air Force Institute of Technology (ATC)
Wright-Patterson AFB, OH 45433

A THEORETICAL AND EXPERIMENTAL STUDY ON THE APPLICATION OF STIMULATED RAMAN SPECTROSCOPY

THESIS

David Charles Slater
AFIT/GEP/PH/80-9 2nd Lt USAF

Approved for public release; distribution unlimited.

(14) AFIT/GEP/PH/80-9

(6) A THEORETICAL AND EXPERIMENTAL STUDY ON THE APPLICATION OF STIMULATED RAMAN SPECTROSCOPY.

(9) Master's THESIS,

PRESENTED TO THE FACULTY OF THE SCHOOL OF ENGINEERING

OF THE AIR FORCE INSTITUTE OF TECHNOLOGY

AIR UNIVERSITY (ATC)

IN PARTIAL FULFILLMENT OF THE

REQUIREMENTS FOR THE DEGREE OF

MASTER OF SCIENCE

BY

(10) DAVID CHARLES SLATER B.S.

SECOND LIEUTENANT USAF

GRADUATE ENGINEERING PHYSICS

(12) 140

(11) DEC [redacted] 80

Approved for public release; distribution unlimited.

012225

Preface

The Raman scattering process is one of Nature's fascinating yet subtle phenomena which is just beginning to be explored as one of Man's Tools to further his understanding of the properties of matter and radiation, and their intimate interactions. I enjoyed immensely the study and application of this subtle phenomenon. The theoretical aspects of this thesis greatly increased my understanding of optics, signal analysis, electromagnetic theory and its application to the study of the interaction of light with matter. The experimental aspects taught me that experimental research follows a long, winding path which takes you on many roads full of potholes and deadends.

Noise was the villain in this thesis which prevented the Ramán signal from ever popping its head high enough to be observed. The noise was fought during my alloted time but in the end the noise remained the villain. The fight, however, led to my increased understanding of this phenomenon and alternate ways to defeat the noise for those few brave souls who wish to continue the battle in the future.

I am greatly indebted to my advisor Dr. Roh who guided me through this research. He taught me a great deal about working in a laboratory environment and how to think as an experimentalist.

I would also like to thank George Gergal, Ron Gabriel, and Jim Miskimen for their technical help with the laboratory equipment used at AFIT.

Contents

Preface ii

List of Figures v

List of Tables vi

List of Symbols vii

Abstract x

I Introduction 1

Background 1
Purpose and Scope 6

II Theory 8

Introduction 8
Stimulated Raman Gain Using Maxwell's Equations 9
Classical Susceptibility Using the Nuclear Harmonic Oscillator Model 17

III Variational Techniques of SRS 25

Introduction 25
Direct SRS 27
Description 27
Signal Analysis-Amplitude Modulation of Pump Beam (AM Case) 28
Signal Analysis-Phase Modulation of Pump Beam (PM Case) 31
Signal-Noise Analysis 34
RIKES (Raman-Induced Kerr Effect) 44
Description 44
Signal Analysis-Amplitude Modulation of Pump Beam (AM Case) 45
Signal-Noise Analysis 49
OHD RIKES (Optical Heterodyned RIKES) 54
Description 54
Signal Analysis-Amplitude Modulation of Pump Beam (AM Case) 55
Signal Analysis-Phase Modulation of Pump Beam (PM Case) 57
Signal-Noise Analysis 59

IV Experimental Apparatus 65

Introduction 65
Lasers 68
Ar^+ Laser 68
Pump Laser 68
Probe Laser..... 69
Optical System 70
Optical Modulators 70
Lenses, Beamsplitters, Filters and Grating 71
Monochromator and Sample Cells 71
Detection System 72

V Experimental Procedure and Results..... 73

Introduction 73
Experimental Procedure 73
Optical Alignment 74
Direct SRS Polarization Alignment 78
RIKES Polarization Alignment 78
OHD RIKES Polarization Alignment 79
Results 80
Results of Spectral Runs 80
Discussion of Results 81

VI Conclusions and Recommendations 94

Bibliography 98

Appendix A: Derivation of Raman Signals Using Amplitude Modulation 100

Appendix B: Derivation of Raman Signals Using Phase Modulation 115

Appendix C: Noise Spectra of Pump Dye Laser and AR^+ Laser 123

List of Figures

Figure		Page
1	Energy Level Diagram for Stimulated Raman Scattering Process	3
2	General Optical Arrangement for Direct SRS, RIKES, and OHD RIKES	27
3	Noise Power Spectral Density for Probe Laser	42
4	RIKES Polarization Configuration	45
5	OHD RIKES Polarization Configuration	54
6	$SNR\|_{\substack{OHD \\ RIKES}}$ VS. θ	63
7	Experimental SRS System for Liquid Benzene Sample	65a
8	Experimental SRS System for Solid Silicon Sample	65b
9	Experimental Arrangement for Recording Noise Spectrum of HeNe Laser	84
10	HeNe Noise Spectrum: Multi-Mode and Single Mode	85
11	Noise Spectrum of HeNe Laser with RF Power Supply	91
12	Superimposed HeNe Noise Spectra	92
A-1	Intensity Modulated Pump Beam	101
A-2	Frequency Domain Representation of Amplitude Modulated Pump Field	102
A-3	Polarization Configuration for OHD RIKES	111
B-1	Frequency Domain Representation of Phase Modulated Pump Field	117
C-1	Noise Spectra of Pump Dye Laser and Ar^+ Laser	124

List of Tables

Table		Page
I	Values of $\delta_s^{\frac{1}{2}}$ of HeNe Probe Laser Operated Both Multi-Mode and Single-Mode	88
II	Values of S' and SNR For All Three Variational Techniques of SRS	89
III	Minimum Modulation Frequency for Direct SRS and OHD RIKES	93
C-I	Values of $\delta_p^{\frac{1}{2}}$ and $\delta_{Ar^+}^{\frac{1}{2}}$ VS. Frequency	125

List of Symbols

Raman Letter Symbols

c	Speed of light (3.0×10^{10} cm/sec)
e	Charge on electron (1.6×10^{-19} coulomb)
E_p	Electric field of pump beam (statvolt cm^{-1})
E_s	Electric field of probe beam (statvolt cm^{-1})
$\hbar$	Planck's constant divided by 2π (1.055×10^{-34} joules sec.)
I_{po}	Intensity of pump beam (erg sec^{-1} cm^{-2})
I_{so}	Intensity of probe beam (erg sec^{-1} cm^{-2})
$\bar{I}$	Average current (ampere)
$\bar{I}_s$	Average signal current (ampere)
i_d	Average dark current (ampere)
k	Boltzmann's constant (1.38×10^{-23} joule K^{-1})
k_s	Wavevector of probe beam (cm^{-1})
N	Number of molecules per unit volume (m^{-3})
P_{po}	Power of pump beam (erg sec^{-1})
P_{so}	Power of probe beam (erg sec^{-1})
q	Internuclear distance coordinate (m)
R_{eff}	Effective load resistance of detection system (ohms)
$\frac{dR}{dT}$	Derivative of reflectivity with respect to temperature
$S_{SRS}(t)$	Direct SRS fractional gain in probe beam (unitless)

$S_{RIKES}(t)$	RIKES fractional gain in probe beam (unitless)
$S_{\substack{OHD \\ RIKES}}(t)$	OHD RIKES fractional gain in probe beam (unitless)
SNR	Signal-Noise Ratio
T_n	First order dispersion and attenuation of $\omega_s + n\omega_m$ component of Stokes field.
T	Temperature of detection load (Kelvin)

Greek Letter Symbols

$\alpha_{k\ell}$	Molecular polarizability
α	Raman gain factor (cm^{-1})
β	Raman dispersion factor (cm^{-1})
Γ	Damping coefficient (sec^{-1})
γ_n	First order dispersion of $\omega_s + n\omega_m$ component of Stokes field
δ	Modulation index
δ_p	Mean-squared fractional deviation of pump beam intensity
δ_s	Mean-squared fractional deviation of probe beam intensity
ε_n	First order attenuation of $\omega_s + n\omega_m$ component of Stokes field
ε_s	Fraction of probe power that leaks through analyzer
η	Quantum efficiency of detector
θ	Angle of probe beam polarization from x-y diagonal
$\lambda(t)$	Rate function
$\Delta\nu$	Detection bandwidth (Hz)
$\chi^{(3)}$	Third order non-linear susceptibility ($cm^3\ erg^{-1}$)

ψ_{rs}	Imaginary part of $\chi^{(3)}$ $(\omega_p + r\omega_m, -(\omega_p + s\omega_m), \omega_s)$
ϕ_{rs}	Real part of $\chi^{(3)}$ $(\omega_p + r\omega_m, -(\omega_p + s\omega_m), \omega_s)$
ω_s	Circular frequency of probe beam (sec^{-1})
ω_p	Circular frequency of pump beam (sec^{-1})
ω_v	Circular vibrational frequency of molecule or lattice (sec^{-1})
ω_m	Circular modulation frequency

Abstract

An analysis of the stimulated Raman scattering process has been carried out for three variational techniques of stimulated Raman spectroscopy (SRS) using low power CW lasers and synchronous detection techniques. The three variational techniques of SRS examined are direct SRS, Raman-Induced Kerr Effect (RIKES) and Optically Heterodyned RIKES (OHD RIKES). In this analysis the Raman scattered signals for all three variational techniques were derived using Maxwell's equations for both amplitude and phase modulation techniques. The noise contributions for each technique were also examined. It was found that the main source of noise for each technique was due to probe laser intensity fluctuations.

The results of this analysis were utilized on an experimental SRS system using low power CW lasers and synchronous detection which was built to record Raman spectra. This technique would provide the Air Force with a valuable diagnostic tool for potential use in many areas such as combustion research, chemical kinetics and solid state technology. This system failed to record Raman resonance of liquid benzene at 992 cm^{-1} and solid silicon at 520 cm^{-1}. This was due to poor signal-noise ratios of less than one caused primarily by probe laser intensity fluctuations. The results of the analysis on this system yielded the minimum necessary modulation frequencies for each variational technique in order to detect the Raman resonance in benzene.

A THEORETICAL AND EXPERIMENTAL STUDY ON THE APPLICATION OF STIMULATED RAMAN SPECTROSCOPY

I Introduction

Background

The spontaneous Raman scattering process is a non-linear optical effect caused by an inelastic scattering of radiation due to molecular vibrations in the case of gases and liquids and lattice vibrations in the case of solids. This process was predicted in 1928 by Chandrasekhara Raman (Ref 1:44). The Raman process results in an upward and downward shifting of the incident radiation frequency by an amount equal to the vibrational frequency of the interacting molecule or lattice vibration. The downward shifted radiation is called the Stokes wave and the upward shifted radiation is called the anti-Stokes wave. Before the laser was developed Raman scattering was a very difficult phenomenon to observe. This was due to the extreme weakness of the Raman scattered radiation. With the advent of the laser, spontaneous Raman scattering has become a very useful tool for studying molecular vibrations, molecular structure and symmetry as well as the structure and vibrations of solids (Ref 2:V).

A slightly modified form of spontaneous Raman scattering, called stimulated Raman scattering, was observed by Eckhardt et al (Ref 3:455-457). Stimulated Raman scattering occurs when two overlapping radiation fields, which differ in frequency by an amount equal to the vibrational frequency of the interacting molecule or lattice, are both incident onto the sample. These two fields are supplied by two laser sources whose beams are made to overlap in the sample. The higher frequency field will be called the pump wave and the lower frequency field will be called the probe wave in this thesis. When the pump wave interacts with the sample, the Stokes field created due to the nonlinear properties of the sample, will be at the same frequency as the probe wave. This allows the Stokes field to be stimulated by the presence of the probe field, hence, the name stimulated Raman scattering. The stimulated Stokes field propagates in the same direction and is phase coherent to the probe field. The energy density of the Stokes field is proportional to the energy density of the probe field. This process results in the net gain of the probe wave at the expense of the pump wave.

Figure 1 is an energy level diagram which depicts the stimulated Raman scattering process. The incident pump photon ($\hbar\omega_p$) raises the molecular system from the ground

vibrational state to a virtual energy level. The molecular system is then stimulated to decay from the virtual level to the first excited vibrational state by the presence of the probe field ($n\hbar\omega_s$ where n is the number of photons in the probe radiation field). This results in the emission of a Stokes photon having energy $\hbar\omega_s$ which is of the same energy as the photons which make up the probe field. Hence, the number of photons in the probe field is increased by one everytime this scattering takes place. The stimulated Raman scattering process converts part of the incident energy of the pump field to molecular (or lattice) vibrations and the remaining energy leaves as a photon of reduced energy.

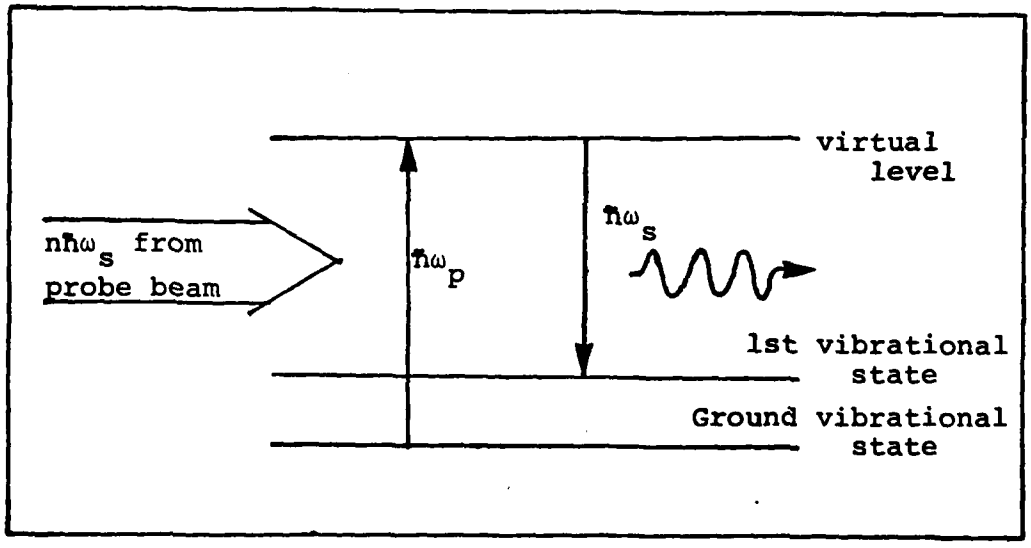

Figure 1. Energy Level Diagram for Stimulated Raman Scattering Process

The scattered light of the stimulated Raman process is generally of much greater intensity than the scattered light of the spontaneous Raman process (Ref 4:209). Much of the work involving the stimulated Raman process has been in the generation of the Stokes' components in various gas, liquid and solid state samples. The stimulated Raman scattering process provides high resolution Raman spectra limited only by the linewidths of the lasers used (Ref 5:1) and is free of interference from background nonlinearities (Ref 6:100D). This has led to an endeavor to develop the stimulated Raman process as a spectroscopic tool known as stimulated Raman spectroscopy (SRS). SRS provides Raman spectra which is directly proportional to both the imaginary part of the third order nonlinear susceptability $\chi^{(3)}$ and the input pump power (Ref 6:100D). Several variational techniques have been developed and analyzed in the recent years to enhance the stimulated Raman signal. These techniques include the direct SRS (Ref 7:192-193), Raman-induced Kerr effect (RIKES)(Ref 8), and optically heterodyned RIKES (OHD RIKES) (Ref 7:193-195;9;10).

Of particular interest in this thesis is the development of SRS using low power CW lasers. Owyoung has recently demonstrated SRS in liquid benzene, as well as in mixtures of common solvents using low power CW lasers for both the

pump and probe sources (Ref 7:197-200;11;12). Owyoung has incorporated the use of a multipass Raman cell which enhances the output stimulated Raman signal in several common solvents (Ref 11). Owyoung has also obtained high resolution stimulated Raman spectra of the $Q_{01}(1)$ transition in molecular hydrogen using CW lasers (Ref 13). Recently, Levine et al have examined and proposed the use of SRS for studying monolayers. They also propose a surface Raman ellipsometry technique analogous to the RIKES technique for further signal-to-noise enhancement of solid state samples (Ref 14).

The development of SRS techniques will provide the Air Force with a valuable tool which can be used in a wide variety of scientific study. Indeed, SRS is being developed into a gas diagnostic tool to determine the temperature and concentrations of major species in combustion environments such as the hot exhaust of a rocket engine without perturbing it (Ref 15). These results can lead to the improvement of fuel burning efficiency and the reduction of pollutants. Other uses of SRS include the following: understanding basic physics such as the examination of nonlinear susceptability tensor elements, dephasing and decay times and the determination of rotational constants for various substances (Ref 1:49); the study of crystals and amorphous solids; provide a wealth of useful surface information of solid

state samples and hence complement other surface vibrational techniques such as electron energy loss spectroscopy and IR absorption (Ref 14:1431); provide a means to examine lattice damage, measure dopant ion concentrations and the location of the dopant ions of an ion implanted semiconductor both before and after the annealing process.

Purpose and Scope

The purpose of this thesis is twofold: first, to derive and analyze the signal and noise of three variational techniques of SRS, which include direct SRS, RIKES and OHD RIKES for both an amplitude and phase modulated pump beam; and second, to develop and demonstrate an experimental SRS system using low power CW lasers and synchronous detection based on Owyoung's SRS system (Ref 12), which could be used to obtain and study Raman spectra of liquids and solids. The signal and noise analysis will complement the experimental aspects of this thesis, allowing a comparison of the experimental results to the predicted results, as well as, a complete diagnosis of each variational SRS technique.

A liquid benzene sample was used to demonstrate the experimental setup because of its well-characterized Raman resonance at 992 cm^{-1}. All three techniques, direct SRS, RIKES and OHD RIKES were tried on the benzene sample, but resonance was never observed. This was attributed to a

poor signal-noise ratio (SNR), due primarily to a noisy probe laser source and too low a modulation frequency of 1KHz. This forced a look at the noise power spectral density of the probe laser beam to determine its noise content. Finally, a sample of silicon was tried using an amplitude modulated pump source. Thermal background noise was observed which completely washed out the Raman resonance at 520 cm^{-1}. In order to suppress the thermal background noise, phase modulation must be used instead of amplitude modulation in the case where the sample is an absorptive solid (Ref 14:1427).

The thesis is organized in the following manner. Chapter II discusses the basic theory behind the stimulated Raman scattering process. In Chapter III, the basic results of Chapter II are utilized to derive the signal strengths for the three variational SRS techniques assuming an amplitude and phase modulated pump beam. This is followed by a signal-noise analysis for each technique. Chapters IV and V discuss the experimental apparatus, procedures and results. Finally, Chapter VI discusses the conclusions and recommendations.

II Theory

Introduction

There are many references which discuss the theory behind stimulated Raman scattering. Some authors treat this phenomenon using classical mechanics and classical electromagnetic field theory, whereas others choose to describe the phenomenon using quantum mechanics and quantum field theory. A quantum treatment of this phenomenon is, however, very limited because the matrix elements involved are very difficult to calculate (Ref 16:473). When the photon densities of the pump and probe beams are low, the quantum treatment gives the most accurate results. However, in most cases where the photon densities are high, classical field theory is adequate enough to describe this phenomenon (Ref 16:484). Hence, the discussion to follow will treat the stimulated Raman scattering phenomenon using the classical approach.

In the first section of this chapter the stimulated Raman gain experienced by the probe beam during Raman resonance will be derived using Maxwell's electromagnetic field equations. The following section will treat the phenomenon using a classical harmonic oscillator model for the vibrations of the medium. This will allow the third-order nonlinear susceptability tensor $\chi^{(3)}_{ijkl}(\omega_1,\omega_2,\omega_3)$,

which describes this nonlinear phenomenon, to be explicitly calculated. The form of $\chi^{(3)}_{ijkl}(\omega_1,\omega_2,\omega_3)$ is very important in this analysis, since the Raman signal is related to it.

Stimulated Raman Gain Using Maxwell's Equations

The magnitude of the stimulated Stokes field created in a sample of transparent material, where there is no magnetization and no currents due to free charges, is determined using Maxwell's electromagnetic field equations. The equations, in Gaussian units, are:

$$\underline{\nabla} \times \underline{E} = -\frac{1}{c}\frac{\partial \underline{H}}{\partial t} \qquad \underline{\nabla} \times \underline{H} = \frac{1}{c}\frac{\partial \underline{D}}{\partial t} \tag{1}$$

$$\underline{\nabla} \cdot D = 0 \qquad \underline{\nabla} \cdot \underline{H} = 0 \tag{2}$$

The displacement vector $\underline{D}$ is related to the electric field $\underline{E}$ by the relation

$$\underline{D} = \underline{E} + 4\pi \underline{P} \tag{3}$$

where $\underline{P}$ is the electric polarization of the sample.

The classical wave equation for the electric field is obtained by combining the above field equations. This gives

$$\nabla^2 \underline{E}(z,t) - \frac{1}{c^2}\frac{\partial^2 \underline{E}(z,t)}{\partial t^2} = \frac{4\pi}{c^2}\frac{\partial^2 \underline{P}(t)}{\partial t^2} \tag{4}$$

This is an inhomogeneous wave equation with the polarization $\underline{P}(t)$ acting as a source term.

The $\underline{E}$ and $\underline{P}$ fields are assumed harmonic with identical frequencies ω, given by

$$\underline{E}(z,t) = \frac{1}{2} \left[\underline{E}(\omega) e^{j\omega t} + \text{c.c.} \right] \tag{5a}$$

$$\underline{P}(t) = \frac{1}{2} \left[P(\omega) e^{j\omega t} + \text{c.c.} \right] \tag{5b}$$

After substitution of equations (5a) and (5b) into equation (4), we get

$$\nabla^2 \underline{E}(\omega) + \frac{\omega^2}{c^2} \underline{E}(\omega) = \frac{-4\pi}{c^2} \omega^2 \underline{P}(\omega) \tag{6}$$

The polarization $\underline{P}(\omega)$ is made up of a linear term and nonlinear terms of the electric field, so that the total polarization is written as

$$\underline{P}(\omega) = \underline{P}^{(1)}(\omega) + \underline{P}^{(2)}(\omega) + \underline{P}^{(3)}(\omega) + \ldots \tag{7}$$

where

$$P_i^{(n)}(\omega) = \int_{-\infty}^{\infty} \chi_{ijkl\ldots p}^{(n)}(\omega_1, \omega_2, \omega_3, \ldots \omega - \omega_1 - \omega_2 - \ldots - \omega_{n-1}) E_j(\omega_1) E_k(\omega_2) E_l(\omega_3) \ldots E_p(\omega - \omega_1 - \omega_2 - \ldots - \omega_{n-1}) d\omega_1 d\omega_2 d\omega_3 \ldots d\omega_{n-1} \tag{8}$$

where $\chi^{(n)}_{ijk\ell\ldots p}(\omega_1,\omega_2,\omega_3\ldots\omega-\omega_1-\omega_2-\ldots-\omega_{n-1})$ is the nth order susceptibility tensor of rank n+1, and repeated indices are summed over (Ref 17:256). $P_i^{(n)}(\omega)$ follows from taking the Fourier transform of the polarization $\underline{P}^{(n)}(t)$ as given by Butcher (Ref 18:17).

All even order terms of the polarization are zero for media which have inversion symmetry (Ref 17:256). The linear term $\underline{P}^{(1)}(\omega)$ is expressed as

$$P_i^{(1)}(\omega) = \chi_{ij}^{(1)}(\omega)E_j(\omega) \tag{9}$$

The linear susceptibility is related to the dielectric constant of the media $\varepsilon_{ij}(\omega)$, by the well-known relation

$$\varepsilon_{ij}(\omega) = 1 + 4\pi\,\chi_{ij}^{(1)}(\omega) \tag{10}$$

so that equation (9) becomes

$$P_i^{(1)}(\omega) = \frac{1}{4\pi}\,(\varepsilon_{ij}(\omega)-1)E_j(\omega) \tag{11}$$

Substituting equations (11) and (7) into equation (6), setting all even order terms to zero and ignoring all odd order terms greater than the third, we get

$$\nabla^2\underline{E}(\omega) + k^2\underline{E}(\omega) = \frac{-4\pi}{c^2}\,\omega^2\underline{P}^{(3)}(\omega) \tag{12}$$

where

$$k^2 = \frac{\varepsilon\omega^2}{c^2}$$

In general, the electric field may be written as a linear superposition of harmonic fields. Thus, equation (12) may be written for a single harmonic component. In this analysis, the Stokes field is of interest, so we write equation (12) as

$$\nabla^2 \underline{E}_s(\omega_s) + k_s^2 \underline{E}(\omega_s) = \frac{-4\pi\omega_s^2}{c^2} \underline{P}^{(3)}(\omega_s) \qquad (13)$$

where $\underline{E}_s(\omega_s)$ and $\underline{P}^{(3)}(\omega_s)$ are the Stokes electric field and the third-order polarization in the frequency domain, respectively, and $\underline{k}_s$ is the Stokes wavevector. The solution of equation (13) will determine the magnitude of the gain of the Stokes field.

To solve equation (13) the envelope of the Stokes field is allowed to vary with distance z inside the medium. The envelope of the field takes the form $\underline{E}_s(\omega_s) = \tilde{\underline{E}}_s(z) e^{jk_s z}$. The Laplacian of equation (13) is written as

$$\nabla^2 \underline{E}_s(\omega_s) = \frac{\partial^2}{\partial z^2} \underline{E}_s(\omega_s)$$

$$= \left[\frac{\partial^2 \tilde{\underline{E}}_s(z)}{\partial z^2} + 2jk_s \frac{\partial \tilde{\underline{E}}_s(z)}{\partial z} - k_s^2 \tilde{\underline{E}}(z) \right] e^{jk_s z}$$

Since the gain in the Stokes field is known to be small, the change in amplitude of the envelope with respect to z must be small, so it is safe to assume that

$$\left| jk_s \frac{\partial \underline{E}_s(z)}{\partial z} \right| >> \left| \frac{\partial^2 \tilde{\underline{E}}_s(z)}{\partial z^2} \right| \tag{15}$$

The Laplacian becomes

$$\nabla^2 \underline{E}_s(\omega_s) \simeq (-k_s^2 \tilde{\underline{E}}_s(z) + 2jk_s \frac{\partial \tilde{\underline{E}}_s(z)}{\partial z}) e^{jk_s z} \tag{16}$$

Substituting this back into equation (13) gives

$$\frac{\partial \tilde{\underline{E}}_s(z)}{\partial z} = j \frac{2\pi\omega_s^2}{c^2 k_s} \underline{P}^{(3)}(\omega_s) e^{-jk_s z} \tag{17}$$

The impinging electric field onto the sample is composed of the pump wave and the probe wave and is given by

$$\underline{E}(z,t) = \frac{1}{2} [\underline{E}_s(\omega_s) e^{j\omega_s t} + \underline{E}_p(\omega_p) e^{j\omega_p t} + c.c.] \tag{18}$$

where $\underline{E}_s(\omega_s)$ is the probe electric field amplitude, $\underline{E}_p(\omega_p)$ is the pump electric field amplitude, ω_s and ω_p are the circular frequencies of the probe and pump waves, respectively. Substituting the Fourier transform of the combined electric field impinging onto the sample [equation (18)] into equation (8) yields $P^{(3)}(\omega_s)$ as

$$\begin{aligned} P^{(3)}(\omega_s) &= 6 \underline{\chi}^{(3)}(\omega_p, -\omega_p, \omega_s) \underline{E}_p(\omega_p) \underline{E}_p^*(\omega_p) \underline{E}_s(\omega_s) \\ &+ 3\underline{\chi}^{(3)}(\omega_s, -\omega_s, \omega_s) \underline{E}_s(\omega_s) \underline{E}_s^*(\omega_s) \underline{E}_s(\omega_s) \end{aligned} \tag{19}$$

where the indices of $\underline{\underline{\chi}}^{(3)}$ have been suppressed. The second term on the right hand side of equation (19) is a non-resonant term which is much smaller than the first term and thus is neglected in this discussion.

Substitution of equation (19) into equation (17) gives

$$\frac{\partial \tilde{\underline{E}}_s(z)}{\partial z} = j \frac{12\pi\omega_s^2}{c^2 k_s} \underline{\underline{\chi}}^{(3)}(\omega_p,-\omega_p,\omega_s)\underline{E}_p(\omega_p)\underline{E}_p^*(\omega_p) \quad \tilde{\underline{E}}_s(z) \tag{20}$$

This may be rewritten as

$$\frac{\partial \tilde{\underline{E}}_s(z)}{\partial z} = j \frac{96\pi^2\omega_s^2}{c^3 k_s} \chi^{(3)}(\omega_p,-\omega_p,\omega_s) I_p(z) \tilde{\underline{E}}_s(z) \tag{21}$$

where $I_p(z) = \frac{c}{8\pi} |E_p|^2$ is the intensity of the pump beam, and $\chi^{(3)}(\omega_p,-\omega_p,\omega_s)$ are those tensor components which contribute to the Stokes gain. Since the intensity of the pump beam is assumed larger than the probe beam, the comparative depletion of the pump beam is insignificant to the probe beam, so $I_p(z)$ may be considered constant. This allows an easy solution to equation (21), namely

$$\tilde{\underline{E}}_s(z) = \tilde{\underline{E}}_{so}(z=0)e^{jRI_p z} \tag{22}$$

where

$$R = \frac{96\pi^2\omega_s^2}{c^3 k_s} \chi^{(3)}(\omega_p,-\omega_p,\omega_s) \tag{23}$$

All the phase terms have cancelled out so that the stimulated Raman scattering process is a self phased-matched interaction. Hence, this phenomenon is insensitive to any effect which could cause phase changes in either the pump or probe beam, such as birefringence or optical dispersion caused by the optical elements used in an SRS experiment (Ref 11:324).

In order to see the gain more clearly we let $jRI_p = \alpha+j\beta$ and also allow $\chi^{(3)}$ to have real and imaginary components. Thus we have

$$\alpha = Re\{jRI_p\} = \frac{-96\pi^2\omega_s^2 I_p}{c^3 k_s} Im\{\chi^{(3)}(\omega_p,-\omega_p,\omega_s)\} \qquad (24a)$$

$$\beta = Im\{jRI_p\} = \frac{96\pi^2\omega_s^2 I_p}{c^3 k_s} Re\{\chi^{(3)}(\omega_p,-\omega_p,\omega_s)\} \qquad (24b)$$

It will be shown in the following section that $Im\{\chi^{(3)}\}<0$ so α, which is the gain per unit length of the Stokes field, is a positive quantity indicating that the Stokes beam emerges from the medium with a greater amplitude than it had upon entering the medium. This comes about through the transfer of energy from the pump field to the probe field.

Since the gain is small, the exponential function of equation (22) may be written as

$$\tilde{\underline{E}}_s(z) = \tilde{\underline{E}}_{so}(1 + \alpha z + j\beta z) \tag{25}$$

$$= \tilde{\underline{E}}_{so} + \delta\tilde{\underline{E}}_s \tag{26}$$

where

$$\delta\tilde{\underline{E}}_s = \tilde{\underline{E}}_{so}\ (\alpha + j\beta)z \tag{27}$$

The development so far does not take into account the possibility that the pump field maybe composed of other frequency components besides ω_p. This will be the case if the pump field is modulated in some way, as is commonly done in order to use synchronous detection techniques. In order to account for these additional frequency components, the $\chi^{(3)}$ is examined in greater detail. *Using equation* (8), $P^{(3)}(\omega)$ may be written as

$$P^{(3)}(\omega) = \int_{-\infty}^{\infty}\int_{-\infty}^{\infty}\chi^{(3)}(\omega_1,\omega_2,\omega-\omega_1-\omega_2)E(\omega_1)E(\omega_2)E(\omega-\omega_1-\omega_2)$$

$$d\omega_1 d\omega_2 \tag{28}$$

In the case of a finite number of possible frequencies for $\pm\omega_1$ and $\pm\omega_2$, for example the set of frequencies $\{\omega_{-n}, \omega_{-n+1}..\omega_n\}$, the integral of equation (28) reduces to a finite sum over these possible frequencies. Thus, equation (28) reduces to

$$P^{(3)}(\omega) = \sum_{i=-n}^{n}\sum_{j=-n}^{n} \chi^{(3)}(\omega_i,\omega_j,\omega-\omega_i-\omega_j)E(\omega_i)E(\omega_j)$$

$$E(\omega-\omega_i-\omega_j) \qquad (29)$$

This is now substituted into equation (17) which when solved gives

$$\tilde{\underline{E}}_s(z) = \tilde{\underline{E}}_{so}(z=0)\ e^{jR'z} \qquad (30)$$

where

$$R' = \frac{12\pi\omega_s^2}{c^2k_s}\sum_{i=-n}^{n}\sum_{j=-n}^{n} \chi^{(3)}(\omega_i,-\omega_j,\omega_s)E_p(\omega_i)\ E_p^*(\omega_j) \qquad (31)$$

This leads to the modified expressions for α and β:

$$\alpha = \frac{-12\pi\omega_s^2}{c^2k_s}\sum_{i=-n}^{n}\sum_{j=-n}^{n} \mathrm{Im}\{\chi^{(3)}(\omega_i,-\omega_j,\omega_s)\}E_p(\omega_i)\ E_p^*(\omega_j) \qquad (32a)$$

$$\beta = \frac{12\pi\omega_s^2}{c^2k_s}\sum_{i=-n}^{n}\sum_{j=-n}^{n} \mathrm{Re}\{\chi^{(3)}(\omega_i,-\omega_j,\omega_s)\}E_p(\omega_i)\ E_p^*(\omega_j) \qquad (32b)$$

Classical Susceptibility Using the Nuclear Harmonic Oscillator Model

Stimulated Raman scattering can be explained very simply by treating the Raman active medium as a collection of N uncoupled harmonic oscillators per unit volume where

each harmonic oscillator represents a molecule. If q is the generalized coordinate representing the amplitude of molecular vibration from the equilibrium position, then the equation of motion for the molecular vibration is

$$\frac{d^2q}{dt^2} + \Gamma \frac{dq}{dt} + \omega_v{}^2 q = \frac{F}{m} \tag{33}$$

where Γ is the damping coefficient due to collisions, ω_v is the natural vibrational frequency of the molecule, F is the driving force applied to the molecule, and m is the reduced mass of the molecule.

When an electric field is applied to the molecule, the field causes the electron cloud surrounding the molecule to distort or polarize. The amount of polarization induced by the field is given by (using indicial notation)

$$P_k = N\alpha_{kl}E_l \tag{34}$$

where P_k is the k^{th} component of the induced polarization, N is the number of molecules per unit volume, α_{kl} is the molecular polarizability tensor and E_l is the l^{th} component of the electric field. Since the polarization is the product of charge and the distance between the charges, it seems reasonable to expect that the polarizability tensor

is a weak function of the internuclear coordinate q. As q changes, the electrons surrounding the molecule see a slightly different potential and hence, will distort differently. To express this mathematically, the polarizability tensor is Taylor expanded around q = 0 :

$$\alpha_{kl} = \alpha^{\circ}_{kl} + \left(\frac{\partial \alpha_{kl}}{\partial q}\right)_{q=0} q + \ldots \tag{35}$$

The electrostatic energy of the polarized molecules in the medium is expressed by the interaction Hamiltonian H_I as

$$H_I = \frac{-1}{2} \underline{P}.\underline{E} = \frac{-1}{2} P_k E_k \tag{36}$$

The force on one molecule is

$$F = \frac{-1}{N} \frac{\partial H_I}{\partial q} \tag{37}$$

$$= \frac{-1}{N} \frac{\partial}{\partial q} \left[\frac{-N}{2}(\alpha^{o}_{kl} + \left(\frac{\partial \alpha_{kl}}{\partial q}\right)_o q + \ldots) E_k E_l\right]$$

$$= \frac{1}{2} \left(\frac{\partial \alpha_{kl}}{\partial q}\right)_o E_k E_l \tag{38}$$

after substitution of equations (34), (35) and (36) into (37). The molecular polarization changes the potential seen by the nuclear elements of the molecule, which causes an applied force to exist on those nuclear elements. Substituting equation (38) into (33) gives

$$\frac{d^2q}{dt^2} + \Gamma \frac{dq}{dt} + \omega_v{}^2 q = \frac{1}{2m} \left(\frac{\partial \alpha_{kl}}{\partial q}\right)_o E_k E_l \tag{39}$$

as the equation of motion for q. Assuming a harmonic time dependence for q, of the form $q(t) = \frac{1}{2}[q(z)e^{j\omega t} + q^*(z) e^{-j\omega t}]$, substituted into equation (39) yields

$$q(z) = \frac{1}{(\omega_v{}^2 - \omega^2) + j\Gamma\omega} 2\frac{1}{m} \left(\frac{\partial \alpha_{kl}}{\partial q}\right)_o E_k E_l \tag{40}$$

The electric field impinging on the molecule is composed of the probe field plus the pump field. Hence,

$$\underline{E} = \frac{1}{2}[\underline{E}_p(\omega_p)e^{j\omega_p t} + \underline{E}_s(\omega_s)e^{j\omega_s t} + c.c.] \tag{41}$$

Substitution of equation (41) into equation (40) will lead to frequency components of q at $\pm 2\omega_p, \pm 2\omega_s, \pm(\omega_p - \omega_s)$, $\pm(\omega_p + \omega_s)$ and a d.c. component. The pump and probe fields are normally in the optical region of the electromagnetic spectrum and ω_v is normally in the infrared region. Hence, the $\pm(\omega_p - \omega_s)$ frequency components of q cause resonance when $\omega_p - \omega_s \simeq \omega_v$.

Carrying out the substitution of equation (41) into equation (40) yields

$$q(t) = \frac{1}{8m}\left(\frac{\partial \alpha_{kl}}{\partial q}\right)_o \frac{E_{pk}(\omega_p) E_{sl}^{*}(\omega_s) e^{j(\omega_p-\omega_s)t}}{\omega_v^2-(\omega_p-\omega_s)^2+j\Gamma(\omega_p-\omega_s)} + c.c \qquad (42)$$

Since the polarizability α_{kl} is a weak function of q, as seen in equation (35), substitution of equation (42) into equation (35) will yield a polarizability which is modulated at $\omega_p - \omega_s$. The induced molecular vibration caused by the overlapping pump and probe fields reacts back into the impinging electric field of equation (41). This shows up in equation (34) where the product of α_{kl}, which exists at the frequency $\omega_p - \omega_s$, and E_l, which exists at frequencies ω_s and ω_p, cause the polarization P_k to exist at frequencies $+\omega_s, +(2\omega_s-\omega_p), -(2\omega_p-\omega_s), -\omega_p$, etc. In the stimulated Raman process the ω_s component is detected. The nonlinear polarization at frequency ω_s becomes, after substituting equation (42) into equation (39),

$$P_i^{NL}(\omega_s) = \frac{N}{8m}\left(\frac{\partial \alpha_{ij}}{\partial q}\right)_o \left(\frac{\partial \alpha_{kl}}{\partial q}\right)_o \frac{E_{pj}(\omega_p) E_{pk}^{*}(\omega_p) E_{sl}(\omega_s)}{\omega_v^2-(\omega_p-\omega_s)^2+j\Gamma(\omega_p-\omega_s)} \qquad (43)$$

The third order polarization is given by

$$P_i^{(3)} = 6\chi_{ijkl}^{(3)}(\omega_p, -\omega_p, \omega_s) E_{pj}(\omega_p) E_{pk}^{*}(\omega_p) E_{sl}(\omega_s) \qquad (44)$$

as derived in equation (19).

Comparing equation (44) with equation (43) yields

$$\chi^{(3)}_{ijkl}(\omega_p,-\omega_p,\omega_s) = \frac{N}{48m}\left(\frac{\partial\alpha_{ij}}{\partial q}\right)_o\left(\frac{\partial\alpha_{kl}}{\partial q}\right)_o \frac{1}{\omega_v^2-(\omega_p-\omega_s)^2+j\Gamma(\omega_p-\omega_s)} \tag{45}$$

Near resonance where $\omega_p-\omega_s\simeq\omega_v$ the denominator of equation (45) becomes

$$\frac{1}{\omega_v^2-(\omega_p-\omega_s)^2+j\Gamma(\omega_p-\omega_s)} \simeq \frac{1}{\omega_v}\cdot\frac{1}{2(\omega_v+\omega_s-\omega_p)+j\Gamma} \tag{46}$$

Hence, equation (45) reduces to

$$\chi^{(3)}_{ijkl}(\omega_p,-\omega_p,\omega_s) = \frac{N}{48m}\left(\frac{\partial\alpha_{ij}}{\partial q}\right)_o\left(\frac{\partial\alpha_{kl}}{\partial q}\right)_o \frac{1}{\omega_v[2(\omega_v+\omega_s-\omega_p)+j\Gamma]} \tag{47}$$

which is Lorentzian. The real and imaginary components of $\chi^{(3)}_{ijkl}$ are

$$\mathrm{Re}\{\chi^{(3)}_{ijkl}\} = \frac{N}{48m}\left(\frac{\partial\alpha_{ij}}{\partial q}\right)_o\left(\frac{\partial\alpha_{kl}}{\partial q}\right)_o \frac{1}{\omega_v}\frac{A}{A^2+\Gamma^2} \tag{48}$$

$$\mathrm{Im}\{\chi^{(3)}_{ijkl}\} = -\frac{N}{48m}\left(\frac{\partial\alpha_{ij}}{\partial q}\right)_o\left(\frac{\partial\alpha_{kl}}{\partial q}\right)_o \frac{1}{\omega_v}\frac{\Gamma}{A^2+\Gamma^2}$$

where $A = 2\,(\omega_v + \omega_s - \omega_p)$ (49)

Hence, it is shown that the imaginary part of $\chi^{(3)}_{ijkl}$ is a negative quantity and exhibits a Lorentzian shape much like the first order susceptibility for normal attenuation. Likewise, the real part of $\chi^{(3)}_{ijkl}$ exhibits a shape much like the first order susceptibility for normal dispersion.

In general, the $\chi^{(3)}_{ijkl}$ tensor is composed of 81 components. Fortunately, symmetry considerations reduce the number of nonvanishing elements. For an isotropic medium, which is considered in this thesis, the number of components is reduced to 21. Of these 21 components only 3 are independent. These components are displayed below:

$$\chi^{(3)}_{1111} = \chi^{(3)}_{2222} = \chi^{(3)}_{3333}$$

$$\chi^{(3)}_{1122} = \chi^{(3)}_{2211} = \chi^{(3)}_{1133} = \chi^{(3)}_{3311} = \chi^{(3)}_{2233} = \chi^{(3)}_{3322}$$

$$\chi^{(3)}_{1212} = \chi^{(3)}_{2121} = \chi^{(3)}_{1313} = \chi^{(3)}_{3131} = \chi^{(3)}_{2323} = \chi^{(3)}_{3232}$$

$$\chi^{(3)}_{1221} = \chi^{(3)}_{2112} = \chi^{(3)}_{1331} = \chi^{(3)}_{3113} = \chi^{(3)}_{2332} = \chi^{(3)}_{3223}$$

and $\chi_{1111} = \chi_{1122} + \chi_{1212} + \chi_{1221}$ (Ref 18:49-50)

where subscripts 1, 2 and 3 are the x, y and z directions, respectively.

III Variational Techniques of SRS

Introduction

Synchronous detection is the method employed in this thesis to detect the stimulated Raman gain induced in the sample. In order to utilize this method, the detected signal must be modulated. This is accomplished by modulating the pump beam. Doing so causes the stimulated Raman gain of the probe beam to be modulated through the gain's dependence on the pump field, as seen in equations (32a, b). The Raman gain is synchronously detected with a lock-in amplifier referenced to the modulation frequency.

Amplitude modulation is the most common method when working with transparent liquids or gases. However, for the case of absorptive solids such as silicon, amplitude modulating the pump beam causes the temperature at the surface of the sample to fluctuate at the modulation frequency. This change in temperature induces a change in the reflectivity of the probe beam $(\frac{dR}{dT})$ which is synchronously detected by the lock-in amplifier. The signal due to this change in reflectivity is typically 10^4 times greater than the Raman signal, hence it obliterates the chance of recording Raman spectra. In order to prevent the temperature from fluctuating, the pump beam must be phase modulated.

As will be shown, phase modulation at frequency ω_m causes the Raman signal to be amplitude modulated at ω_m which allows it to be synchronously detected by the lock-in amplifier (Ref 14:1427).

This chapter will examine the stimulated Raman scattered intensities assuming both an amplitude and phase modulated pump source for the three variational SRS techniques: direct SRS, RIKES, and OHD RIKES. Each of these techniques will be treated separately in three sections. Each section will begin with a description of the technique, followed by a signal analysis where the two modulation schemes are assumed. This will be followed by a signal-noise analysis which will include a discussion of the advantages and disadvantages of each technique. The details of the signal analysis are presented in Appendix A for the AM (amplitude modulation) modulation scheme and Appendix B for the PM (phase modulation) modulation scheme.

The general optical arrangement which is considered in this analysis for direct SRS, RIKES and OHD RIKES is shown in Figure 2. The pump beam, emitted by a tunable dye laser, is passed through a modulator before entering the sample. The probe beam, emitted from a fixed frequency laser, is aligned so that it overlaps the pump beam. After the two beams pass through the sample they hit a grating which spatially separates them. The probe beam then passes

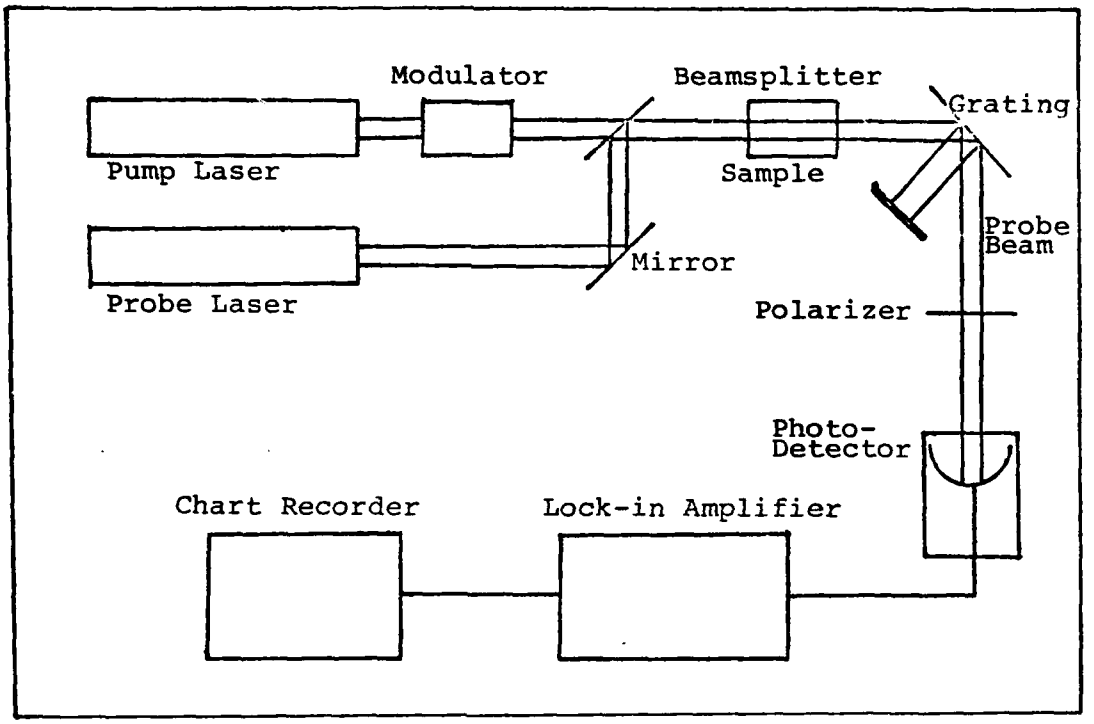

Figure 2: General optical arrangement for direct SRS, RIKES and OHD RIKES.

through a polarizer, which acts as an analyzer, before impinging on the photodetector. To record the Raman spectrum, the pump laser is slowly scanned in wavelength so that when the frequency difference between the pump and probe lasers match the vibrational frequency of the sample the induced modulated Raman signal is synchronously detected by the lock-in amplifier.

Direct SRS

Description. In the direct SRS technique the pump and

probe beams, which enter the sample, are both linearly polarized along the same direction. The detected probe beam is analyzed along this direction. Hence, the component of the third order non-linear susceptibility which is responsible for the scattering in this configuration is the $\chi^{(3)}_{1111}$ (Note, the first subscript of the susceptibility is the analyzed direction, the following two subscripts are the pump polarization directions and the last subscript is the probe polarization direction).

Signal Analysis - Amplitude Modulation of Pump Beam (AM Case). Amplitude modulation of the pump beam is accomplished by utilizing either a mechanical chopper or electro-optic crystal modulator placed in the path of the beam just after it emerges from the laser. The intensity of the pump beam will be assumed to vary sinusoidally at a frequency of ω_m. The pump intensity becomes

$$I_p(t) = \frac{I_{po}}{2} \quad (1 + \cos \omega_m t) \tag{50}$$

where I_{po} is the intensity of the pump beam before entering the modulator. The complex electric field $\tilde{E}_p$ of the modulated pump beam becomes

$$\tilde{E}_p = \frac{1}{2} \quad E_{po} \left[e^{j(\omega_p + \frac{\omega_m}{2}) t} + e^{j(\omega_p - \frac{\omega_m}{2}) t} \right] \tag{51}$$

The pump and probe beams interact in a distance ℓ in the sample giving rise to a gain in the probe beam. The total probe field which leaves the sample is given by equation (25) with α and β given by equations (32a) and (32b). After substitution of equations (31a) and (32b) into equation (25) we have

$$\tilde{E}_s\ (z = \ell, t) = E_{so}\Big[T_o - T_n \frac{12\pi\omega_s^2 \ell}{c^2 k_s} \sum_{r=-\frac{1}{2}}^{\frac{1}{2}} \sum_{s=-\frac{1}{2}}^{\frac{1}{2}} \tilde{E}_p(\omega_p + r\omega_m) \cdot$$

$$\tilde{E}_p^*\ (\omega_p + s\omega_m)\ \Psi_{rs}^{1111} + j\ T_n \frac{12\pi\omega_s^2 \ell}{c^2 k_s} \sum_{r=-\frac{1}{2}}^{\frac{1}{2}} \sum_{s=-\frac{1}{2}}^{\frac{1}{2}} \tilde{E}_p(\omega_p + r\omega_m) \cdot$$

$$\tilde{E}_p^*\ (\omega_p + s\omega_m)\ \phi_{rs}^{1111}\Big] e^{j\omega_s t} \qquad (52)$$

where

$$\Psi_{rs}^{1111} \equiv \mathrm{Im}\ \{\chi_{1111}^{(3)}\ (\omega_p + r\omega_m, -(\omega_p + s\omega_m), \omega_s)\}$$

$$\phi_{rs}^{1111} \equiv \mathrm{Re}\ \{\chi_{1111}^{(3)}\ (\omega_p + r\omega_m, -(\omega_p + s\omega_m), \omega_s)\}$$

$T_n = e^{-\varepsilon_n} - j\gamma_n$ describes the linear dispersion and attenuation of the $\omega_s + n\omega_m$ component of the Stokes field. $n = -1, 0, -1$ for AM.

$\varepsilon_n = \frac{\alpha_n \ell}{2}$ where α_n is the 1^{st} order attenuation coefficient for $\omega_s + n\omega_m$ component of the Stokes field.

$$\gamma_n = \eta_n \ell \frac{(\omega_s + n\omega_m)}{c}$$ where η_n is the index of refraction for $\omega_s + n\omega_m$ component of the Stokes field.

The total intensity of the probe beam after travelling through the sample is

$$I_s\ (z=\ell,t) = \frac{c}{8\pi} |\tilde{E}_s(z=\ell,t)|^2 \tag{53}$$

After substituting equation (51) for $\tilde{E}_p$ into equation (52) then calculating $I_s(z=\ell,t)$ using equation (53), the total intensity of the probe beam which is incident onto the photodetector in Gaussian units becomes (see Appendix A for details of calculation)

$$I_s(z=\ell,t)\Big|_{\substack{\text{direct SRS} \\ \text{AM}}} = I_o + I_1 \cos \omega_m t + I_2 \sin \omega_m t + I_3(t) \tag{54}$$

where

$$I_o = \text{d.c. terms} \tag{54a}$$

$$I_1 = \frac{-48\pi^2 \omega_s^2 \ell}{c^3 k_s} I_{so} I_{po} (\psi^{1111}_{-\frac{1}{2}\frac{1}{2}} + \psi^{1111}_{\frac{1}{2}-\frac{1}{2}}) e^{-2\varepsilon_o} \tag{54b}$$

$$I_2 = \frac{48\pi^2\omega_s^2}{c^3 k_s} \ell I_{so} I_{po} (\phi^{1111}_{-\frac{1}{2}\frac{1}{2}} - \phi^{1111}_{\frac{1}{2}-\frac{1}{2}}) e^{-2\varepsilon_o} \qquad (54c)$$

$$I_3(t) = \text{terms proportional to } \psi^2 \text{ and } \phi^2 \qquad (54d)$$

The in-phase term I_1 is directly proportional to the sum of the imaginary components of the $\chi^{(3)}_{1111}$ tensor, whereas, the quadrature component I_2 is directly proportional to the difference in the real components of $\chi^{(3)}_{1111}$, which makes I_2 less intense than I_1. The real and imaginary components of $\chi^{(3)}_{1111}$ may be detected separately by properly adjusting the reference phase on the lock in amplifier but the signal due to $\mathrm{Re}\chi^{(3)}$ is very weak. I_3 is proportional to ψ^2 and ϕ^2 which makes detection of I_3 much more difficult due to the small magnitude of ψ^2 and ϕ^2.

Signal Analysis - Phase Modulation of Pump Beam (PM Case). Phase modulation of the pump beam is accomplished by utilizing an electro-optic (E/O) modulator aligned such that the polarization of the pump beam is along one of the principal axis of the E/O crystal. When a sinusoidal field is brought across the crystal the phase velocity of the pump beam will vary sinusoidally, hence the beam emerges from the crystal phase modulated. The electric field of

the sinusoidally phase modulated pump beam becomes

$$\tilde{E}_p(t) = E_{po} \sum_{n=-\infty}^{\infty} J_n(\delta) \exp[j(\omega_p + n\omega_m)t] \tag{55}$$

(Ref 19:15)

where E_{po} is the amplitude of the electric field of the pump beam, δ is the modulation index, J_n are the Bessel functions of order n, and ω_m is the modulation frequency. The modulation index δ is given by

$$\delta = \frac{\pi n_o^3 r_{63} E_m \ell}{\lambda} \tag{56}$$

where n_o is the ordinary index of refraction of the E/O crystal, r_{63} is the 63 element of the electro-optic tensor, E_m is the magnitude of the electric field which drives the modulator, ℓ is the length the beam travels through the crystal, and λ is the wavelength of the pump beam (Ref 20:260). For $\delta << 1$ the modulated pump field of equation (55) reduces to

$$\tilde{E}_p(t) = E_{po}[e^{j\omega_p t} + \frac{\delta}{2}(e^{j(\omega_p+\omega_m)t} - e^{j(\omega_p-\omega_m)t})] \tag{57}$$

The total probe field which leaves the sample is given by equation (52) with the exception that r and s are now summed over -1, 0, 1 and n goes from -2 to 2 in unit steps.

Equation (57) is substituted in for the pump field. The intensity of the probe field is found after substituting the resultant $\tilde{E}_s$ field into equation (53). The result of this laborious calculation gives the intensity of the probe field in Gaussian units as (see Appendix B for details of calculation)

$$I_s(z=\ell,t)\Big|_{\substack{\text{direct SRS}\\ \text{PM}}} = I_o + I_1 \cos \omega_m t + I_2 \sin \omega_m t + I_3 \cos 2\omega_m t + I_4 \sin 2\omega_m t + I_5(t) \tag{58}$$

where

$$I_o = \text{d.c. terms} \tag{58a}$$

$$I_1 = \frac{96\pi^2 \omega_s^2 \ell}{c^3 k_s} I_{po} I_{so} e^{-2\varepsilon_o} \delta \, (\psi_{0-1}^{1111} - \psi_{01}^{1111}) \tag{58b}$$

$$I_2 = \frac{96\pi^2 \omega_s^2 \ell}{c^3 k_s} I_{po} I_{so} e^{-2\varepsilon_o} \delta \, (\phi_{0-1}^{1111} + \phi_{01}^{1111} - 2\phi_{10}^{1111}) \tag{58c}$$

$$I_3 = \frac{96\pi^2 \omega_s^2 \ell}{2c^3 k_s} I_{po} I_{so} e^{-2\varepsilon_o} \delta^2 \, (\psi_{1-1}^{1111} + \psi_{-11}^{1111}) \tag{58d}$$

$$I_4 = \frac{96\pi^2 \omega_s^2 \ell}{2c^3 k_s} I_{po} I_{so} e^{-2\varepsilon_o} \delta^2 \, (\phi_{1-1}^{1111} - \phi_{-11}^{1111}) \tag{58e}$$

$$I_5(t) = \text{terms proportional to } (\delta\psi)^2 \text{ and } (\delta\phi)^2 \qquad (58f)$$

The in-phase and quadrature signals at ω_m are proportional to δ, whereas, the signal at $2\omega_m$ are proportional to δ^2. Hence, the stronger signal exists at ω_m due to the small value of δ ($\sim$.1 or .01 typically). If ω_m is small compared to the width of the $\chi^{(3)}$ resonance, then I_1 is proportional to the first derivative of ψ^{1111} and I_2 is proportional to the second derivative of ϕ^{1111}. The in-phase and quadrature signals at $2\omega_m$ (I_3 and I_4) are smaller than the signals at ω_m by a factor of δ. Finally, the remaining signals existing in the term $I_5(t)$ are proportional to ψ^2 and ϕ^2 which, because of the small values of ψ and ϕ, are considered negligible.

Signal-Noise Analysis. It is very important not only to examine the amount of Raman signal that can be detected but also to examine the amount of noise associated with the signal. The ultimate factor which will determine whether or not the signal can be detected is the signal-noise ratio (SNR).

In general, the basic contributions to the noise arises from signal shot noise, dark current noise of the detector, Johnson noise arising from the detection electronics and intensity fluctuations of the lasers.

The shot noise, given by the variance of the signal current, is $2e\bar{I}\,\Delta\nu$ where e is the charge on an electron, $\bar{I}$ is the average signal current and $\Delta\nu$ is the detection bandwidth (Ref 20:281). The average signal current $\bar{I}$ is given by

$$\bar{I} = e\,\lambda\,(t) \tag{59}$$

where $\lambda(t)$, known as the rate function, is given by

$$\lambda(t) = \frac{\eta}{\hbar\omega_s}\int_{A_d} |\tilde{E}_s\,(\bar{r},t)|^2\,d\bar{r} \tag{60}$$

The quantum efficiency of the detector is given by η, $\hbar$ is Planck's constant divided by 2π, ω_s is the Stokes frequency, A_d is the area of the detector, and $\tilde{E}_s$ is the detected Stokes field. The greatest contribution to $\lambda(t)$ comes from the d.c. term involving the unaffected part of the probe beam as it passes through the sample. This d.c. term is seen as the first term in equation (52). Equation (60) becomes

$$\lambda(t) \cong \frac{\eta}{\hbar\omega_s}\,P_{so} \tag{61}$$

where P_{so} is the power of the probe beam in MKS units incident onto the detector. Substituting equations (59)

and (61) into $2e\bar{I}\Delta\nu$ gives the variance of the signal current due to shot noise as

$$\text{Var[current due to shot noise]} = \frac{2e^2\eta}{\hbar\omega_s} P_{so}\Delta\nu \qquad (62)$$

The mean-squared deviations of the pump and probe laser powers are given by $P_{po}^2\,\delta_p$ and $P_{so}^2\,\delta_s$, respectively. The factors δ_p and δ_s are defined as the mean-squared *fractional deviations* of the pump and probe powers within the detection bandwidth centered at the modulation frequency (Ref 9:47). Direct SRS allows the unaffected probe beam to be detected, as well as, the small Raman gain. Hence, the detector is able to see the intensity fluctuations of the probe beam. The variance of the current due to the probe laser fluctuations is

$$\text{Var[current due to probe fluctuations]} = \delta_s\left(\frac{e\eta}{\hbar\omega_s} P_{so}\right)^2 \qquad (63)$$

The fluctuations of the pump beam do not enter directly into the detector since the pump beam is spatially separated from the probe beam before detection. However, the fluctuations of the pump beam causes the Raman field to fluctuate due to the dependence of the Raman gain on the

intensity of the pump field. To evaluate the noise due to this fluctuation, the signal $S_{srs}(t)$ is defined for the AM case as

$$S_{srs}(t) = \frac{1}{I_{so}} (I_1 \cos \omega_m t + I_2 \sin \omega_m t + I_3(t)) \quad (64a)$$

where I_1, I_2 and $I_3(t)$ are given by equations (54b), (54c) and (54d), respectively. $S_{srs}(t)$ for the PM case is defined as

$$S_{srs}(t) = \frac{1}{I_{so}} (I_1 \cos \omega_m t + I_2 \sin \omega_m t + I_3 \cos 2\omega_m t + I_4 \sin 2\omega_m t + I_5(t)) \quad (64b)$$

where I_1 through $I_5(t)$ are given by equations (58b) through (58f), respectively. To take account of the fluctuations in the pump and probe intensities, I_{po}^2 and I_{so}^2 are replaced by $I_{po}^2 (1 + \delta_p)$ and $I_{so}^2 (1 + \delta_s)$, respectively. Thus, the square of the Raman gain part of the total signal becomes

$$I_{so}^2 (1 + \delta_s) I_{po}^2 (1 + \delta_p) \frac{[S_{srs}(t)]^2}{I_{po}^2} \quad (65a)$$

which expanded is

$$I_{so}^2 \, [S_{srs}(t)]^2 \, [1 + \delta_p + \delta_s + \delta_p \, \delta_s] \tag{65b}$$

The first term of equation (65b) is the unfluctuating part of the Raman scattered intensity. The second, third and fourth terms are the fluctuations in the Raman intensity due to both the pump and probe fluctuations. In most cases, when a dye laser is being used as the pump source and a gas laser is being used for the probe source, the pump beam fluctuations are much greater than the probe beam fluctuations ($\delta_p > \delta_s$). Thus equation (65b) reduces to

$$I_{so}^2 \, [S_{srs}(t)]^2 + I_{so}^2 \, \delta_p [S_{srs}(t)]^2 \tag{66}$$

The variance of the signal current due to the pump beam fluctuations becomes

$$\text{Var [current due to pump fluctuations]} = \delta_p \left(\frac{en}{\hbar\omega_s} P_{so} S_{srs}(t)\right)^2 \tag{67}$$

Combining all the noise terms of equations (62), (63), (67) along with the Johnson and dark current noise, the total variance of the signal current is

Var [current due to all noise sources] =

$$\frac{2e^2\eta}{\hbar\omega_s} P_{so}\,\Delta\nu + \frac{4kT}{R_{eff}}\,\Delta\nu + 2ei_d\Delta\nu + \left(\frac{e\eta}{\hbar\omega_s}\right)^2 .$$

$$P_{so}^2\,\delta_s + \left(\frac{e\eta}{\hbar\omega_s}\right)^2 P_{so}^2\,[S_{srs}(t)]^2\,\delta_p \qquad (68)$$

The first term in equation (68) is due to shot noise. The second term is due to Johnson noise (Ref 20:284), where T is the effective temperature of the detection load and R_{eff} is the effective load resistance. The third term is due to the detector dark current where i_d is the average detector dark current. The fourth and fifth terms are due to the laser fluctuations. The fifth term is considered negligible due to its dependence on $[S_{srs}(t)]^2$ which is typically a very small quantity. If the probe laser power is made sufficiently strong such that $P_{so} >> \frac{\hbar\omega_s}{2e^2\eta}\left[\frac{4kT}{R_{eff}} + 2ei_d\right]$ then the Johnson and dark current noise become negligible compared to the shot noise. This condition is easily satisfied for normal values of T and laser powers in the milliwatt range. Thus, the variance of the signal reduces to

$$\frac{2e^2\eta}{\hbar\omega_s} P_{so}\,\Delta\nu + \left(\frac{e\eta}{\hbar\omega_s}\right)^2 P_{so}^2\,\delta_s \qquad (69)$$

To form the signal-noise ratio the signal must be evaluated. The intensity of the detected signal has already been worked out in equation (54) for the AM case and equation (58) for the PM case. The average electrical signal is given by

$$\bar{I}_s = e\lambda(t) * h(t) \tag{70}$$

where $\lambda(t)$ is the rate function as defined in equation (60) and $h(t)$ is the impulse response function of the detector. If the detection bandwidth is considered constant around the referenced frequency and zero at d.c. then

$$\bar{I}_s = \frac{e\eta}{h\omega_s} P_{so} S'_{srs}(t) \tag{71}$$

where $S'_{srs}(t)$ is that part of $S_{srs}(t)$ which falls within the detection bandwidth. For example, if the lock-in is referenced at the frequency ω_m for the AM case then $S'_{srs}(t) = \frac{I_1 \cos \omega_m t}{I_{so}}$ where I_1 is given by equation (54b).

The signal-noise ratio (SNR) is defined as

$$SNR = \frac{\bar{I}_s}{\{\text{Var}[\text{current due to all noise sources}]\}^{\frac{1}{2}}} \tag{72}$$

Substituting equation (69) and (71) into equation (72) the SNR for direct SRS becomes

$$SNR|_{\text{direct SRS}} = \frac{S'_{srs}(t)}{\left[\frac{2\hbar\omega_s}{\eta P_{so}}\Delta\nu + \delta_s\right]^{\frac{1}{2}}} \qquad (73)$$

As P_{so} is increased, the shot noise term in the denominator decreases but the term δ_s due to laser fluctuation stays constant. Hence, the main barrier to shot noise limited detection is the noise due to probe laser fluctuations (Ref 7:193). Thus, it is very important to eliminate as much probe laser noise as possible. It has been observed by Levine and Bethea (Ref 21:86) that inserting an etalon into the probe laser cavity, so that the laser is operated single-mode, the d.c. intensity of the beam is reduced by a factor of 2, whereas, the noise is reduced an order of magnitude. Another noise suppressing device that is available on many HeNe lasers is an RF quieting circuit which helps to stabilize the plasma in the discharge tube of the laser.

The amount of laser noise which enters the system, given by δ_p and δ_s, is determined by the value of the modulation frequency ω_m and the bandwidth of detection system. The noise power spectral density, as shown in Figure 3 for a typical laser, is used to determine the

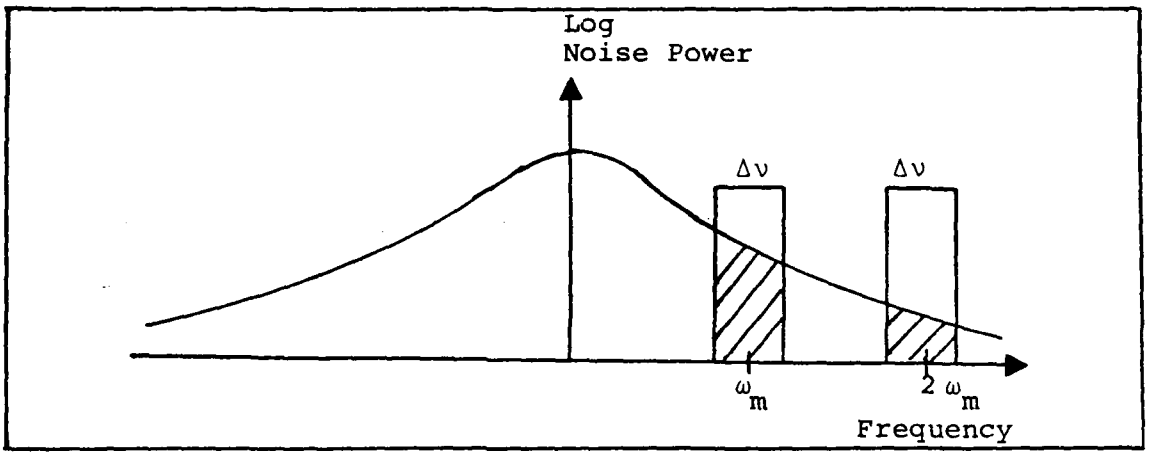

Figure 3: Noise power spectral density for probe laser.

values of δ_p and δ_s. The bandwidth of the detection system is shown in Figure 3 as a box centered at ω_m with a width of $\Delta\nu$. The amount of noise power that enters the system is represented by the area under the noise power density inside the box. It can be easily seen that the noise power entering the system is described by either narrowing the bandwidth (making $\Delta\nu$ smaller) or increasing the modulation frequency ω_m (allowing the noise power density curve to drop). Hence, it is important to choose a high enough modulation frequency ω_m and a narrow enough

bandwidth so that δ_s or δ_p is sufficiently small to allow the signal to be easily detected.

When AM modulation is used on absorptive samples such as silicon, there exists a synchronous thermal background noise, discussed in the introduction to this chapter due to absorption of the pump beam, which contributes to the variance of the signal current. If this noise is assumed to have a noise spectral density of height N_o, then the variance of the signal current due to this thermal background noise is

$$\text{Var[current due to thermal background]} = N_o \Delta\nu \qquad (74)$$

The SNR for direct SRS becomes

$$\text{SNR}|_{\text{direct SRS}} = \frac{S'_{srs}(t)}{\left[\frac{2\hbar\omega_s \Delta\nu}{\eta P_{so}} + \delta_s + N_o \Delta\nu \left(\frac{\hbar\omega_s}{e\eta}\right)^2 \frac{1}{P_{so}^2}\right]^{\frac{1}{2}}} \qquad (75)$$

The thermal background noise increases with increasing pump power making N_o a function of P_{po}^2. This thermal background noise has been reported by Levine et al (Ref 14:1427) as being 10^4 times greater in amplitude than the Raman signal, making the third term in the denominator of equation (75) the dominant term. Hence, phase modulation

must be used, in which case the thermal background noise terms would not exist.

RIKES (Raman-Induced Kerr Effect)

Description. RIKES is an optical configuration which greatly reduces any non-resonant Raman scattering due to electrons (second term in equation (19)) and reduces the effect of probe laser fluctuations which was found to be the main noise contribution for direct SRS. The polarization configuration used for the RIKES experiment is shown in Figure 4. The pump beam is linearly polarized along the x direction and the probe beam is linearly polarized along the x-y diagonal. This polarization configuration will induce birefringence in the sample which results in the emission of a Raman signal perpendicular to the initial probe beam polarization. This field passes through the analyzer and is detected. The x component of the Stokes field is proportional to $\chi^{(3)}_{1111} + \chi^{(3)}_{1112}$ and the y component is proportional to $\chi^{(3)}_{2111} + \chi^{(3)}_{2112}$. For isotropic media $\chi^{(3)}_{1112}$ and $\chi^{(3)}_{2112}$ are both zero.

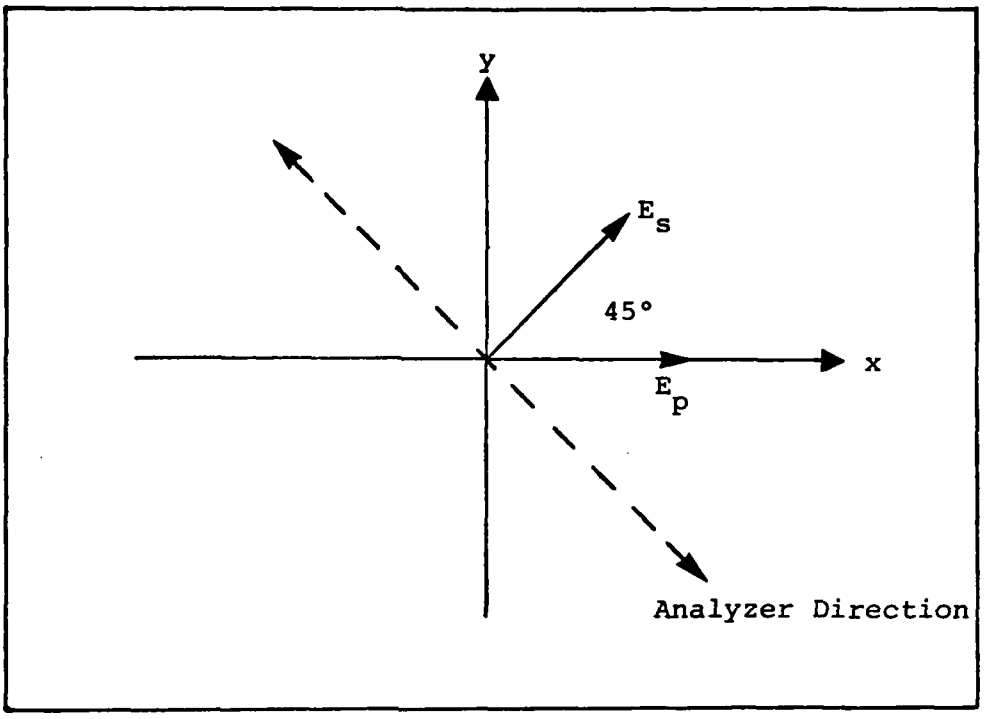

Figure 4: RIKES polarization configuration.

Signal Analysis - Amplitude Modulation of Pump Beam (AM Case). The detected Stokes field, which is derived in Appendix A, is given by (eq. (A-12))

$$\tilde{E}_s\ (z=\ell, t) = \frac{1}{\sqrt{2}} (\delta\tilde{E}_{sx} - \delta\tilde{E}_{sy}) \tag{76}$$

where

$$\delta\tilde{E}_{sx} = \frac{E_{so}}{\sqrt{2}} \ell T_n \alpha_x e^{j\omega_s t} + j\frac{E_{so}}{\sqrt{2}} \ell T_n \beta_x e^{j\omega_s t} \tag{76a}$$

$$\delta\tilde{E}_{sy} = \frac{E_{so}}{\sqrt{2}} \ell T_n \alpha_y e^{j\omega_s t} + j\frac{E_{so}}{\sqrt{2}} \ell T_n \beta_y e^{j\omega_s t} \qquad (76b)$$

and α_x, α_y are given by equation (32a) with ψ_{rs} ($\psi_{rs} = \text{Im}\{\chi^{(3)}\}$) replaced by ψ_{rs}^{1111} for α_x and ψ_{rs}^{2112} for α_y. Likewise, β_x and β_y are given by equation (32b) with ϕ_{rs} ($\phi_{rs} = \text{Re}\{\chi^{(3)}\}$) replaced by ϕ_{rs}^{1111} for β_x and ϕ_{rs}^{2112} for β_y. The intensity of the detected Stokes field is given by substituting equation (76) into equation (53). This yields the Stokes intensity in Gaussian units as

$$I_s(z=\ell,t)\Big|_{\substack{\text{RIKES}\\\text{AM}}} = I_o + I_1 \cos \omega_m t + I_2 \sin \omega_m t + I_3 \cos 2\omega_m t + I_4 \sin 2\omega_m t \qquad (77)$$

where

$$I_o = \text{d.c. terms} \qquad (77a)$$

$$I_1 = \frac{288\pi^4 \omega_s^4 \ell^2}{c^6 k_s^2} I_{so} I_{po}^2 e^{-2\varepsilon_o}$$

$$[(\psi^{1111}_{-\frac{1}{2}-\frac{1}{2}} + \psi^{1111}_{\frac{1}{2}\frac{1}{2}})(\psi^{1111}_{-\frac{1}{2}\frac{1}{2}} + \psi^{1111}_{\frac{1}{2}-\frac{1}{2}}) + (\psi^{2112}_{-\frac{1}{2}-\frac{1}{2}} + \psi^{2112}_{\frac{1}{2}\frac{1}{2}})(\psi^{2112}_{-\frac{1}{2}\frac{1}{2}} + \psi^{2112}_{\frac{1}{2}-\frac{1}{2}})$$

$$-(\psi^{1111}_{-\frac{1}{2}-\frac{1}{2}} + \psi^{1111}_{\frac{1}{2}\frac{1}{2}})(\psi^{2112}_{-\frac{1}{2}\frac{1}{2}} + \psi^{2112}_{\frac{1}{2}-\frac{1}{2}}) - (\psi^{1111}_{-\frac{1}{2}\frac{1}{2}} + \psi^{1111}_{\frac{1}{2}-\frac{1}{2}})(\psi^{2112}_{-\frac{1}{2}-\frac{1}{2}} + \psi^{2112}_{\frac{1}{2}\frac{1}{2}})$$

$$+(\phi^{1111}_{-\frac{1}{2}-\frac{1}{2}} + \phi^{1111}_{\frac{1}{2}\frac{1}{2}})(\phi^{1111}_{-\frac{1}{2}\frac{1}{2}} + \phi^{1111}_{\frac{1}{2}-\frac{1}{2}}) + (\phi^{2112}_{\frac{1}{2}\frac{1}{2}} + \phi^{2112}_{-\frac{1}{2}-\frac{1}{2}})(\phi^{2112}_{-\frac{1}{2}\frac{1}{2}} + \phi^{2112}_{\frac{1}{2}-\frac{1}{2}})$$

$$-(\phi^{1111}_{-\frac{1}{2}-\frac{1}{2}} + \phi^{1111}_{\frac{1}{2}\frac{1}{2}})(\phi^{2112}_{-\frac{1}{2}\frac{1}{2}} + \phi^{2112}_{\frac{1}{2}-\frac{1}{2}}) - (\phi^{2112}_{-\frac{1}{2}-\frac{1}{2}} + \phi^{2112}_{\frac{1}{2}\frac{1}{2}})(\phi^{1111}_{-\frac{1}{2}\frac{1}{2}} + \phi^{1111}_{\frac{1}{2}-\frac{1}{2}})] \quad (77b)$$

I_2 = term similar to I_1 but proportional to cross product of ψ and ϕ. (77c)

$$I_3 = \frac{288\pi^4\omega_s^4\ell^2}{c^6k_s^2} I_{so}I_{po}^2 e^{-2\varepsilon_o}[\psi^{1111}_{\frac{1}{2}-\frac{1}{2}}(\psi^{1111}_{-\frac{1}{2}\frac{1}{2}} - \psi^{2112}_{-\frac{1}{2}\frac{1}{2}}) +$$

$$\psi^{2112}_{\frac{1}{2}-\frac{1}{2}}(\psi^{2112}_{-\frac{1}{2}\frac{1}{2}} - \psi^{1111}_{-\frac{1}{2}\frac{1}{2}}) + \phi^{1111}_{\frac{1}{2}-\frac{1}{2}}(\phi^{1111}_{\frac{1}{2}-\frac{1}{2}} - \phi^{2112}_{-\frac{1}{2}\frac{1}{2}}) + \phi^{2112}_{\frac{1}{2}-\frac{1}{2}}(\phi^{2112}_{-\frac{1}{2}\frac{1}{2}} - \phi^{1111}_{-\frac{1}{2}\frac{1}{2}})] \quad (77d)$$

I_4 = term similar to I_3 but proportional to cross product of ψ and ϕ.

If ω_m is small compared to the linewidth of $\chi^{(3)}$, then $\psi^{1111}_{\frac{1}{2}\frac{1}{2}} \simeq \psi^{1111}_{-\frac{1}{2}-\frac{1}{2}} \simeq \psi^{1111}_{\frac{1}{2}-\frac{1}{2}} \simeq \psi^{1111}_{-\frac{1}{2}\frac{1}{2}} \equiv \psi^{1111}$, and likewise for all the components of ψ^{2112}, ϕ^{1111} and ϕ^{2112}. Equation (77b) reduces to

$$I_1 \simeq \frac{288\pi^4\omega_s{}^4\ell^2}{c^6k_s{}^2} I_{so}I_{po}^2 e^{-2\varepsilon_o}[(\psi^{1111} - \psi^{2112})^2 + (\phi^{1111} - \phi^{2112})^2] \quad (78)$$

The RIKES intensity at ω_m (equation (78)) is seen to be proportional to the square of the difference between the x and y components of ψ and of ϕ. The form of I_1 is also seen to be Lorentzian. Comparing equation (78) with the direct SRS intensity given by equation (54b) shows that the RIKES signal is considerably weaker due to its quadratic dependence on ψ and ϕ as opposed to the linear dependence for direct SRS. However, a signal-noise analysis of RIKES will demonstrate whether or not it is advantageous over direct SRS.

The phase modulation case for RIKES will not be discussed because the signal levels turn out to be very weak. Such signals would be proportional to $(\delta\psi)^2$ and $(\delta\phi)^2$

which would be at least 2 orders of magnitude weaker than the AM case.

Signal-Noise Analysis. For the signal-noise analysis $S_{RIKES}(t)$ is defined as

$$S_{RIKES}(t) = \frac{I_s(z=\ell,t)}{I_{so}} \tag{79}$$

where $I_s(z=\ell,t)$ is given by equation (77). This allows the rate function $\lambda(t)$ to be written as

$$\lambda(t) = \frac{\eta}{\hbar\omega_s} P_{so} S_{RIKES}(t) \tag{80}$$

where P_{so} is the power of the probe in MKS units and $S_{RIKES}(t)$ is calculated using Gaussian units. The average current given by substitution of equation (80) into equation (59) gives the variance of the signal current due to shot noise as

$$\text{Var[current due to shot noise]} = \frac{2e^2\eta}{\hbar\omega_s} P_{so} S_{RIKES}(t)\ \Delta\nu \tag{81}$$

The other contributions to the noise include Johnson noise, dark current noise and noise due to laser fluctuations. Since the main portion of the probe beam is blocked by the

analyzer the only contribution to the noise by the laser fluctuations comes about through the dependence of the Raman gain on the intensities of both the pump and probe beam intensities, as well as, light leakage of the probe beam through the analyzer which adds incoherently to the RIKES signal. This leakage is caused by strains in the optics or sample which induce birefringence (Ref 9:46).

The fluctuations in the Raman gain due to the laser fluctuations are analyzed by replacing I_{so}^2 and I_{po}^2 by $I_{so}^2 (1 + \delta_s)$ and $I_{po}^2 (1 + \delta_p)$, respectively, into equation (77). The square of the RIKES intensity becomes

$$I_s^2(z=\ell,t) = I_{so}^2 I_{po}^4 (1 + \delta_s)(1 + \delta_p)^2 \frac{[S_{RIKES}(t)]^2}{I_{po}^4}$$

$$= I_{so}^2 [S_{RIKES}(t)]^2 [1 + \delta_s + 2\delta_p + 2\delta_s\delta_p$$

$$+ \delta_p^2 + \delta_s\delta_p^2] \qquad (82)$$

Neglecting terms of order δ^2, one can approximate the variance of the signal current due to laser fluctuations in the Raman gain to be (assuming $\delta_p > \delta_s$)

$$\text{Var[current due to laser fluctuations]} = 2 \left(\frac{e\eta}{\hbar\omega_s}\right)^2$$

$$P_{so}^2[S_{RIKES}(t)]^2\delta_p \tag{83}$$

To determine the noise due to the leakage of the probe beam through the analyzer, the fraction of probe power which leaks through is defined as ε_s. The variance of the signal current due to this leakage becomes

$$\text{Var[current due to probe beam leakage]} = \left(\frac{e\eta}{\hbar\omega_s}\right)^2 P_{so}^2\varepsilon_s^2\delta_s \tag{84}$$

Combining all the noise terms of equations (81), (83), (84) along with the Johnson and dark current noise, the total variance of the signal current is

$$\text{Var[current due to all noise sources]} = \frac{2e^2\eta}{\hbar\omega_s}P_{so}S_{RIKES}(t')\Delta\nu + \frac{4kT}{R_{eff}}\Delta\nu + 2ei_d\Delta\nu + 2\left(\frac{e\eta}{\hbar\omega_s}\right)^2 P_{so}^2[S_{RIKES}(t)]^2\delta_p + \left(\frac{e\eta}{\hbar\omega_s}\right)^2 P_{so}^2\varepsilon_s^2\delta_s \tag{85}$$

The fourth term is considered negligible here due to its dependence on $[S_{RIKES}(t)]^2$ which is very small.

The detected electrical signal is given by equation (71) with $S'_{srs}(t)$ replaced by $S'_{RIKES}(t)$, where $S'_{RIKES}(t)$ is that part of $S_{RIKES}(t)$ which falls within the detection bandwidth. The resultant electrical signal is

$$\bar{I}_s = \frac{e\eta}{\hbar\omega_s} P_{so} S'_{RIKES}(t) \tag{86}$$

Substituting equations (85) and (86) in equation (72) gives the SNR for RIKES as

$$SNR|_{RIKES} = \frac{S'_{RIKES}(t)}{\left[\frac{2\hbar\omega_s}{\eta P_{so}} S_{RIKES}(t)\Delta\nu + \frac{4kT}{R_{eff}}\left(\frac{\hbar\omega_s}{e\eta}\right)^2 \frac{\Delta\nu}{P_{so}^2} + 2ei_d\left(\frac{\hbar\omega_s}{e\eta}\right)^2 \frac{\Delta\nu}{P_{so}^2} + \varepsilon_s^2\delta_s\right]^{\frac{1}{2}}} \tag{87}$$

Due to the shot noise dependence on $S_{RIKES}(t)$, it is much more difficult using RIKES to increase P_{so} in order to make the Johnson and dark current noise negligible. In order for the shot noise to be great enough to allow the Johnson and dark current noise terms to become negligible, for typical values of T, R_{eff}, i_d and ω_s, the probe power P_{so} would have to be at least 10^{10} watts. In fact, for these same typical values and assuming a probe laser power

in the milliwatt range, the shot noise and the dark current noise are considered negligible to the Johnson noise. Hence, the dominant noise terms for RIKES is due to Johnson noise and that due to the leakage of the probe beam through the analyzer.

If this analysis is carried further, by comparing the two noise terms left, then it is discovered that as soon as the leakage of the probe beam becomes 0.01% or greater (assuming $\delta_s = 10^{-12}$) then the Johnson noise becomes negligible. It is unlikely that the leakage can be held to that low a figure, which means that the main barrier to the detection of the RIKES signal is due to the probe laser fluctuations which leak through the analyzer.

The main advantage of RIKES is that it suppresses the amount of probe fluctuations which enter the detector by a factor of ε_s over the direct SRS case. However, due to the extremely weak RIKES signal ($\sim 10^{-12} P_{so}$) in conjunction with typical values of ε_s of 0.25% or greater, the SNR of RIKES is about 3 orders of magnitude below that for direct SRS. This really puts RIKES at a disadvantage compared to direct SRS. Another disadvantage of RIKES is that it does not allow the real and imaginary components of the $\chi^{(3)}$ to be separated, thus not allowing the values of ψ and ϕ to be found.

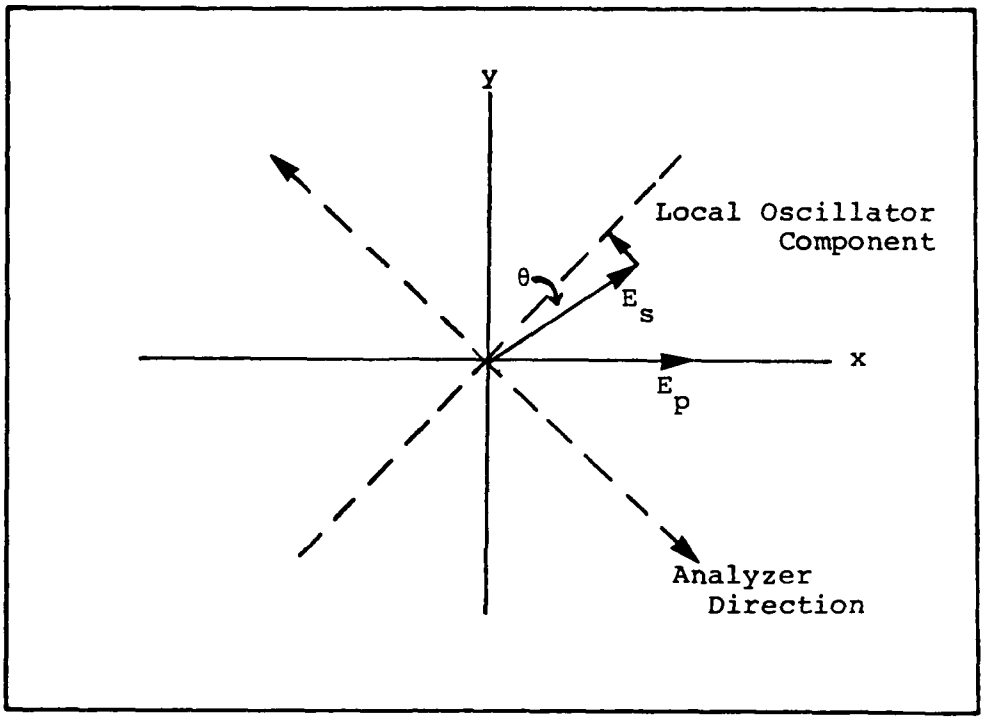

Figure 5: OHD RIKES polarization configuration.

OHD RIKES (Optical Heterodyned RIKES)

Description. The polarization configuration for OHD RIKES is very similar to that of RIKES. The pump beam is linearly polarized along the x-axis as in RIKES. The probe beam is linearly polarized a small angle θ from the x-y diagonal. The signal is analyzed along the perpendicular to the x-y diagonal as in RIKES. This polarization configuration is shown in Figure 5.

This polarization configuration allows a small component of the probe field to pass through the analyzer which acts as a local oscillator and heterodynes with the Raman induced Kerr signal. The component that passes through the analyzer is either in-phase or in quadrature to the Kerr signal allowing either the real or imaginary part of $\chi^{(3)}$ to be detected. The output signal will be shown to be directly proportional to $\chi^{(3)}$ so there is a greater gain in signal over RIKES.

Signal Analysis - Amplitude Modulation of Pump Beam (AM Case). The detected Stokes field which is derived in Appendix A is given by (Eq. A-20)

$$\tilde{E}_s(z=\ell,t) = E_{so}T_o\theta e^{j\omega_s t} + \frac{1}{\sqrt{2}}[\delta\tilde{E}_{sx} - \delta\tilde{E}_{sy}] \tag{88}$$

where $\delta\tilde{E}_{sx}$ and $\delta\tilde{E}_{sy}$ are given approximately by equations (76a) and (76b), respectively and θ is the angle between the x-y diagonal and the direction of polarization of the probe beam. The intensity of the detected Stokes field in Gaussian units is given by (see Appendix A for details of calculation)

$$I_s(z=\ell,t)\Big|_{AM}^{OHD} = I_o + I_1 \cos\omega_m t + I_2 \sin\omega_m t + I_3(t) \tag{89}$$

where

$$I_o = \text{d.c. terms} \tag{89a}$$

$$I_1 = \frac{24\pi^2\omega_s{}^2\ell}{c^3k_s} I_{so}I_{po}\theta e^{-2\varepsilon_o}[(\psi^{2112}_{\frac{1}{2}-\frac{1}{2}} + \psi^{2112}_{-\frac{1}{2}\frac{1}{2}}$$

$$- (\psi^{1111}_{\frac{1}{2}-\frac{1}{2}} + \psi^{1111}_{-\frac{1}{2}\frac{1}{2}})] \tag{89b}$$

$$I_2 = \frac{24\pi^2\omega_s{}^2\ell}{c^3k_s} I_{so}I_{po}\theta e^{-2\varepsilon_o}[(\phi^{2112}_{\frac{1}{2}-\frac{1}{2}} - \phi^{2112}_{-\frac{1}{2}\frac{1}{2}})$$

$$+ (\phi^{1111}_{-\frac{1}{2}\frac{1}{2}} - \phi^{1111}_{\frac{1}{2}-\frac{1}{2}})] \tag{89c}$$

$I_3(t)$ = higher order terms proportional to ψ^2 and ϕ^2. (89d)

The in-phase OHD RIKES intensity at ω_m (equation (89b)) is seen to be linearly proportional to the difference between the x and y components of ψ. The quadrature component at ω_m (equation (89c)) is directly proportional to the difference of ϕ separated by ω_m of the same directional component of ϕ. Comparing the intensity terms of OHD RIKES in equation (89) with that of RIKES in equation (77) shows that the OHD RIKES signal is stronger due to its linear dependence on ψ and ϕ as opposed to the

quadratic dependence for RIKES. In addition, the OHD RIKES technique allows the real and imaginary components of $\chi^{(3)}$ to be detected separately.

Signal Analysis - Phase Modulation of Pump Beam (PM Case). Using equation (88) for the detected Stokes field and equation (57) for the phase modulated pump beam, the intensity in Gaussian units of the detected Stokes field is (see Appendix B for details of calculation)

$$I_s(z=\ell,t)\Big|_{PM}^{OHD} = I_o + I_1 \cos \omega_m t + I_2 \sin \omega_m t + I_3 \cos 2\omega_m t + I_4 \sin 2\omega_m t + I_5(t) \tag{90}$$

where

$$I_o = \text{d.c. terms} \tag{90a}$$

$$I_1 = \frac{48\pi^2\omega_s^2\ell}{c^3 k_s} I_{so} I_{po} \theta e^{-2\varepsilon_o} \delta[(\psi_{0-1}^{1111} - \psi_{01}^{1111}) + (\psi_{01}^{2112} - \psi_{0-1}^{2112})] \tag{90b}$$

$$I_2 = \frac{48\pi^2\omega_s^2\ell}{c^3 k_s} I_{so} I_{po} \theta e^{-2\varepsilon_o} \delta[(\phi_{0-1}^{1111} + \phi_{01}^{1111} - 2\phi_{10}^{1111})$$

$$- (\phi_{01}^{2112} + \phi_{0-1}^{2112} - 2\phi_{10}^{2112})] \tag{90c}$$

$$I_3 = \frac{24\pi^2\omega_s^2\ell}{c^3k_s} I_{so}I_{po}\theta e^{-2\varepsilon_o}\delta^2[(\psi_{1-1}^{1111} + \psi_{-11}^{1111})$$

$$- (\psi_{1-1}^{2112} + \psi_{-11}^{2112})] \tag{90d}$$

$$I_4 = \frac{24\pi^2\omega_s^2\ell}{c^3k_s} I_{so}I_{po}\theta e^{-2\varepsilon_o}\delta^2[(\phi_{1-1}^{1111} - \phi_{-11}^{1111})$$

$$+ (\phi_{-11}^{2112} - \phi_{1-1}^{2112})] \tag{90e}$$

$$I_5(t) = \text{terms proportional to } (\delta\psi)^2 \text{ and } (\delta\phi)^2. \tag{90f}$$

If ω_m is small compared to the linewidth of the $\chi^{(3)}$ resonance, then I_1 is proportional to the sum of the first derivatives of the x and y components of ψ. I_2 becomes proportional to the difference of the second derivatives of the x and y components of ϕ. Hence, I_2 is smaller than I_1. I_3 and I_4 are one to two orders of magnitude weaker than I_1 and I_2 due to the quadratic dependence on δ. $I_5(t)$ is the weakest contribution to the OHD RIKES intensity because of its quadratic dependence on both $\delta\psi$ and $\delta\phi$.

One of the advantages phase modulation offers over amplitude modulation is that with phase modulation very weak Raman signals which change rapidly during the spectral scan can be more easily detected due to the first and second derivative dependence of the phase modulated Raman intensities. This is true for both direct SRS and OHD RIKES using phase modulation.

Signal-Noise Analysis. For the signal-noise analysis of OHD RIKES, $S_{OHD}(t)$ is defined for the AM case as

$$S_{OHD}(t) = \frac{1}{I_{so}\theta}(I_1 \cos \omega_m t + I_2 \sin \omega_m t + I_3(t)) \quad (91a)$$

where I_1, I_2 and $I_3(t)$ are given by equations (89b), (89c) and (89d), respectively. $S_{OHD}(t)$ is defined for the PM case as

$$S_{OHD}(t) = \frac{1}{I_{so}\theta}(I_1 \cos \omega_m t + I_2 \sin \omega_m t + I_3 \cos 2\omega_m t + I_4 \sin 2\omega_m t + I_5(t)) \quad (91b)$$

where I_1 through $I_5(t)$ are given by equations (90b) through (90f), respectively. The rate function for OHD RIKES, defined in equation (60), becomes

$$\lambda(t) = \frac{\eta}{\hbar\omega_s} P_{so} \left(\theta^2 + \theta S_{OHD}(t)\right) \tag{92}$$

The main contributions to the noise for OHD RIKES that are considered in this analysis are shot noise, Johnson noise, dark current noise, and noise due to laser fluctuations. The variance of the signal current due to shot noise is, after substituting $\bar{I} = e\lambda(t)$ and equation (92) into $2e\bar{I}\Delta\nu$,

$$\text{Var[current due to shot noise]} = \frac{2e^2\eta}{\hbar\omega_s} P_{so}\theta^2\Delta\nu \tag{93}$$

The noise due to laser fluctuations arise from three sources: 1) fluctuations in the probe component which acts as the local oscillator, 2) fluctuations in the Raman gain due to pump beam fluctuations, 3) probe beam leakage through the analyzer due to strains in the optics and sample. The variance of the signal current due to the local oscillator probe fluctuations is exactly that found in equation (63) for the direct SRS case, except with $P_{so}\theta^2$ replacing P_{so}. Hence,

Var[current due to local oscillator fluctuations] =

$$\left(\frac{e\eta}{\hbar\omega_s} P_{so}\,\theta^2\right)^2 \delta_s \tag{94}$$

The variance of the signal current due to the Raman gain's dependence on the pump beam fluctuations (here assuming $\delta_p >> \delta_s$)

$$\text{Var[current due to pump fluctuations]} = \left(\frac{e\eta}{\hbar\omega_s}\right) P_{so} \theta \, S_{OHD}(t) \,)^2 \, \delta_p \tag{95}$$

This term can be discarded, as before, due to its dependence on $[S_{OHD}(t)]^2$ which is very small. The variance of the signal current due to the leakage of the probe beam through the analyzer is the same as that for RIKES (equation (84)):

$$\text{Var[current due to probe beam leakage]} = \left(\frac{e\eta}{\hbar\omega_s}\right)^2 P_{so}{}^2 \varepsilon_s{}^2 \delta_s \tag{84}$$

Combining all the noise terms of equations (84), (93), and (94) along with the Johnson and dark current noise, the total variance of the signal current is

$$\text{Var[current due to all noise sources]} = \frac{2e^2\eta}{\hbar\omega_s} \cdot P_{so}\theta^2\Delta\nu + \tag{96}$$

$$+ \frac{4kT}{R_{eff}} \Delta\nu + 2ei_d\Delta\nu + \left(\frac{e\eta}{\hbar\omega_s}\right)^2 P_{so}{}^2\theta^4\delta_s + \left(\frac{e\eta}{\hbar\omega_s}\right)^2 P_{so}{}^2\varepsilon_s{}^2\delta_s$$

The average signal current $\bar{I}_s$ given by equation (70) becomes, after substituting equation (92) for $\lambda(t)$,

$$\bar{I}_s = \frac{e\eta}{\hbar\omega_s} P_{so}\theta\, S'_{OHD}(t) \tag{97}$$

where $S'_{OHD}(t)$ is that part of $S_{OHD}(t)$ which falls within the detection bandwidth.

The SNR for OHD RIKES becomes, after substitution of equations (96) and (97) into equation (72)

$$SNR|_{\substack{OHD\\RIKES}} = \frac{S'_{OHD}(t)\theta}{\left[\frac{2\hbar\omega_s}{\eta P_{so}}\theta^2\Delta\nu + \frac{4kT}{R_{eff}}\left(\frac{\hbar\omega_s}{e\eta}\right)^2\frac{\Delta\nu}{P_{so}^2} + 2ei_d\left(\frac{\hbar\omega_s}{e\eta}\right)^2\frac{\Delta\nu}{P_{so}^2}\right.}$$

$$\left. + \theta^4\delta_s + \varepsilon_s^2\delta_s\right]^{\frac{1}{2}} \tag{98}$$

For the experimentally typical values of T, R_{eff}, and i_d, the Johnson noise term (2^{nd} term in denominator of equation (98)) is approximately 4 orders of magnitude greater than the dark current term (3^{rd} term in denominator of equation (98)).

For small values of θ (assuming a fixed probe power), the $SNR|_{\substack{OHD\\RIKES}}$ increases linearly with θ, whereas, for

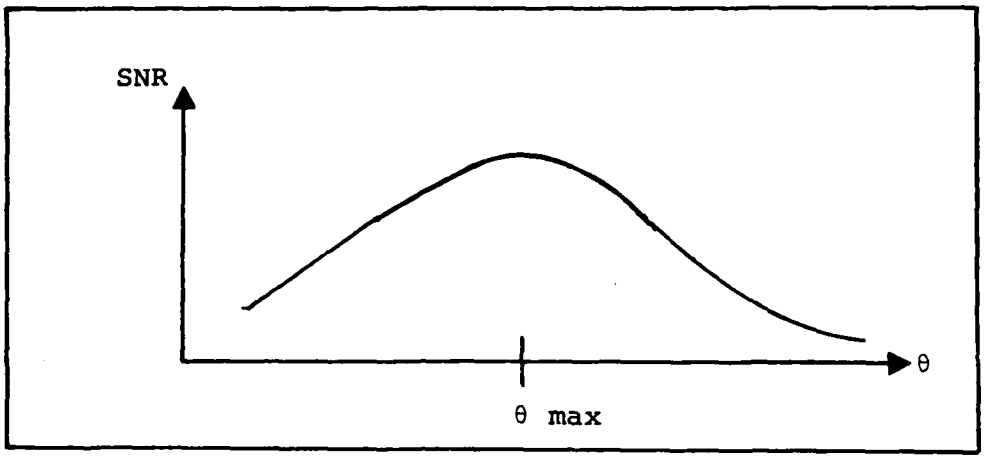

Figure 6: $SNR|_{\substack{OHD \\ RIKES}}$ VS. θ

large values of θ the $SNR|_{\substack{OHD \\ RIKES}}$ decreases as $\frac{1}{\theta}$. Somewhere in between the $SNR|_{\substack{OHD \\ RIKES}}$ reaches a maximum at θmax as depicted in Figure 6. To maximize the $SNR|_{\substack{OHD \\ RIKES}}$, θmax is chosen so that

$$\theta max = \left[\frac{4kT}{R_{eff}} \left(\frac{\hbar\omega_s}{e\eta}\right)^2 \frac{\Delta\nu}{P_{so}^2 \delta_s} + \varepsilon_s^2\right]^{\frac{1}{4}} \qquad (99)$$

In most cases the second term in equation (99) is larger than the first term. Hence, the value of θ which maximizes the $SNR|_{\substack{OHD \\ RIKES}}$ is that which causes the noise due to leakage of the probe beam to be equivalent to the noise due to

the component of the probe beam which acts as the local oscillator. If θ is chosen greater than θ_{max} the dominant noise term is that due primarily to the probe fluctuations which belong to the probe component which acts as the local oscillator. If θ is less than θ_{max} the dominant noise term is that due to the leakage of the probe beam through the analyzer.

Comparing the $SNR|_{\substack{OHD \\ RIKES}}$ of equation (98) with the $SNR|_{\substack{direct \\ SRS}}$ of equation (73) shows that if $\delta_s >> \frac{\hbar\omega_s}{\eta P_{so}} \Delta\nu$, which is very common for narrow bandwidth detection systems and most low power lasers, the $SNR|_{\substack{OHD \\ RIKES}}$ is greater than $SNR|_{direct\ SRS}$ by a factor of $\frac{1}{2\sqrt{2}\theta_{max}}$, where θ_{max} is given by equation (99). Hence, OHD RIKES gives rise to the highest SNR of all three variational techniques.

IV Experimental Apparatus

Introduction

The experimental SRS system is shown in Figure 7 for a liquid and Figure 8 for a solid sample. The system consists of the pump and probe lasers, optics, and the detection electronics.

The pump beam emanates from a vertically polarized tunable dye laser which is excited by an argon ion laser. The pump beam passes through a modulator which either amplitude or phase modulates the beam. The modulated pump beam then passes through a cutoff filter (F 1) which prevents that portion of the dye power, existing at and below the probe frequency, from entering the system. This alleviates a potential noise source due to the pump beam's intensity fluctuations which may exist at the probe wavelength. The pump beam then hits a beam splitter (BS 1) where it is allowed to combine collinearly with the probe beam.

The probe beam emanates vertically polarized from a HeNe gas laser. For direct SRS, the polarization of the HeNe laser is kept vertical, whereas, for RIKES the polarization must be 45° from the vertical and for OHD RIKES it must be an angle $45°+\theta$ from the vertical (see Figures 4 and 5). A half-wave plate (P 1) is used to rotate the

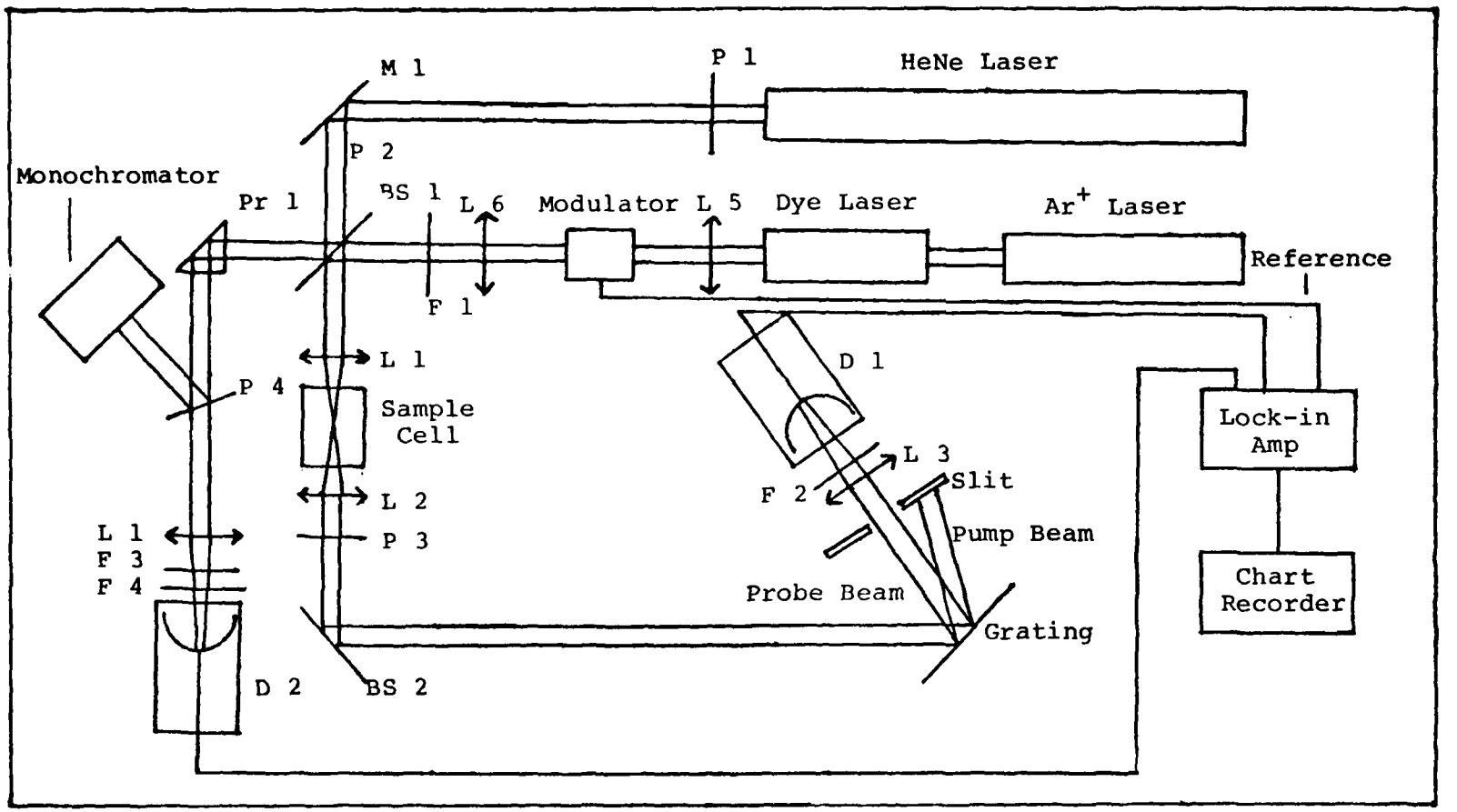

Figure 7: Experimental SRS System for Liquid Sample

BS 1, BS 2: Beamsplitters
D 1 : Signal Detector
D 2 : Reference Detector
F 1 : Cutoff Filter
F 3 : Neutral Density Filter
F 2, F 4 : Narrow Bandpass Filters
L 1 - L 6 : Lenses
M 1 : Mirror
P 1 : Half-Wave Plate
P 2, P 3, P 4: Polarizers

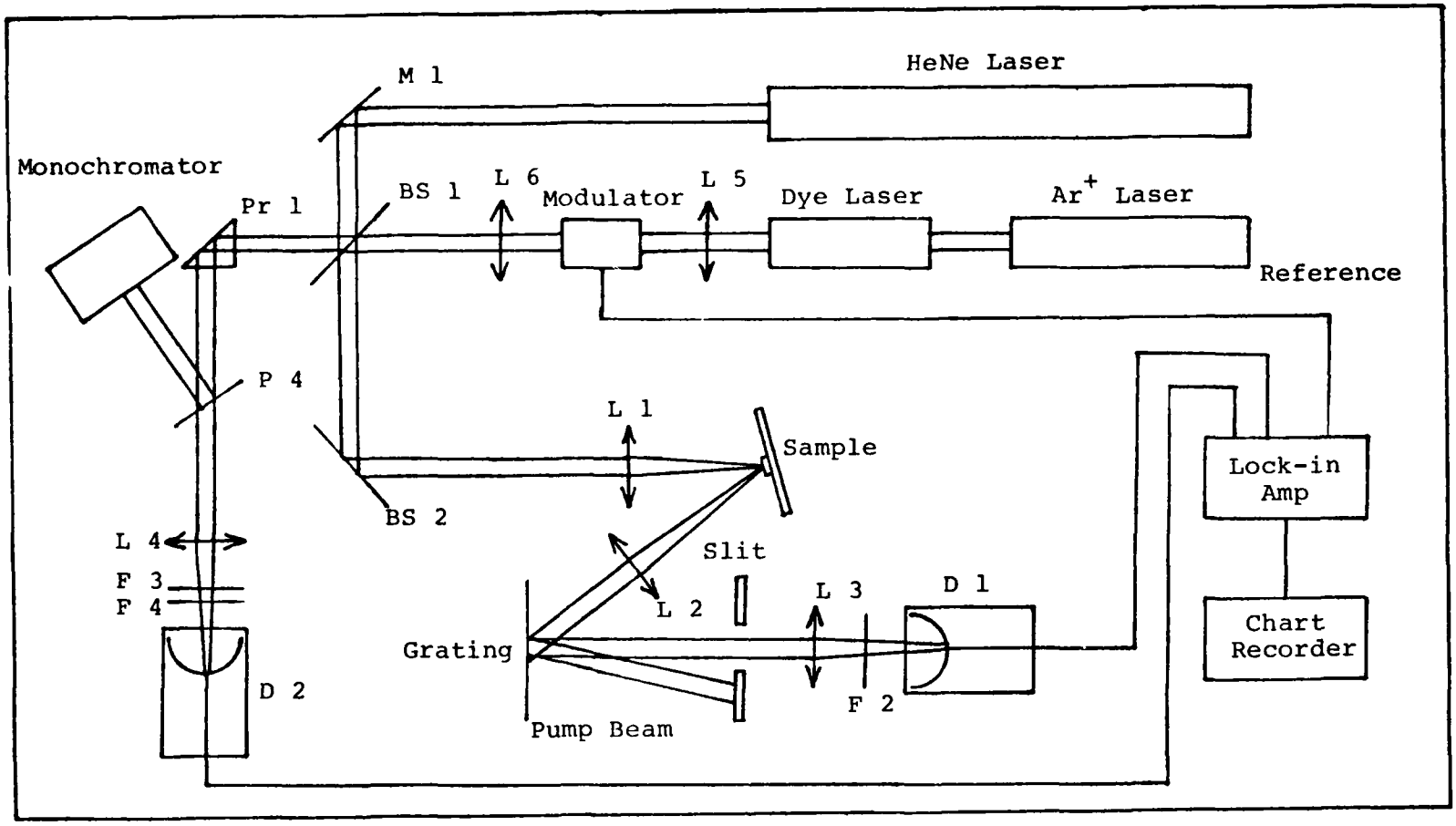

Figure 8: Experimental SRS System for Solid Sample

BS 1, BS 2: Beamsplitters
D 1 : Signal Detector
D 2 : Reference Detector
F 3 : Neutral Density Filter
F 2, F 4 : Narrow Bandpass Filters
L 1 - L 6: Lenses
M 1 : Mirror
P 4 : Polarizer

vertically polarized probe beam. A polarizer (P 2) cleans up the polarization of the probe beam before combining with the pump beam at the beam splitter BS 1.

With the pump and probe beams aligned collinearly at the beamsplitter BS 1, one arm of the combined beams is focussed into the sample by a lens (L 1). For the liquid benzene sample, the two beams pass through the sample and are recollimated by the lens L 2 as shown in Figure 7. For the solid silicon sample, the two beams reflect off the sample and are recollimated by the lens L 2, as shown in Figure 8. After the beams have been recollimated, they pass through an analyzer (P 3) which picks off the component of the Stokes field to be detected. For direct SRS, the analyzer is rotated such that it passes the vertical component, whereas, for both RIKES and OHD RIKES the analyzer is rotated so that the component 45° from the pump beam polarization is detected (see Figures 4 and 5). After passing through the polarizer P 3, the beams hit another beamsplitter (BS 2) and then a ruled reflection grating. The grating spatially separates the pump and probe beams. The probe beam continues, passing through a slit which isolates the probe beam and stops the pump beam. A lens (L 3) focuses the probe beam onto the signal detector D 1. A narrow band pass filter (F 2) of 80Å

bandwidth centered at 6328Å (the probe wavelength) is used to prevent stray background light, particularly that of the pump beam, from entering the detector.

The other arm of the combined pump and probe beams, beginning at the beamsplitter BS 1, is used to both monitor the wavelength of the pump beam and to suppress probe laser intensity fluctuations in the detected signal. The pump and probe beams reflect off a prism (Pr 1) to a polarizer (P 4) rotated such that part of the probe and pump power is reflected to the slit of the monochromator and part of it is transmitted through. The monochromator is used to monitor the wavelength of the pump beam. The pump and probe power, which is transmitted through the polarizer, is filtered by a narrow bandpass filter (F 4) equivalent to the filter F 2 so that only the probe beam is allowed to hit the detector D 2. The d.c. level of the detected probe beam at detector D 2 is matched to the d.c. level of the probe beam at detector D 1 by the neutral density filter F 3 and the polarizer P 4. By rotating the polarizer P 4 the d.c. level of the detected probe beam at detector D 2 may be continuously changed. The two signals from the detectors D 1 and D 2 are plugged into the differential mode of the lock-in amplifier. The lock-in subtracts the two signals before demodulation which effectively subtracts out much of the noise.

The dye laser is scanned very slowly until the frequency difference between it and probe laser match a vibrational mode of the sample. When this occurs, an induced Stokes field is created which gives rise to a modulated gain in the probe beam. This gain is synchronously detected by the lock-in amplifier and recorded by a chart recorder.

Laser

Ar^+ Laser. The dye laser was pumped utilizing a Spectra-Physics Model 165 Argon Ion Laser capable of delivering a maximum of 5 watts of power, however, no more than 3 watts were ever used. This laser was used in the broadband mode allowing the lines between 4579Å and 5145Å pump the dye laser. High stability in output power was achieved by operating the laser in the "light control mode" which allowed only a $\pm$0.5% fluctuation in output power.

Pump Laser. A Spectra-Physics Model 370 Tunable Dye Laser with the Spectra-Physics Model 371 Dye Circulator was used as the pump source. The dye utilized in this system was Rhodamine 6G which allowed continuous tuning from 540 nm to 630 nm. The linewidth of this laser is given as 0.25Å. The required wavelength for Raman resonance in benzene is 595.4 nm. At this wavelength the output power of the dye laser was found to be 300 mW with an input power

of 3 watts from the Ar^+ laser. Normally, only 1 watt of input power is all the dye laser is able to take without burning the dye cell windows. However, this laser has the capability of receiving greater input power by a readjustment of the position of the input lens. It was found that this dye laser could accommodate up to 3 watts of input power before the dye cell windows began to burn.

The required wavelength of the dye laser to induce Raman resonance in silicon was 612.6 nm. At this wavelength, the maximum output power of the dye laser was found to be 95 mW with an input pump power of 3 watts from the Ar^+ laser.

The dye laser was automatically scanned in wavelength using a small electric motor which rotated the wavelength selection dial at a rate of 1 Å/min.

Probe Laser. A Spectra-Physics Model 125A Helium-Neon Gas Laser, capable of delivering a maximum of 50 mW of output power, was utilized as the probe source. The Spectra-Physics Model 261 RF/DC Exciter was used to supply the energy to the laser plasma tube. This laser comes with a removable intracavity etalon which allowed single-mode operation with the etalon in the cavity or multi-mode operation with the etalon removed. The maximum power measured in the multi-mode configuration was 50 mW, whereas,

the maximum power measured in the single-mode configuration was 10 mW. This laser also has an optional RF power supply which is designed to reduce laser output noise by quenching noise in the plasma. This unit, however, was under repair throughout the experimental phase of this thesis. The peak to peak stability of this laser is reported to be less than 1%.

Optical System

Optical Modulators. A mechanical chopper capable of intensity modulating the pump beam as a square wave at 1 KHz was utilized as the amplitude modulator. The pump beam was focussed in the plane of the chopper blades and then recollimated by two lenses of 101.6 cm focal length (L 5 and L 6 in Figure 7). A 1 KHz reference square wave was available from the small power package which powered the chopper.

To phase modulate the pump beam an Isomet Corporation Model TFM-503 transverse electro-optic modulator utilizing KD*P as the crystal was used. This E/O modulator was driven by a sinusoidal signal from a Wavetek Model III Signal Generator. This modulator had to be oriented and supported so that the vertically polarized pump beam was parallel to one of the induced birefringent axes of the

crystal. This required building a stand which supported the modulator in this configuration.

Lenses, Beamsplitters, Filters and Grating. All the lenses (L 1 through L 4 in Figures 7 and 8) were positive with a focal length of 10 cm. The two beamsplitters (BS 1 and BS 2) reflected 75% of the dye power and 70% of the HeNe power. This allowed 15 mW of probe power (operated multi-mode) and 225 mW of pump power (operating at 5954Å) to enter the sample cell. The narrow bandpass filters (F 2 and F4) had maximum transmission at 6328Å with a transmission bandwidth of 80Å. A Jarrell-Ash reflection grating of 295 grooves/mm was used to spatially separate the pump and probe beams before detection.

Monochromator and Sample Cells. A Jarrell-Ash 1/4 meter monochromator was used to monitor the pump beam wavelength as it was scanned.

The sample cell used to hold the liquid benzene was a rectangular glass container with optical windows on either end which allowed the laser beams to pass through with little distortion. This cell was filled with liquid benzene and capped to prevent evaporation.

The sample cell used to hold the silicon sample was an NRC Model MM-2A optical holder. A 1cm x 1cm piece of silicon was glued to a piece of aluminum sheeting which was then mounted in the optical holder.

Detection System

Two EG&G SGD-100A PIN photodiodes were used for the detectors D 1 and D 2. The bandwidth of this photodiode is 45 MHz. The dark current is rated at <10 nanoamps.

The signals from these two detectors were fed into an Ithaco Model 353 Phase-Lock Amplifier operated in the differential mode. This lock-in amplifier was referenced at the modulation frequency by the mechanical chopper power supply when the chopper was used, or by the Wavetek Signal Generator when the E/O modulator was used. The lock-in amplifier was utilized at the 1 μ Volt sensitivity setting which gave a total gain of 10,000. The time constant was set at 10 seconds for all the spectral runs, which is an equivalent noise bandwidth of ~0.01 Hz. The demodulated signal was fed to an Omegaline Chart Recorder set at 0.4"/min scan speed. The oscilloscope used in the optical alignment procedure was a Ballantine 1066S oscilloscope.

V Experimental Procedure and Results

Introduction

The experimental procedure for the three variational SRS techniques (direct SRS, RIKES, OHD RIKES) will be discussed in this chapter, as well as, the experimental results of these techniques.

Direct SRS, RIKES, and OHD RIKES were all attempted on the liquid benzene sample using both amplitude and phase modulation. The three techniques proved unsuccessful in obtaining the sought-after Raman mode at 992 cm^{-1}. Direct SRS, using both amplitude and phase modulation, was tried on the silicon sample. Again, this proved unsuccessful in obtaining the Raman mode at 520 cm^{-1}. However, the thermal background noise reviewed in Chapter III, was observed using an amplitude modulated pump source. These results will be discussed in light of the signal-noise analysis of Chapter III.

Experimental Procedure

The procedure for setting up the experimental SRS system is basically the same for both the liquid benzene sample and the solid silicon sample. The only difference lies in the placement of the optics and detectors. The

procedure for the alignment of the optics will be discussed first. The procedures for performing direct SRS, RIKES and OHD RIKES will follow. This entire discussion will be in reference to Figures 7 and 8.

Optical Alignment. After all the optical components were set in their proper positions, as shown in Figures 7 and 8, the task that followed was to align these components. The HeNe probe laser was turned on first and allowed to warm up for approximately one hour. This gave the laser sufficient time to stabilize. This was followed by turning on the Ar^+ laser (as instructed in the manual for the Ar^+ laser) to power level of 2 Watts which was sufficient to cause the dye laser to begin lasing. (It is assumed here that the dye laser has already been properly aligned with the Ar^+ laser)

For the AM case, the first task was to align the mechanical chopper. Lens L 5 was positioned so that it focussed the dye beam directly onto the slit of the chopper (where the blades come together). Lens L 6 was positioned behind the chopper such that it recollimated the diverged beam from lens L 5. One of the detectors was then placed behind lens L 6 (with the filter F 1 temporarily removed) to intercept the dye laser beam. The signal from this detector was fed directly into the oscilloscope. The chopper

was turned on and incrementally moved back and forth in a lateral direction to the dye beam until a fully modulated square wave was displayed on the oscilloscope. This guaranteed the proper positioning of the chopper. At this time it was convenient to adjust the phase on the lock-in amplifier for maximum d.c. output signal. This was done by connecting the modulated signal of the dye laser to the "A" input of the lock-in amplifier. The reference signal from the chopper power supply was connected to the reference input of the lock-in amplifier. With the lock-in amplifier turned on and a sensitivity of 1 mV selected, the phase control knob was adjusted for maximum deflection of the output voltmeter. This insured proper phase matching of the input signal to the reference signal.

For the PM case, the E/O modulator was placed so that the dye laser beam passed clearly through the modulator. With the modulator turned on, the detector could not "see" any a.c. signal because the intensity of the pump beam does not fluctuate while being phase modulated. In order to adjust the phase on the lock-in amplifier a signal from the Wavetek signal generator was plugged into both the "A" input of the lock-in amplifier and the reference input. The phase was adjusted until there was a maximum deflection of the output voltage meter. The next step was to set the

modulator driving voltage from the Wavetek to insure that $\delta << 1$. The voltage was set at 0.5 Volt utilizing equation (53).

After the modulator was properly aligned and the phase properly adjusted on the lock-in amplifier, the next task was to align the HeNe and dye laser beams so they travelled collinearly to the sample. Mirror M 1 was adjusted so that the HeNe beam fell on top of the dye laser beam at the beamsplitter BS 1. The sample cell was removed from its position and replaced by a 20 μm pinhole. This pinhole was aligned so that the HeNe beam passed directly through it which produced a Fresnel diffraction pattern immediately behind it. Next, the beamsplitter BS 1 was rotated along a vertical and horizontal axis until the dye beam passed through the pinhole producing a Fresnel diffraction pattern which overlapped the HeNe pattern. This insured that the HeNe and dye laser beams were overlapping at the pinhole. A further check of the collinearity of the two beams was done by allowing the beams to propagate to a nearby wall. If the beams overlapped at the wall the alignment was satisfactory, however, if they diverged from each other the whole process had to be repeated.

After the two laser beams were satisfactorily aligned by the above method, the sample cell was replaced in a

position such that the beams properly focussed in the sample. This was followed by positioning lens L 2 such that the beams became recollimated. The beams then proceeded to the reflection grating. The grating was positioned to allow the third diffraction order of the probe beam to pass through the slit which subsequently was focussed by the lens L 3 onto the detector D 1. Detector D 1 was then connected to the "A" input of the lock-in amplifier.

The background detector D 2 was aligned to intercept the probe beam. This detector was connected to the "B" input of the lock-in amplifier which was subsequently set to the "A-B" differential mode. The amplified signal, that the lock-in amplifier was receiving, was monitored by connecting the output from the amplifier section of the lock-in (before demodulation) to the oscilloscope. The polarizer P 4 was rotated until the d.c. level of detector D 2 matched the d.c. level of D 1. When this occurred, the difference in the two signals greatly reduced the effective noise of the HeNe laser, which could be seen on the oscilloscope.

The monochromator was positioned so that the reflection of the beams off the polarizer P 4 entered the monochromator. The wavelength of the pump beam was read directly off the wavelength scale on the monochromator. This scale had been previously calibrated using a mercury lamp.

Direct SRS Polarization Alignment. To perform direct SRS the pump and probe beams had to be polarized in the same direction. Since the two lasers were both already polarized vertically there was no need for the half-wave plate P 1. Polarizer P 2 was adjusted so that it passed a minimum amount of the probe beam. It was then rotated 90 degrees to allow full passage. This insured that a clean polarized probe beam entered the sample. Polarizer P 3 was not needed for this technique, so it was removed.

RIKES Polarization Alignment. In performing RIKES it was very important to insure that the pump and probe beams were polarized exactly 45 degrees from each other when entering the sample, and that the signal was analyzed in a direction 90 degrees from the polarization of the probe beam. The half-wave plate P 1 was adjusted so that the polarized beam from the probe laser was rotated 45 degrees from the vertical. The probe beam was then allowed to propagate to the beamsplitter BS 1. As the beam passed through BS 1 it experienced a slight rotation in the direction of polarization due to the induced birefringence caused by strain in the beamsplitter. Not only did the direction of polarization change, but also the beam experienced a slight phase retardation in one of the quadrature components which left the beam no longer linearly polarized but actually

elliptically polarized. The rotation of the polarized beam was corrected for by rotating the half-wave plate so that the pump and probe beams remained polarized 45 degrees from each other as they entered the sample. Polarizer P 2 was adjusted, as before in the direct SRS case, to clean up the polarization of the probe beam. Polarizer P 3 was adjusted so that it nulled out as much of the probe beam as possible. However, due to the slight ellipticity of the probe beam, a small component was able to "leak" through. This leakage allowed laser intensity fluctuations into the detection system which contributed to the noise.

OHD RIKES Polarization Alignment. In this technique, the same procedure as outlined in the previous paragraph for RIKES was followed. After completing the above procedure, the half-wave plate P 1 was rotated by the small angle θ to allow the local oscillator component of the probe beam to pass through the analyzer P 3 and heterodyne with the RIKES signal. The angle θ was typically varied from 1 to 5 degrees.

After the polarization of the pump and probe beams were properly aligned for the technique being used, the following procedure was performed. The output power of Ar^+ laser was turned up to 3 Watts. The sensitivity on the lock-in amplifier was set at 1 μV which provided a total

gain of 10,000. The time constant was set at 10 seconds. The lock-in amplifier was now ready to detect the in-phase signal component. If the quadrature component was to be detected, the phase was offset 90 degrees from the in-phase setting. When liquid benzene was being analyzed, the dye laser wavelength was set at 5970Å and allowed to scan through the Raman resonance at 5954Å and stopped around 5940Å. The chart recorder was turned on at the beginning of the scan at a setting of 0.4"/min. This scan took approximately 30 minutes. When silicon was being analyzed, the dye laser was set at 6135Å and allowed to scan through Raman resonance at 6126Å and stopped around 6110Å. This scan took about 25 minutes. Scans of both benzene and silicon were tried using amplitude and phase modulation. The scans utilizing phase modulation were done on both samples with modulation frequencies of 1 KHz, 10 KHz, up through 50 KHz in 10 KHz steps.

Results

Results of Spectral Runs. All three variational techniques of SRS (direct SRS, RIKES, OHD RIKES) with the probe HeNe laser operating both multi-mode and single-mode proved unsuccessful in recording the Raman resonance at 992 cm^{-1} for the liquid benzene sample utilizing both amplitude and phase modulation schemes. Likewise, the direct SRS

technique was unsuccessful with the silicon sample for both amplitude and phase modulation schemes. However, the thermal background noise was observed when utilizing an amplitude modulated pump beam. With a pump beam power of 70 mW and a probe beam power of 15 mW hitting the silicon sample, a d.c. signal of 0.25 μVolt, due to the synchronous detection of the thermal background noise, was easily recorded. This signal swamped out the Raman resonance signal at 520 cm^{-1}.

Discussion of Results. The lack of ability of the experimental SRS system to record the Raman resonance in benzene stimulated the need to understand why the system was not working. The signal-noise ratios derived in Chapter III could be utilized to provide a clue as to why the sensitivity of the system was not enough to see the Raman resonance, as well as, indicate what improvements could be made to the system to increase its sensitivity.

The first task was to find out the numerical values of the variables of the experimental system needed to calculate the signal-noise ratios of equations (69), (80) and (91) for direct SRS, RIKES and OHD RIKES, respectively. The values for all these variables, except δ_s and ε_s are tabulated below:

$T = 300°K$

$R_{eff} = 10^3 \Omega$

$\omega_s = 3 \times 10^{15}$ sec^{-1}

$\Delta\nu = 0.01$ Hz ($\Delta\nu = \frac{1}{8\tau}$; $\tau = 10$ sec.)

$i_d = 10^{-9}$ amp

$\psi = 15.9 \times 10^{-14} \frac{cm^3}{erg}$ (Ref 12:153)

$I_{po} = 7.2 \times 10^9 \frac{ergs}{cm^2 sec}$ (225 mW focussed to a beam dia. of 0.02 cm)

$k_s = 99292$ rad/cm

$\varepsilon_o \simeq 0$

$P_{so} = 15$ mW

$\delta \simeq 0.1$

To obtain a value for the light leakage parameter ε_s, the following procedure was carried out. The probe HeNe laser beam's power was first measured directly from the laser using a Scientech 362 power meter. This was followed by measuring the probe beam power after passing through a polarizer rotated so that it nulled out as much of the beam as possible. It was found that approximately 0.25% of the probe beam was able to leak through the polarizer. This gave a value for ε_s of 2.5×10^{-3}.

In order to find δ_s for the experimental system (δ_s is the mean-squared fractional deviation of the intensity of the HeNe beam) it was necessary to examine the noise power spectral density of the HeNe laser. This was accomplished using a spectrum analyzer which was able to

AD-A094 418 AIR FORCE INST OF TECH WRIGHT-PATTERSON AFB OH SCHOO--ETC F/G 20/6
A THEORETICAL AND EXPERIMENTAL STUDY ON THE APPLICATION OF STIM--ETC(U)
DEC 80 D C SLATER
UNCLASSIFIED AFIT/GEP/PH/80-9 NL

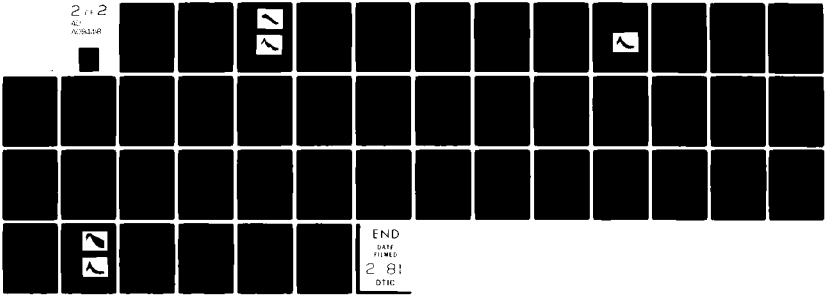

provide a display of the noise spectrum. The experimental arrangement for recording the noise spectrum is shown in Figure 9.

The HeNe beam was detected with one of the photodiode detectors used in the original experimental SRS setup. The signal from the detector was amplified by a factor of 100 using a Keithley Model 104 Wideband Amplifier. The amplified signal was fed into the input of a Hewlett-Packard 8556A Low Frequency plug-in module capable of receiving signals between 20 Hz and 300 KHz. This plug-in module was connected to a Hewlett-Packard 8552A IF unit and a Hewlett-Packard 141T Spectrum Analyzer Display. The vertical axis of the display was calibrated to show the laser power per unit frequency on a log scale, and the horizontal axis was calibrated in units of frequency on a linear scale. The noise spectrum of the HeNe beam operating both multi-mode and single-mode is shown in Figure 10. These noise spectra are very similar to those obtained by Cole for HeNe gas lasers (Ref 22:1023).

The peak of the noise curves shown in Figure 10 correspond to very low frequencies close to d.c. (the actual d.c. power level is filtered out by the analyzer and thus does not show up on the display). Each horizontal division is 20 KHz. Hence, the noise spectrum in these photographs

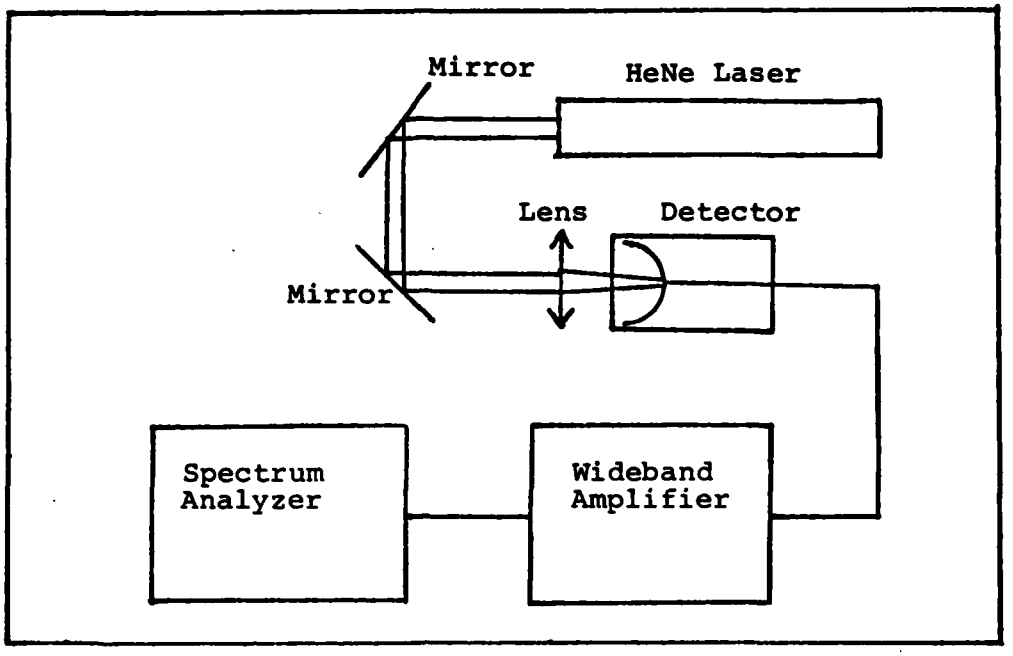

Figure 9: Experimental Arrangement for Recording Noise Spectrum of HeNe Laser.

run from d.c. to 160 KHz. The amplitude modulation frequency of 1 KHz is very close to the peak of the spectral curve. In order to get a number for δ_s at 1 KHz, the height of the spectral curve at 1 KHz had to be known with respect to the d.c. signal level of the HeNe beam. The d.c. signal level was measured with an oscilloscope to be 0.5 volt. A sinusoidal reference signal of 0.5 volt amplitude from the Wavetek signal generator was plugged into the input of the spectrum analyzer. The sensitivity knobs on the analyzer, which control the vertical gain of the display, were adjusted so the 0.5 volt signal from the Wavetek

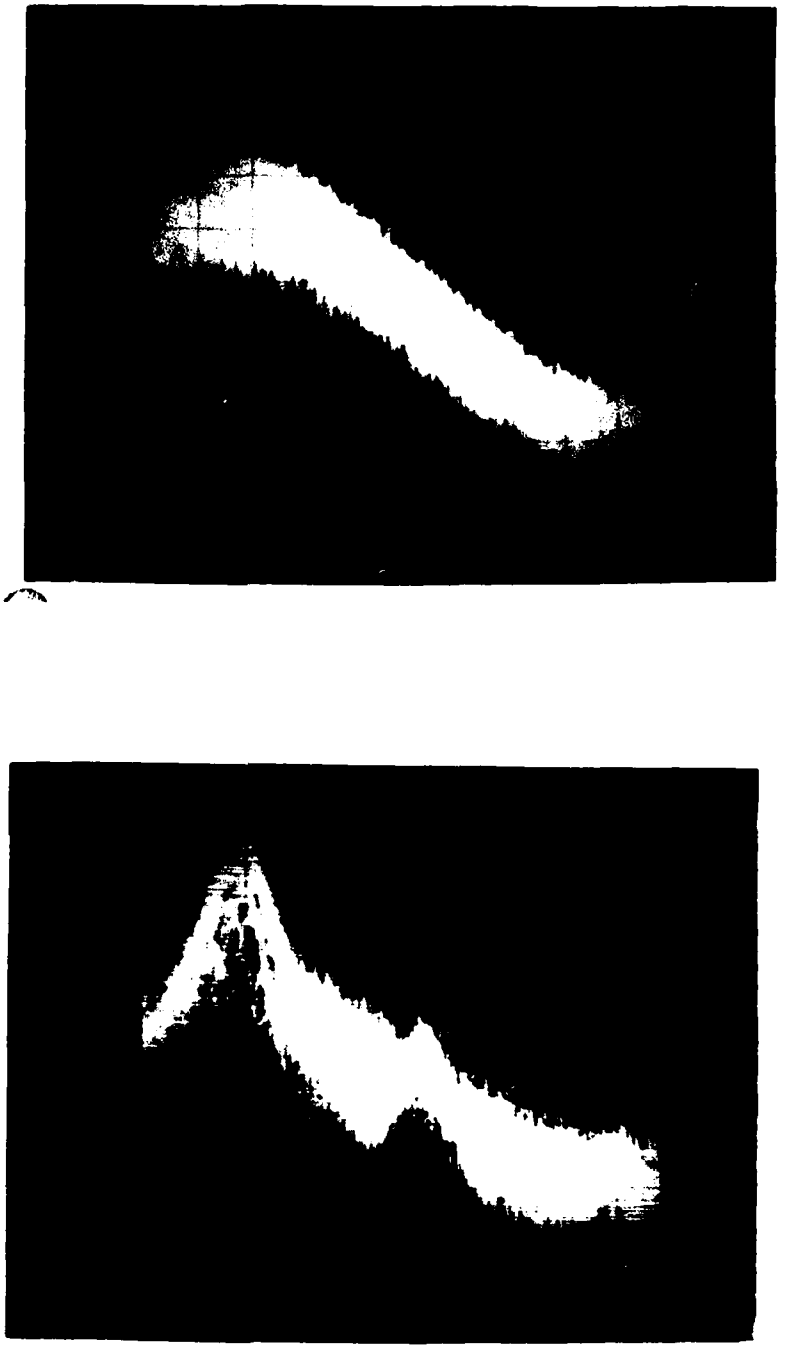

Figure 10: Top, HeNe Noise Spectrum Operated Multi-Mode. Bottom, HeNe Noise Spectrum Running Single-Mode. Each Horizontal Division in 20 KHz. Top of Photo is Reference Line.

signal generator reached the top reference line on the display (the reference line is the very last horizontal line at the top portion of the display). Each vertical division below the top reference line corresponds to a 10db decrease in signal strength. This allowed the noise power of the HeNe laser to be evaluated with respect to the d.c. power of the HeNe laser.

The first photograph of Figure 10 shows the noise spectrum of the HeNe laser operated multi-mode. The top of the spectral curve at 1 KHz is about 10 dB below the reference line. Using the equation $dB = 20 \log (\frac{V_2}{V_1})$, where V_2 is the d.c. voltage proportional to the d.c. power of the HeNe beam and V_1 is the amplified noise voltage proportional to the a.c. power amplitude fluctuations of the HeNe beam, the equation used to calculate the root-mean-square power fluctuations $\delta_s^{\frac{1}{2}}$ was derived. This equation is

$$\delta_s^{\frac{1}{2}} = \frac{1}{\sqrt{2}} \frac{V(\text{noise})}{V\ (\text{d.c.})} \Delta\nu = \frac{10^{-[\frac{dB}{20} + 4]}}{\sqrt{2}} \qquad (100)$$

where V(noise) is the noise voltage amplitude from the detector due to the power fluctuations of the HeNe laser, V(d.c.) is the d.c. voltage from the detector, $\Delta\nu$ is the detection bandwidth and dB is the difference in height

measured from the top reference line to the spectral curve. If the spectral curve lies below the reference line, dB is a positive quantity. If the spectral curve lies above the reference line, dB is a negative quantity. For example, in the first photograph of Figure 10, the peak of the spectral curve is 10 dB below the top reference line. The value of $\delta_s^{\frac{1}{2}}$ at the peak (corresponding to a frequency of ~ 1 KHz) is 2.2×10^{-5} using equation (100). The values of $\delta_s^{\frac{1}{2}}$ decrease with increasing modulation frequencies, as is easily seen by the downward slope of the noise curve. Values of $\delta_s^{\frac{1}{2}}$ are tabulated in Table I for both a multimode and single mode operated HeNe laser at various frequencies.

At about the same time these results were obtained the RF power supply was returned from repair. This unit was plugged into the probe power supply and a noise spectrum was taken as shown in Figure 11. The values of $\delta_s^{\frac{1}{2}}$ were found from this spectrum and are also presented in Table I.

TABLE I

Values of $\delta_s^{\frac{1}{2}}$ of HeNe probe laser operated multi-mode, single-mode and multi-mode with RF power supply.

FREQUENCY (KHz)	$\delta_s^{\frac{1}{2}}$ MULTI-MODE ($\times 10^{-8}$)	$\delta_s^{\frac{1}{2}}$ SINGLE-MODE ($\times 10^{-8}$)	$\delta_s^{\frac{1}{2}}$ MULTI-MODE W/RF POWER SUPPLY ($\times 10^{-8}$)
1	2236	7070	4460
10	1260	2236	1260
20	707	500	280
40	398	224	70
60	126	100	22
80	56	40	13
100	22	22	7
120	13	13	6
140	7	13	5.6
160	7	13	5.6

Table I shows that the HeNe laser intensity fluctuations, when operated single-mode, were approximately 3 times greater than the fluctuations when operated multi-mode at 1 KHz. Between 20 KHz and 100 KHz the single-mode HeNe was

approximately 1.5 times quieter than the HeNe operated multi-mode.

With all the variables required to calculate the signal-noise ratios for all three variational SRS techniques known, the ratios were calculated assuming the HeNe probe laser was operated multi-mode. These values are tabulated in Table II. Along with the SNR values are the values of S' as defined on page 37 for direct SRS and which is similarly defined for RIKES and OHD RIKES. S' is the fractional gain of the probe laser power during Raman resonance.

TABLE II

Values of S' and SNR (Signal-noise ratio) for all three variational techniques of SRS. (Modulation frequency indicated in parenthesis).

VARIATIONAL TECHNIQUE	S'	SNR
Direct SRS AM Case (1 KHz)	1.8×10^{-6}	0.08
Direct SRS PM Case (40 KHz)	3.6×10^{-7}	0.09
RIKES AM Case (1 KHz)	4.0×10^{-13}	0.0000075
OHD RIKES ($\theta=\theta$ max) AM Case (1 KHz)	0.9×10^{-6}	0.57
OHD RIKES ($\theta=\theta$ max) PM Case (40 KHz)	1.8×10^{-7}	0.64

Table II shows clearly why the Raman resonance of liquid benzene was never observed. For each variational technique the signal-noise ratio was less than one making it virtually impossible to detect the Raman signal. The source of the noise which buried the signal in each case was due to the laser intensity fluctuations in the HeNe probe beam existing at 1 KHz for the AM case and from 1 KHz up to 40 KHz for the PM case.

In order for the direct SRS technique to yield an SNR greater than 1, $\delta_s^{\frac{1}{2}}$ must be less than 180×10^{-8} when using AM modulation and less than 36×10^{-8} when using PM modulation. This means that within the 0.01 Hz detection bandwidth the probe laser power must be stable to at least 1 part in 10^6. Table I shows that with the experimental SRS system, signal-noise ratios greater than one can be achieved when modulating above 60 KHz for AM and 100 KHz for PM.

Table II shows that RIKES is a highly undesirable technique due to the extremely small SNR. OHD RIKES, on the other hand, offers the greatest SNR of the three techniques. In order for OHD RIKES to yield an SNR greater than one, $\delta_s^{\frac{1}{2}}$ must be less than 1300×10^{-8} using AM modulation and less than 255×10^{-8} using PM modulation.

Table I shows that signal-noise ratios greater than one can be achieved when modulating above 10 KHz for AM and above 60 KHz for PM.

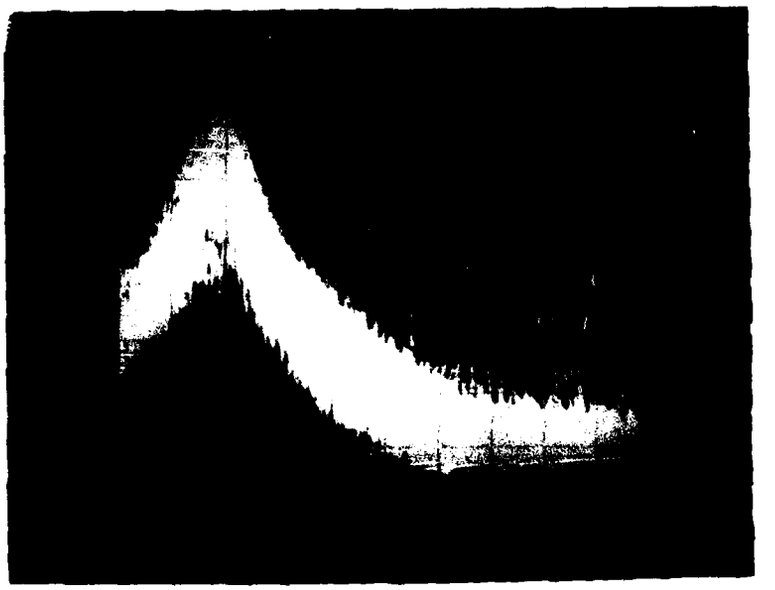

Figure 11: Noise Spectrum of HeNe with RF Power Supply.

Comparing the values of $\delta_s^{\frac{1}{2}}$ without the RF power supply (first column in Table I) with those values with the RF power supply (last column in Table I) shows that the RF power supply dampens the power fluctuations of the HeNe probe laser by a factor of approximately 5 between 10 KHz and 100 KHz. In this case, direct SRS will yield an SNR greater than one for modulation frequencies above 20 KHz for AM modulation and above 60 KHz for PM modulation. OHD RIKES will yield an SNR greater than one for modulation frequencies above 10 KHz for AM and above 20 KHz for PM. All of the minimum modulation frequencies required in order to effectively see Raman resonance in liquid benzene are tabulated in Table III.

Figure 12 below shows all three noise spectra found in Figures 10 and 11 superimposed on top of each other in order to make direct comparisons.

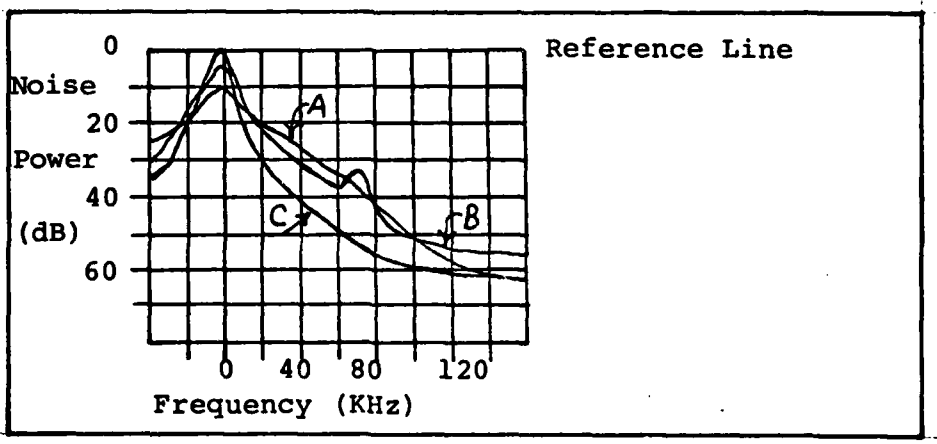

Figure 12: Superimposed HeNe Noise Spectra. Curve A-Multimode Operation W/O RF Power Supply; Curve B-Single Mode W/O RF Power Supply; Curve C-Multimode W/RF Power Supply.

TABLE III

The minimum modulation frequency for direct SRS and OHD RIKES are given in order to record the Raman resonance of liquid benzene. Two cases are considered: HeNe with and without RF power supply.

VARIATIONAL TECHNIQUE	MULTI-MODE W/O RF MINIMUM MOD. FREQ (KHz)	MULTI-MODE W/ RF MINIMUM MOD. FREQ (KHz)
DIRECT SRS AM CASE	60	20
DIRECT SRS PM CASE	100	60
OHD RIKES AM CASE	10	10
OHD RIKES PM CASE	60	20

VI Conclusions and Recommendations

In this study the signal and noise of the three variational SRS techniques (direct SRS, RIKES and OHD RIKES) utilizing amplitude and phase modulation were derived and applied to an experimental SRS system using low power CW lasers with samples of liquid benzene and solid silicon. The conclusions drawn from the signal and noise analysis are the following:

1. For each variational technique, amplitude modulation yields greater Raman signals than phase modulation.

2. If the modulation frequency ω_m is small compared to the linewidth of $\chi^{(3)}$ then phase modulation yields Raman signals which are proportional to the first derivative of the imaginary part of $\chi^{(3)}$ and the second derivative of the real part of $\chi^{(3)}$ for both direct SRS and OHD RIKES. Hence, phase modulation is advantageous over amplitude modulation when detecting weak Raman signals with sharp spectral structures.

3. The main source of noise for all three variational techniques is the intensity fluctuations of the probe laser. RIKES and OHD RIKES detect less probe fluctuations than direct SRS, however, the intensity of the Raman signals for RIKES and OHD RIKES is less than for direct SRS. The RIKES

signal is so small, due to its quadratic dependence on $\chi^{(3)}$, that it is considered an impractical technique for low power CW systems. The OHD RIKES signal is smaller than the direct SRS signal by a factor of $\frac{\theta}{2}$, however, OHD RIKES is better able to suppress the probe fluctuations entering the detector by a factor of $\frac{1}{\sqrt{2}\theta^2_{max}}$. Hence, the signal-noise ratio (SNR) of OHD Rikes is greater than the SNR of direct SRS by a factor of $\frac{1}{2\sqrt{2}\theta_{max}}$ making OHD RIKES the most favorable SRS technique.

The conclusions drawn from the application of the signal and noise analysis to the experimental SRS system are the following:

1. The present state of the experimental SRS system is not able to detect any Raman gain in benzene due to extremely poor signal-noise ratios. This is a result of an excessive amount of probe laser intensity fluctuations at the modulation frequencies of 1 KHz for AM and up to 50 KHz for PM which swamp the Raman signal.

2. The root-mean-squared fractional intensity deviation $(\delta_s^{\frac{1}{2}})$ of the probe laser operated multimode within the effective detection bandwidth of 0.01 Hz at 1 KHz is 2.2×10^{-5}. In order for the Raman signal level of benzene to rise above the noise, $\delta_s^{\frac{1}{2}}$ must be no larger than about 10^{-6} for direct SRS and 10^{-5} for OHD RIKES.

3. The variational technique requiring the lowest modulation frequency, in order to detect the Raman resonance in benzene, is OHD RIKES using amplitude modulation. The lowest modulation frequency which gives an SNR of one for this technique is 10 KHz. The minimum modulation frequencies for the other variational techniques are shown in the left hand column of Table IV.

4. Thermal background noise was observed using amplitude modulation on solid silicon. This swamped the Raman signal at 520 cm^{-1}. Phase modulation was tried but it was not able to pull the Raman signal out of the noise. Again, probe laser intensity fluctuations is the probable cause for not detecting the Raman signal.

The following are recommendations for future work with this system:

1. The 1 KHz chopper should be replaced with a longitudinal electro-optic (E/O) modulator capable of amplitude modulating the pump beam between 10 KHz and 100 KHz, or higher. Modulation at these higher frequencies will allow detection of the Raman signal in benzene. The E/O crystal must not have any natural birefringence which rules out transverse E/O modulators; otherwise, the variation in the wavelength of the pump beam, while the dye laser is being scanned, will upset the polarization of the emerging beam from the E/O modulator.

2. Phase modulation at frequencies higher than 50 KHz, with the E/O modulator already being used in the experimental system, should be tried.

3. The utilization of a more powerful dye laser as the pump source. This will increase the Raman signal due to its dependence on the intensity of the pump beam.

4. The RF power supply, which decreases the probe laser fluctuations in the probe beam, should be used for all future experimental work with this system. Table III shows the reduction in the modulation frequency for each technique if the RF power power supply is used.

5. The use of a multi-pass sample cell (Ref 11), which allows the probe and pump beams to make multiple passes through the sample could be tried. This results in an increase in the gain of the Raman signal.

6. Working with solid samples such as silicon and gallium arsenide should be continued. Further theoretical development of the Raman signals could be carried out for these kinds of solid-state samples.

Bibliography

1. Levenson, Marc D. "Coherent Raman Spectroscopy," Physics Today, 30: 44-49 (May 1977).

2. Weber, A. Raman Spectroscopy of Gases and Liquids. Heidelberg, Germany: Springer-Verlag, 1979.

3. Eckhardt G., R.W. Hellworth, F.J. McClung, S.E. Schwarz, D. Weiner and E.J. Woodbury. "Stimulated Raman Scattering From Organic Liquids," Physical Review Letters, 9:455-457 (December 1, 1962).

4. Maier, M. "Applications of Stimulated Raman Scattering," Applied Physics, 11:209:231 (1976)

5. Owyoung, A. "High Resolution Coherent Raman Spectroscopy of Gases," Unpublished article. Division 4214 Sandia Laboratories, Albuquerque, N.M. 87185.

6. Owyoung, A. "Coherent Detection of Raman Modes by CW Stimulated Gain Spectroscopy," IEEE Journal of Quantum Electronics, QE-13:100D (Sept. 1977).

7. Owyoung, A. "Coherent Raman Gain Spectroscopy Using CW Laser Sources, "IEEE Journal of Quantum Electronics, QE-14:192-203 (March 1978).

8. Heimen, D., R.W. Hellwarth, M.D. Levenson, Graham Martin. "Raman-Induced Kerr Effect," Physical Review Letters, 36:189-192 (26 January 1976).

9. Eesley, Gary L., M.D. Levenson, and William M. Tolles. "Optically Heterodyned Coherent Raman Spectroscopy," IEEE Journal of Quantum Electronics, QE-14:45-49 (January 1978).

10. Levenson, M.D. and G.L. Eesley. "Polarization Selective Optical Heterodyne Detection for Dramatically Improved Sensitivity in Laser Spectroscopy," Applied Physics, 19:1-17 (1979).

11. Owyoung, A. "Sensitivity Limitations for CW Stimulated Raman Spectroscopy," Optics Communications, 22:323-328 (September 1977).

12. Owyoung, A. "Stimulated Raman Spectroscopy Using Low-Power CW Lasers," Optics Letters, 1:152-154 (November 1977).

13. Owyoung, A. "High-resolution CW Stimulated Raman Spectroscopy in Molecular Hydrogen," Optics Letters, 2:91-93 (April 1978).

14. Levine, B.F., C.V. Shank, J.P. Heritage. "Surface Vibrational Spectroscopy Using Stimulated Raman Scattering, "IEEE Journal of Quantum Electronics, QE-15:1418-1432 (December 1979).

15. Rahn, L.A. and P.L. Mattern. "Coherent Raman Spectroscopy for Combustion Applications," SPIE Laser Spectroscopy, 158:76-83 (1978).

16. Yariv, Amnon. Quantum Electronics. New York: John Wiley and Sons, Inc., 1967.

17. Nibler, J.W. and G.V. Knighten. "Coherent Anti-Stokes Raman Spectroscopy." in Raman Spectroscopy of Gases and Liquids, edited by A. Weber. Heidelberg, Germany: Springer-Verlog, 1979.

18. Butcher, P.N. Nonlinear Optical Phenomena. Engineering Experiment Station Bulletin 200, The Ohio State University, Columbus, Ohio (1965).

19. Bjorklund, Gary C. "Frequency-Modulation Spectroscopy: A New Method for Measuring Weak Absorption and Dispersions," Optics Letters, 5: 15-17 (January 1980).

20. Yariv, Amnon. Introduction to Optical Electronics. (Second Edition) New York: Holt, Rinehart and Winston, 1976.

21. Levine, Barry F. and C.G. Bethea. "Ultrahigh Sensitivity Stimulated Raman Gain Spectroscopy," IEEE Journal of Quantum Electronics, QE-16:85-89 (January 1980).

22. Cole, J.H. "Low-Frequency Laser Noise of Several Commercial Lasers," Applied Optics, 19:1023-1025 (1 April 1980).

Appendix A

Deviation of Raman Signals Using Amplitude Modulation

Direct SRS

In this analysis a fully modulated sinusoidal variation in the intensity of the pump beam, as shown in Figure A-1, will be assumed. This sinusoidal variation in the pump intensity can be written as

$$I_p(t) = \frac{I_{po}}{2} [1 + \cos \omega_m t] \qquad \text{(A-1)}$$

where ω_m is the modulation frequency. The electric field of the modulated pump beam is

$$E_p(t) = \frac{1}{2} [\tilde{E}_p + c.c.] \qquad \text{(A-2)}$$

where

$$\tilde{E}_p = \frac{1}{2} E_{po} [e^{j(\omega_p + \frac{\omega_m}{2})t} + e^{j(\omega_p - \frac{\omega_m}{2})t}] \qquad \text{(A-3)}$$

The modulated pump field has frequency components at $\omega_p + \frac{\omega m}{2}$ and $\omega_p - \frac{\omega_m}{2}$.

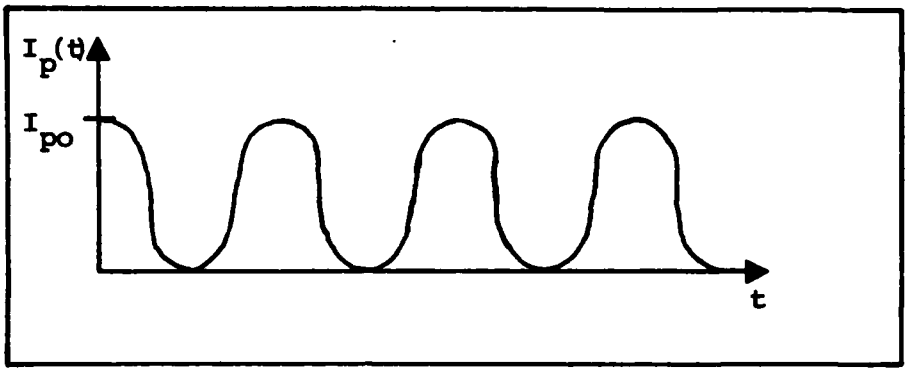

Figure A-1: Intensity Modulated Pump Beam

The spectrum of the pump field is shown in Figure A-2.

The pump and probe beams interact in the medium and the resulting electric field at the Stokes frequency is found by solving Maxwell's equation, as was done in Chapter II. The solution is given by equation (25) which in this analysis is slightly modified by taking into account the first order attenuation and dispersion of the Raman medium. The modified solution becomes

$$\tilde{E}_s(z=\ell,t) = E_{so}T_n\ (1 + \alpha\ell + j\beta\ell)\ e^{j\omega_s t} \qquad \text{(A-4)}$$

where

$T_n = e^{-\varepsilon_n - j\gamma_n}$ describes the linear dispersion and attenuation of the $\omega_s + n\omega_m$ component of the Stokes field. (Here n =-1,0,1)

$$\varepsilon_n = \frac{\alpha_n \ell}{2}$$

α_n is the linear attenuation coefficient and ℓ is the distance the two beams travel together in the sample.

$$\gamma_n = \frac{\eta_n \ell (\omega_s + n\omega_m)}{c}$$

η_n is the first order index of refraction

$$\alpha = \frac{-12\pi\omega_s^2}{c^2 k_s} \sum_{r=-\frac{1}{2}}^{\frac{1}{2}} \sum_{s=-\frac{1}{2}}^{\frac{1}{2}} \tilde{E}_p(\omega_p + r\omega_m) \tilde{E}_p^*(\omega_p + s\omega_m) \psi_{rs}^{1111}$$

$$\beta = \frac{12\pi\omega_s^2}{c^2 k_s} \sum_{r=-\frac{1}{2}}^{\frac{1}{2}} \sum_{s=-\frac{1}{2}}^{\frac{1}{2}} \tilde{E}_p(\omega_p + r\omega_m) \tilde{E}_p^*(\omega_p + s\omega_m) \phi_{rs}^{1111}$$

and

$$\psi_{rs}^{1111} = \mathrm{Im}\{\chi^{(3)}_{1111}(\omega_p + r\omega_m, -(\omega_p + s\omega_m), \omega_s)\}$$

$$\phi_{rs}^{1111} = \mathrm{Re}\{\chi^{(3)}(\omega_p + r\omega_m, -(\omega_p + S\omega_m), \omega_s)\}$$

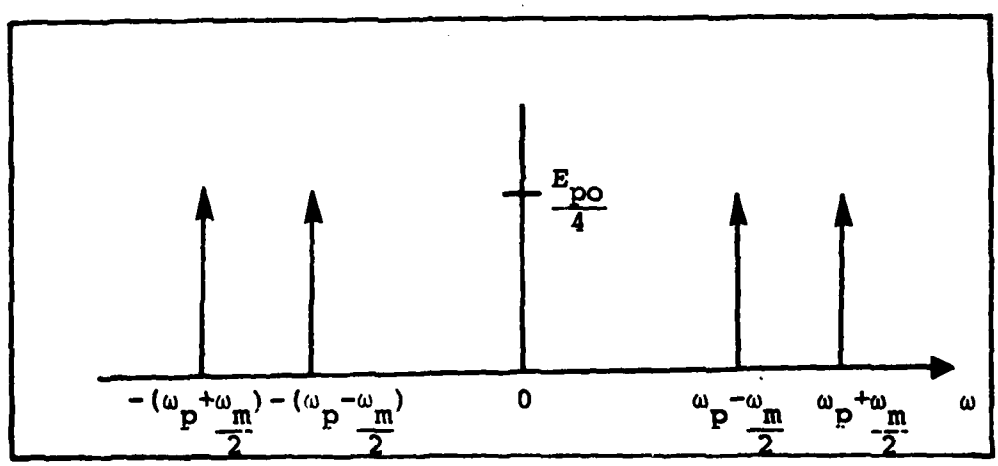

Figure A-2: Frequency Domain Representation of Amplitude Modulated Pump Field.

where r and s take on the values of $+\frac{1}{2}$ and $-\frac{1}{2}$. Equation (A-4) may be written

$$E_s(z=\ell,t) = E_{so}T_o e^{j\omega_s t} + \delta\tilde{E}_s \qquad \text{(A-5)}$$

where

$$\delta\tilde{E}_s = E_{so}\ell T_n \alpha e^{j\omega_s t} + jE_{so}\ell T_n \beta e^{j\omega_s t} \qquad \text{(A-6)}$$

Substitution of α and β from equation (A-4) into equation (A-6), while substituting equation (A-3) for the pump field yields

$$\delta\tilde{E}_s = -E_{so}\ell \frac{12\pi\omega_s^2}{c^2 k_s} \frac{E_{po}^2}{4} [T_o\psi^{1111}_{-\frac{1}{2}-\frac{1}{2}} + T_o\psi^{1111}_{\frac{1}{2}\frac{1}{2}} + T_{-1}\psi^{1111}_{-\frac{1}{2}\frac{1}{2}} e^{-j\omega_m t}$$

$$+ T_1\psi^{1111}_{\frac{1}{2}-\frac{1}{2}} e^{j\omega_m t}]e^{j\omega_s t} + jE_{so}\ell \frac{12\pi\omega_s^2}{c^2 k_s} \frac{E_{po}^2}{4} [T_o\phi^{1111}_{-\frac{1}{2}-\frac{1}{2}} +$$

$$T_o\phi^{1111}_{\frac{1}{2}\frac{1}{2}} + T_{-1}\phi^{1111}_{-\frac{1}{2}\frac{1}{2}} e^{-j\omega_m t} + T_1\phi^{1111}_{\frac{1}{2}-\frac{1}{2}} e^{j\omega_m t}]e^{j\omega_s t} \qquad \text{(A-7)}$$

The total intensity of the Stokes field is given by

$$I_s(z=\ell,t) = \frac{c}{8\pi}|\tilde{E}_s|^2 = \frac{c}{8\pi}|E_{so}T_o e^{j\omega_s t} + \delta\tilde{E}_s|^2 \qquad \text{(A-8)}$$

$$=\frac{c}{8\pi}[E_{so}^2+E_{so}T_o\delta\tilde{E}_s^* e^{j\omega_s t}+E_{so}T_o^*\delta\tilde{E}_s e^{-j\omega_s t}+|\delta\tilde{E}_s|^2]$$

The first term in equation (A-8) is a d.c. term. The second term becomes, after substituting equation (A-7) for $\delta\tilde{E}_s$

$$\frac{c}{8\pi}E_{so}T_o\delta\tilde{E}_s^* e^{j\omega_s t}=\frac{-3\omega_s^2\ell E_{po}^2E_{so}^2}{8ck_s}[\psi^{1111}_{-\frac{1}{2}-\frac{1}{2}}+\psi^{1111}_{\frac{1}{2}\frac{1}{2}}+$$

$$T_oT_{-1}^*\psi^{1111}_{-\frac{1}{2}\frac{1}{2}}e^{j\omega_m t}+T_oT_1^*\psi^{1111}_{\frac{1}{2}-\frac{1}{2}}e^{-j\omega_m t}]-\frac{j3\omega_s^2\ell E_{po}^2E_{so}^2}{8ck_s}$$

$$[\phi^{1111}_{-\frac{1}{2}-\frac{1}{2}}+\phi^{1111}_{\frac{1}{2}\frac{1}{2}}+T_oT_{-1}^*\phi^{1111}_{-\frac{1}{2}\frac{1}{2}}e^{j\omega_m t}+T_oT_1^*\phi^{1111}_{\frac{1}{2}-\frac{1}{2}}e^{-j\omega_m t}] \qquad \text{(A-9)}$$

The third term of equation (A-8) is just the complex conjugate of equation (A-9). Combining all four terms of equation (A-8) gives the total intensity of the Stokes field as

$$I_s(z=\ell,t)=\frac{c}{8\pi}E_{so}^2-\frac{3\omega_s^2\ell E_{po}^2E_{so}^2}{8ck_s}[2\psi^{1111}_{-\frac{1}{2}-\frac{1}{2}}+2\psi^{1111}_{\frac{1}{2}\frac{1}{2}}$$

$$+2e^{-\varepsilon_o-\varepsilon_{-1}}\psi^{1111}_{-\frac{1}{2}\frac{1}{2}}\cos(\omega_m t+\dot{\gamma}_{-1}-\dot{\gamma}_o)+2e^{-\varepsilon_o-\varepsilon_1}\psi^{1111}_{\frac{1}{2}-\frac{1}{2}}$$

$$\cos(\omega_m t+\dot{\gamma}_o-\dot{\gamma}_1)]+\frac{3\omega_s^2\ell E_{po}^2E_{so}^2}{8ck_s}[2\phi^{1111}_{-\frac{1}{2}\frac{1}{2}}e^{-\varepsilon_o-\varepsilon_{-1}}$$

$$\sin(\omega_m t + \gamma_{-1} - \gamma_o) - 2\phi^{1111}_{\frac{1}{2}-\frac{1}{2}} e^{-\varepsilon_o - \varepsilon_1} \sin(\omega_m t + \gamma_o - \gamma_1)]$$

$$+ \frac{c}{8\pi}|\delta\tilde{E}_s|^2 \qquad \text{(A-10)}$$

Since γ_n and ε_n are approximately constant for all values of n (no first order resonance at the Stokes frequency) all differences between the dispersion and attenuation coefficients are zero. The Stokes intensity reduces to

$$I_s(z=\ell,t) = I_o + I_1 \cos\omega_m t + I_2 \sin\omega_m t + I_3(t) \qquad \text{(A-11)}$$

where

I_o = d.c. terms

$$I_1 = \frac{-48\pi^2\omega_s^2}{c^3 k_s} \ell I_{po} I_{so} (\psi^{1111}_{-\frac{1}{2}\frac{1}{2}} + \psi^{1111}_{\frac{1}{2}-\frac{1}{2}}) e^{-2\varepsilon_o}$$

$$I_2 = \frac{48\pi^2\omega_s^2}{c^3 k_s} \ell I_{po} I_{so} (\phi^{1111}_{-\frac{1}{2}\frac{1}{2}} - \phi^{1111}_{\frac{1}{2}-\frac{1}{2}}) e^{-2\varepsilon_o}$$

$I_3(t) = \frac{c}{8\pi}|\delta\tilde{E}_s|^2$ proportional to ψ^2 and ϕ^2.

I_{po} and I_{so} are the initial intensities of the pump and probe beams, respectively.

RIKES

In RIKES, the Stokes field is analyzed in the $\frac{\hat{e}_x - \hat{e}_y}{\sqrt{2}}$ direction, as shown in Figure 4, page 45. Hence, the detected Stokes field becomes

$$\tilde{E}_s(z=\ell,t)\cdot\frac{\hat{e}_x-\hat{e}_y}{\sqrt{2}} = [(\frac{E_{so}}{\sqrt{2}} T_o e^{j\omega_s t+\delta\tilde{E}_{sx}})\hat{e}_x +$$

$$(\frac{E_{so}}{\sqrt{2}}T_o e^{j\omega_s t+\delta\tilde{E}_{sy}})\delta\tilde{E}_{sy})\hat{e}_y]\cdot[\frac{\hat{e}_x-\tilde{e}_y}{\sqrt{2}}]$$

$$= \frac{1}{\sqrt{2}} (\delta\tilde{E}_{sx}-\delta\tilde{E}_{sy}) \qquad \text{(A-12)}$$

where

$\hat{e}_x$ - unit vector in the x direction.

$\hat{e}_y$ - unit vector in the y direction.

$$\delta\tilde{E}_{sx}=\frac{E_{so}}{\sqrt{2}}\ell T_n\alpha_x e^{j\omega_s t}+j\frac{E_{so}}{\sqrt{2}}\ell T_n\beta_x e^{j\omega_s t} \qquad \text{(A-12a)}$$

$$\delta\tilde{E}_{sy}=\frac{E_{so}}{\sqrt{2}}\ell T_n\alpha_y e^{j\omega_s t}+j\frac{E_{so}}{\sqrt{2}}\ell T_n\beta_y e^{j\omega_s t} \qquad \text{(A-12b)}$$

and

$\alpha_x + j\beta_x$ is proportional to $\chi^{(3)}_{1111}$.

$\alpha_y + j\beta_y$ is proportional to $\chi^{(3)}_{2112}$.

The intensity of the detected Stokes field is

$$I_s(z=\ell,t) = \frac{c}{8\pi}\frac{1}{2}\left|\delta\tilde{E}_{sx} - \delta\tilde{E}_{sy}\right|^2 \qquad \text{(A-13)}$$

$$= \frac{c}{8\pi}\frac{1}{2}\left[\left|\delta\tilde{E}_{sx}\right|^2 - \delta\tilde{E}_{sx}\delta\tilde{E}^*_{sy} - \delta\tilde{E}^*_{sx}\delta\tilde{E}_{sy} + \left|\delta\tilde{E}_{sy}\right|^2\right]$$

To simplify the calculation of the Stokes field intensity, we let $\delta\tilde{E}_{sx} = A+jB$ where A and B are both complex. Thus,

$$\left|\delta\tilde{E}_{sx}\right|^2 = AA^* + BB^* + j(BA^* - AB^*) \qquad \text{(A-14)}$$

where

$$A = \frac{-12\pi\omega_s^2\ell}{c^2k_s}\frac{E_{so}}{\sqrt{2}}\frac{E_{po}}{4}^2\left[T_o\psi^{1111}_{-\frac{1}{2}-\frac{1}{2}}e^{j\omega_s t} + T_o\psi^{1111}_{\frac{1}{2}\frac{1}{2}}e^{j\omega_s t}\right.$$

$$\left. + T_{-1}\psi^{1111}_{-\frac{1}{2}\frac{1}{2}}e^{j(\omega_s-\omega_m)t} + T_1\psi^{1111}_{\frac{1}{2}-\frac{1}{2}}e^{j(\omega_s+\omega_m)t}\right] \qquad \text{(A-15)}$$

$$B = \frac{12\pi\omega_s^2 \ell}{c^2 k_s} \frac{E_{so}}{\sqrt{2}} \frac{E_{po}^2}{4} [T_o \phi^{1111}_{-\frac{1}{2}-\frac{1}{2}} e^{j\omega_s t} + T_o \phi^{1111}_{\frac{1}{2}\frac{1}{2}} e^{j\omega_s t}$$

$$+ T_{-1} \phi^{1111}_{-\frac{1}{2}\frac{1}{2}} e^{j(\omega_s - \omega_m)t} + T_1 \phi^{1111}_{\frac{1}{2}-\frac{1}{2}} e^{j(\omega_s + \omega_m)t}] \qquad \text{(A-16)}$$

In this analysis, only the in-phase component of the intensity of the Stokes field will be derived. Hence, the third and fourth term of equation (A-14) will be neglected. The first term of equation (A-14) becomes, after substituting equation (A-15) for A

$$AA^* = \frac{9\pi^2 \omega_s^2 \ell^2 E_{so}^2 E_{po}^4}{c^4 k_s^2} \{\text{d.c. terms} +$$

$$e^{-2\varepsilon_o}[e^{-\varepsilon_o - \varepsilon_{-1}} \psi^{1111}_{-\frac{1}{2}-\frac{1}{2}} \psi^{1111}_{-\frac{1}{2}\frac{1}{2}} \cos(\omega_m t + \gamma_{-1} - \gamma_o) + e^{\varepsilon_o - \varepsilon_1}$$

$$\psi^{1111}_{-\frac{1}{2}-\frac{1}{2}} \psi^{1111}_{\frac{1}{2}-\frac{1}{2}} \cdot$$

$$\cos(\omega_m t + \gamma_o - \gamma_1) + e^{-\varepsilon_o - \varepsilon_{-1}} \psi^{1111}_{\frac{1}{2}\frac{1}{2}} \psi^{1111}_{-\frac{1}{2}\frac{1}{2}} \cos(\omega_m t + \gamma_{-1} - \gamma_o) +$$

$$e^{\varepsilon_o - \varepsilon_1} \psi^{1111}_{\frac{1}{2}\frac{1}{2}} \psi^{1111}_{\frac{1}{2}-\frac{1}{2}} \cos(\omega_m t + \gamma_o - \gamma_1)] + e^{-2\varepsilon_1} \psi^{1111}_{\frac{1}{2}-\frac{1}{2}} \psi^{1111}_{-\frac{1}{2}\frac{1}{2}} [e^{\varepsilon_1 - \varepsilon_{-1}} \cdot$$

$$\cos(2\omega_m t + \gamma_{-1} - \gamma_o)] \qquad \text{(A-17)}$$

The term BB^* is the same as AA^* except ψ_{rs}^{1111} is replaced by ϕ_{rs}^{1111}. Similarly, if a A' and B' are defined for $\tilde{\delta E}_{sy}$ where A' is proportional to ψ_{rs}^{2112} and B' is proportional to ϕ_{rs}^{2112}, then A' and B' are similarly defined as in equations (A-15) and (A-16). The cross terms $\tilde{\delta E}_{sx}\tilde{\delta E}_{sy}^*$ and $\tilde{\delta E}_{sx}^*\tilde{\delta E}_{sy}$ of equation (A-13) are of the same form as equation (A-17), but with the AA^* and BB^* terms proportional to $\psi_{rs}^{1111}\psi_{rs}^{2112}$ and $\phi_{rs}^{1111}\phi_{rs}^{2112}$, respectively. Combining all the terms of equation (A-13) that are in-phase with the modulated pump beam, the resultant Stokes intensity becomes, again letting all differences of ε_n's and γ_n's go to zero,

$$I_s(z=\ell,t) = I_o + I_1 \cos \omega_m t + I_2 \cos 2\omega_m t \qquad \text{(A-18)}$$

where

$$I_o = \text{d.c. terms}$$

$$I_1 = \frac{288\pi^4\omega_s^4}{c^6 k_s^2}\,\ell^2 I_{po}^2 I_{so} e^{-2\varepsilon_o}\left[(\psi_{-\frac{1}{2}-\frac{1}{2}}^{1111}+\psi_{\frac{1}{2}\frac{1}{2}}^{1111})(\psi_{-\frac{1}{2}\frac{1}{2}}^{1111}+\psi_{\frac{1}{2}-\frac{1}{2}}^{1111})\right.$$

$$\left. + (\psi_{-\frac{1}{2}-\frac{1}{2}}^{2112}+\psi_{\frac{1}{2}\frac{1}{2}}^{2112})(\psi_{-\frac{1}{2}\frac{1}{2}}^{2112}+\psi_{\frac{1}{2}-\frac{1}{2}}^{2112}) - (\psi_{-\frac{1}{2}\frac{1}{2}}^{2112}+\psi_{\frac{1}{2}-\frac{1}{2}}^{2112})(\psi_{-\frac{1}{2}-\frac{1}{2}}^{1111}+\psi_{\frac{1}{2}\frac{1}{2}}^{1111})\right.$$

$$- (\psi^{2112}_{-\frac{1}{2}-\frac{1}{2}}+\psi^{2112}_{\frac{1}{2}\frac{1}{2}})(\psi^{1111}_{-\frac{1}{2}\frac{1}{2}}+\psi^{1111}_{\frac{1}{2}-\frac{1}{2}}) + (\phi^{1111}_{-\frac{1}{2}-\frac{1}{2}}+\phi^{1111}_{\frac{1}{2}\frac{1}{2}})(\phi^{1111}_{-\frac{1}{2}\frac{1}{2}}+\phi^{1111}_{\frac{1}{2}\frac{1}{2}})$$

$$+ (\phi^{2112}_{-\frac{1}{2}-\frac{1}{2}}+\phi^{2112}_{\frac{1}{2}\frac{1}{2}})(\phi^{2112}_{-\frac{1}{2}\frac{1}{2}}+\phi^{2112}_{\frac{1}{2}-\frac{1}{2}}) - (\phi^{2112}_{-\frac{1}{2}\frac{1}{2}}+\phi^{2112}_{\frac{1}{2}-\frac{1}{2}})(\phi^{1111}_{-\frac{1}{2}-\frac{1}{2}}+\phi^{1111}_{\frac{1}{2}\frac{1}{2}})$$

$$- (\phi^{2112}_{-\frac{1}{2}-\frac{1}{2}}+\phi^{2112}_{\frac{1}{2}\frac{1}{2}})(\phi^{1111}_{-\frac{1}{2}\frac{1}{2}}+\phi^{1111}_{\frac{1}{2}-\frac{1}{2}})]$$

$$I_2 = \frac{288\pi^4\omega_s^4}{c^6 k_s^2}\,\ell^2 I_{po}^2 I_{so} e^{-2\varepsilon_o}[\psi^{1111}_{\frac{1}{2}-\frac{1}{2}}(\psi^{1111}_{-\frac{1}{2}\frac{1}{2}}-\psi^{2112}_{-\frac{1}{2}\frac{1}{2}})$$

$$+ \psi^{2112}_{\frac{1}{2}-\frac{1}{2}}(\psi^{2112}_{-\frac{1}{2}\frac{1}{2}}-\psi^{1111}_{-\frac{1}{2}\frac{1}{2}})+\phi^{1111}_{\frac{1}{2}-\frac{1}{2}}(\phi^{1111}_{-\frac{1}{2}\frac{1}{2}}-\phi^{2112}_{-\frac{1}{2}\frac{1}{2}})+\phi^{2112}_{\frac{1}{2}-\frac{1}{2}}(\phi^{2112}_{-\frac{1}{2}\frac{1}{2}}-\phi^{1111}_{-\frac{1}{2}\frac{1}{2}})]$$

The quadrature component of the intensity would be proportional to the cross products of ψ and ϕ. This component is neglected, because in most cases it is the in-phase component which is detected.

OHD RIKES

Figure A-3 shows the polarization configuration for OHD RIKES. The Stokes electric field is

$$\tilde{E}_s(z=\ell,t)=(E_{so}T_o e^{j\omega_s t}\cos\phi+\delta\tilde{E}_{sx})\hat{e}_x+(E_{so}T_o e^{j\omega_s t}\sin\phi+\delta\tilde{E}_{sy})\hat{e}_y \qquad \text{(A-19)}$$

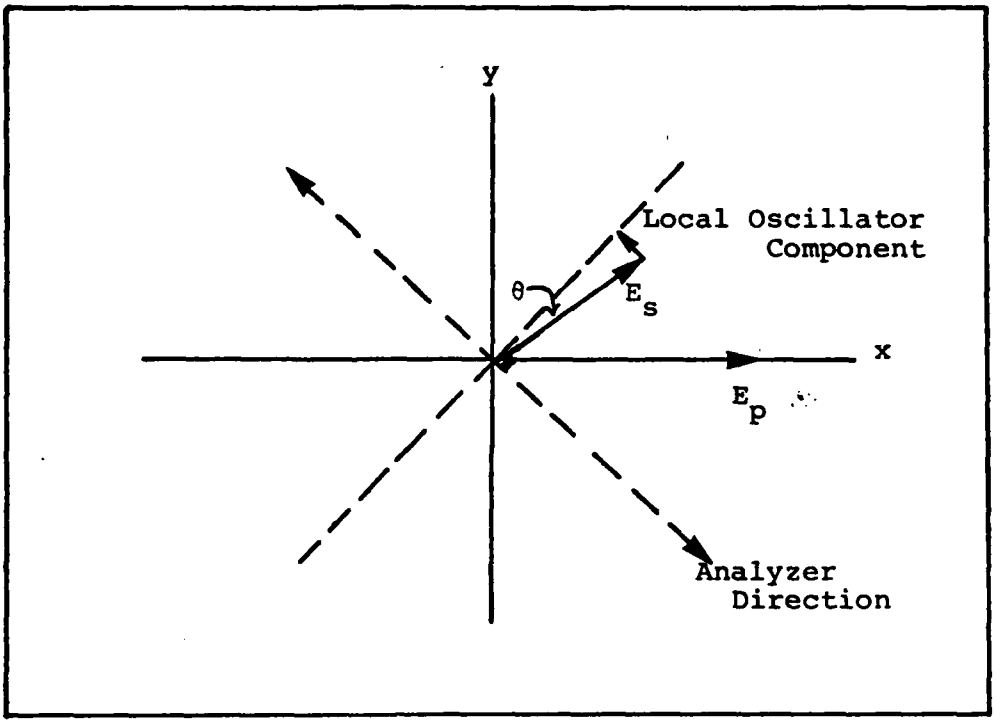

Figure A-3: Polarization Configuration for OHD RIKES

where $\phi = \frac{\pi}{4} - \theta$. For small θ

$$\cos \phi \simeq \frac{1}{\sqrt{2}} (1 + \theta)$$

$$\sin \phi \simeq \frac{1}{\sqrt{2}} (1 - \theta)$$

The Stokes field is analyzed along the $\frac{\hat{e}_x - \hat{e}_y}{\sqrt{2}}$ direction. The analyzed Stokes field becomes

$$\tilde{E}_s(z=\ell,t) \cdot \left(\frac{\hat{e}_x - \hat{e}_y}{\sqrt{2}}\right) = E_{so} T_o \theta e^{j\omega_s t} + \frac{1}{\sqrt{2}}[\delta\tilde{E}_{sx} - \delta\tilde{E}_{sy}] \qquad \text{(A-20)}$$

where $\delta\tilde{E}_{sx}$ and $\delta\tilde{E}_{sy}$ are given by equations (A-12a) and (A-12b), respectively. The intensity of the detected Stokes field is

$$I_s(z=\ell,t) = \frac{c}{8\pi} \left| \tilde{E}_s \cdot \frac{\hat{e}_x - \hat{e}_y}{\sqrt{2}} \right|^2 = \frac{c}{8\pi}\left[E_{so}{}^2\theta^2 + \frac{E_{so}T_o\theta}{\sqrt{2}}(\delta\tilde{E}^*_{sx} - \delta\tilde{E}^*_{sy})e^{j\omega_s t} + \frac{E_{so}T_o{}^*\theta}{\sqrt{2}}(\delta\tilde{E}_{sx} - \delta E_{sy})e^{-j\omega_s t} + \frac{1}{4}|\delta\tilde{E}_{sx} - \delta\tilde{E}_{sy}|^2\right] \qquad \text{(A-21)}$$

The second and third terms of equation (A-21) become

$$\frac{c}{8\pi}\frac{E_{so}\theta}{\sqrt{2}}[T_o(\delta\tilde{E}^*_{sx}-\delta\tilde{E}^*_{sy})e^{j\omega_s t}+T_o^*(\delta\tilde{E}_{sx}-\delta\tilde{E}_{sy})e^{-j\omega_s t}] \quad \text{(A-22)}$$

where

$$\delta\tilde{E}_{sx}=E_{so}\cos\phi\ell T_n\alpha_x e^{j\omega_s t} + jE_{so}\cos\phi\ell T_n\beta_x e^{j\omega_s t}$$

$$\simeq \frac{E_{so}}{\sqrt{2}}(1+\theta)\ell T_n\alpha_x e^{j\omega_s t} + j\frac{E_{so}}{\sqrt{2}}(1+\theta)\ell T_n\beta_x e^{j\omega_s t} \quad \text{(A-23)}$$

and

$$\delta\tilde{E}_{sy}=E_{so}\sin\phi\ell T_n\alpha_y e^{j\omega_s t} + jE_{so}\sin\phi\ell T_n\beta_y e^{j\omega_s t}$$

$$\simeq\frac{E_{so}}{\sqrt{2}}(1-\theta)\ell T_n\alpha_y e^{j\omega_s t} + j\frac{E_{so}}{\sqrt{2}}(1-\theta)\ell T_n\beta_y e^{j\omega_s t}$$

Neglecting terms of order θ^2 in the intensity we get

$$\delta\tilde{E}_{sx} \simeq \frac{E_{so}}{\sqrt{2}}\ell T_n\alpha_x e^{j\omega_s t} + j\frac{E_{so}}{\sqrt{2}}\ell T_n\beta_x e^{j\omega_s t} \quad \text{(A-24)}$$

$$\delta\tilde{E}_{sy} \simeq \frac{E_{so}}{\sqrt{2}}\ell T_n\alpha_y e^{j\omega_s t} + j\frac{E_{so}}{\sqrt{2}}\ell T_n\beta_y e^{j\omega_s t}$$

Letting all differences of $\varepsilon_n'^s$ and $\gamma_n'^s$ to be zero equation (A-22) becomes

$$\frac{c}{8\pi}\frac{E_{so}}{2}\theta\{-E_{so}\ell\frac{12\pi\omega_s^2}{c^2k_s}\frac{E_{po}^2}{4}[\text{d.c. terms} + e^{-2\varepsilon_o}(2\psi^{1111}_{-\frac{1}{2}\frac{1}{2}}\cos\omega_m t$$

$$+ 2\psi^{1111}_{\frac{1}{2}-\frac{1}{2}}\cos\omega_m t - 2\phi^{1111}_{-\frac{1}{2}\frac{1}{2}}\sin\omega_m t + 2\phi^{1111}_{\frac{1}{2}-\frac{1}{2}}\sin\omega_m t - 2\psi^{1111}_{-\frac{1}{2}\frac{1}{2}}\cos\omega_m t$$

$$- 2\psi^{2112}_{\frac{1}{2}-\frac{1}{2}}\cos\omega_m t + 2\phi^{2112}_{-\frac{1}{2}\frac{1}{2}}\sin\omega_m t - 2\phi^{2112}_{\frac{1}{2}-\frac{1}{2}}\sin\omega_m t)]\} \quad \text{(A-25)}$$

The total Stokes intensity is found by combining all the terms of equation (A-21), which becomes

$$I_s(z=\ell,t) = I_o + I_1\cos\omega_m t + I_2\sin\omega_m t + I_3(t) \quad \text{(A-26)}$$

where

I_o = d.c. terms

$$I_1 = \frac{24\pi^2\omega_s^2}{c^3k_s}\ell I_{po}I_{so}\theta e^{-2\varepsilon_o}[(\psi^{2112}_{\frac{1}{2}-\frac{1}{2}}+\psi^{2112}_{-\frac{1}{2}\frac{1}{2}})-(\psi^{1111}_{\frac{1}{2}-\frac{1}{2}}+\psi^{1111}_{-\frac{1}{2}\frac{1}{2}})]$$

$$I_2 = \frac{24\pi^2\omega_s^2}{c^3k_s}\ell I_{po}I_{so}\theta e^{-2\varepsilon_o}[(\phi^{2112}_{\frac{1}{2}-\frac{1}{2}}-\phi^{2112}_{-\frac{1}{2}\frac{1}{2}})+(\phi^{1111}_{-\frac{1}{2}\frac{1}{2}}-\phi^{1111}_{\frac{1}{2}-\frac{1}{2}})]$$

$I_3(t)$ = terms proportional to ψ^2 and ϕ^2.

Appendix B

Derivation of Raman Signals Using Phase Modulation

Direct SRS

The electric field of the pump beam becomes after passing through a phase modulator driven by a sinusoidal field at frequency ω_m,

$$E_p(t) = \frac{1}{2}E_{po}\sum_{n=-\infty}^{\infty} J_n(\delta)\exp[j(\omega_p+n\omega_m)t]+c.c. \qquad (B-1)$$

where E_{po} is the amplitude of the pump electric field, δ is the modulation index, J_n are the Bessel functions of order n. If $\delta<<1$, equation (B-1) can be reduced to

$$\tilde{E}_p(t)=E_{po}[e^{j\omega_p t}+\frac{\delta}{2}(e^{j(\omega_p+\omega_m)t}-e^{j(\omega_p-\omega_m)t})] \qquad (B-2)$$

The phase modulated pump field has frequency components at ω_p (the carrier), $\omega_p+\omega_m$ and $\omega_p-\omega_m$ (the sidebands). The spectrum of the pump field is shown in Figure B-1. The total modulated field is

$$E_p(t)=\frac{1}{2}[\tilde{E}_p(t) + c.c.] \qquad (B-3)$$

The Stokes field is given by equation (A-4). However, equation (B-2) is substituted in for the pump field, r and s take on the values of -1, 0, +1; and n takes on the values of -2, -1, 0, +1, +2. With these changes, equation (A-6) becomes

$$\tilde{\delta E}_s = E_{so}{}^{\ell}T_n \alpha e^{j\omega_s t} + jE_{so}{}^{\ell}T_n \beta e^{j\omega_s t}$$

$$= E_{so}T_n{}^{\ell}\left[\frac{-12\pi\omega_s{}^2}{c^2 k_s}\sum_{r=-1}^{1}\sum_{s=-1}^{1}\tilde{E}_p(\omega_p+r\omega_m)\tilde{E}_p^*(\omega_p+s\omega_m)\psi_{rs}^{1111}\right]e^{j\omega_s t}$$

$$+jE_{so}T_n{}^{\ell}\left[\frac{12\pi\omega_s{}^2}{c^2 k_s}\sum_{r=-1}^{1}\sum_{s=-1}^{1}\tilde{E}_p(\omega_p+r\omega_m)\tilde{E}_p^*(\omega_p+s\omega_m)\phi_{rs}^{1111}\right]e^{j\omega_s t} \qquad \text{(B-4)}$$

Substitution of equation (B-2) for the pump field into the above equation yields

$$\tilde{\delta E}_s = \frac{-12\pi\ell\omega_s{}^2}{c^2 k_s}E_{po}{}^2E_{so}\left[T_o\psi_{oo}^{1111}e^{j\omega_s t}+\frac{\delta}{2}T_{-1}\psi_{o1}^{1111}e^{j(\omega_s-\omega_m)t}\right.$$

$$-\frac{\delta}{2}T_1\psi_{o-1}^{1111}e^{j(\omega_s+\omega_m)t}+\frac{\delta}{2}T_1\psi_{10}^{1111}e^{j(\omega_s+\omega_m)t}+\left(\frac{\delta}{2}\right)^2T_o\psi_{11}^{1111}e^{j\omega_s t}$$

$$\left.-\left(\frac{\delta}{2}\right)^2T_2\psi_{1-1}^{1111}e^{j(\omega_s+2\omega_m)t}-\frac{\delta}{2}T_{-1}\psi_{-10}^{1111}e^{j(\omega_s-\omega_m)t}\right.$$

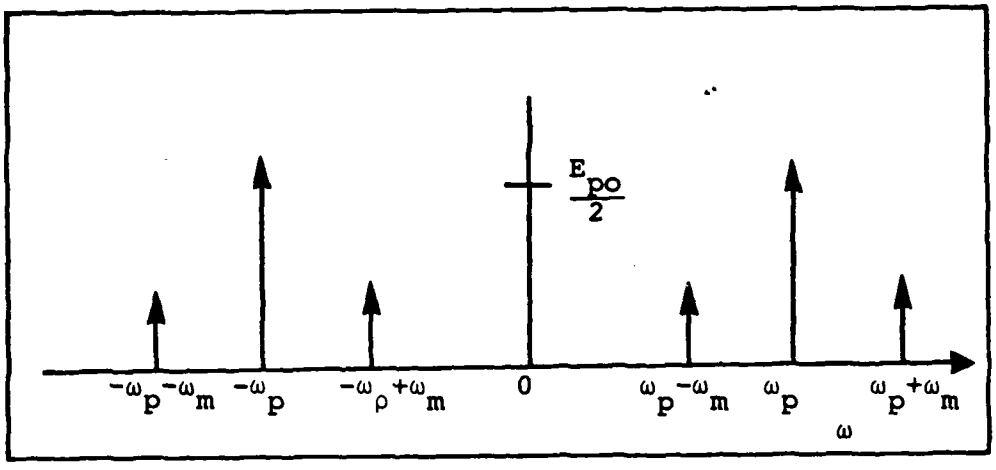

Figure B-1: *Frequency Domain Representation of Phase Modulated Pump Field.*

$$- \left(\frac{\delta}{2}\right)^2 T_{-2}\psi_{-11}^{1111} e^{j(\omega_s-2\omega_m)t} + \left(\frac{\delta}{2}\right)^2 T_o \psi_{-1-1}^{1111} e^{j\omega_s t}]$$

$$+ j\{\text{same terms as above but } \phi_{rs}^{1111} \text{ replaces } \psi_{rs}^{1111}\} \quad \text{(B-5)}$$

The total intensity of the Stokes field is given by equation (A-8). Letting all differences of the first order attenuation and dispersion coefficients go to zero, as was

done in Appendix A, the second term of equation (A-8) becomes, after substitution of equation (B-5) for $\delta\tilde{E}_s$,

$$\frac{c}{8\pi}E_{so}T_o\delta\tilde{E}_s^* e^{j\omega_s t} = \frac{-3\ell\omega_s^2}{2ck_s}E_{po}^2E_{so}^2e^{-2\varepsilon_o}[\psi_{oo}^{1111}$$

$$+ \frac{\delta^2}{4}(\psi_{11}^{1111}+\psi_{-1-1}^{1111})+\frac{\delta}{2}\psi_{o1}^{1111}e^{j\omega_m t}-\frac{\delta}{2}\psi_{o-1}^{1111}e^{-j\omega_m t}$$

$$+ \frac{\delta}{2}\psi_{10}^{1111}e^{-j\omega_m t}-\frac{\delta^2}{4}\psi_{1-1}^{1111}e^{-j2\omega_m t}-\frac{\delta}{2}\psi_{-10}^{1111}e^{j\omega_m t}$$

$$- \frac{\delta^2}{2}\psi_{-11}^{1111}e^{j2\omega_m t}]-j\frac{3\ell\omega_s^2}{2ck_s}E_{po}^2E_{so}^2e^{-2\varepsilon_o}[\phi_{oo}^{1111}+\frac{\delta^2}{4}(\phi_{11}^{1111}+\phi_{-1-1}^{1111})$$

$$+ \frac{\delta}{2}\phi_{01}^{1111}e^{j\omega_m t}-\frac{\delta}{2}\phi_{0-1}^{1111}e^{-j\omega_m t}+\frac{\delta}{2}\phi_{10}^{1111}e^{-j\omega_m t}+\frac{\delta^2}{4}\phi_{1-1}^{1111}e^{-j2\omega_m t}$$

$$- \frac{\delta}{2}\phi_{-10}^{1111}e^{j\omega_m t}-\frac{\delta^2}{4}\phi_{-11}^{1111}e^{j2\omega_m t}] \qquad \text{(B-6)}$$

The third term of equation (A-8) is the complex conjugate of the second term displayed in equation (B-6). Adding up all four terms of equation (A-8), the total Stokes intensity becomes

$$I_s(z=\ell,t)=\text{d.c. terms} + \frac{96\pi^2\omega_s^2}{c^3k_s}\ell I_{po}I_{so}e^{-2\varepsilon_o}$$

$$[\delta(\psi_{0-1}^{1111}-\psi_{01}^{1111}-\psi_{10}^{1111}+\psi_{-10}^{1111})\cos\omega_m t+\frac{\delta^2}{2}(\psi_{1-1}^{1111}+\psi_{-11}^{1111})\cos 2\omega_m t$$

$$+\delta(\phi_{01}^{1111}+\phi_{0-1}^{1111}-\phi_{10}^{1111}-\phi_{-10}^{1111})\sin\omega_m t+\frac{\delta^2}{2}(\phi_{1-1}^{1111}-\phi_{-11}^{1111})\sin 2\omega_m t]$$

$$+\frac{c}{8\pi}|\delta\tilde{E}_s|^2 \qquad \text{(B-7)}$$

Now, $\psi_{10}=\mathrm{Im}\{\chi^{(3)}(\omega_p+\omega_m,-\omega_p,\omega_s)\}$ is equivalent to $\psi_{-10}=\mathrm{Im}\{\chi^{(3)}(\omega_p-\omega_m,-\omega_p,\omega_s)\}$ and $\phi_{10}=\mathrm{Re}\{\chi^{(3)}(\omega_p+\omega_m,-\omega_p,\omega_s)\}$ is equivalent to $\phi_{-10}=\mathrm{Re}\{\chi^{(3)}(\omega_p-\omega_m,-\omega_p,\omega_s)\}$. Hence, equation (B-7) reduces to

$$I_s(z=\ell,t)=I_o+I_1\cos\omega_m t+I_2\sin\omega_m t+I_3\cos 2\omega_m t$$

$$+I_4\sin 2\omega_m t+I_5(t) \qquad \text{(B-8)}$$

where

I_o = d.c. terms

$$I_1=\frac{96\pi^2\omega_s^2}{c^3k_s}\,\ell I_{po}I_{so}e^{-2\varepsilon_o}\,\delta(\psi_{0-1}^{1111}-\psi_{01}^{1111})$$

$$I_2 = \frac{96\pi^2\omega_s^2}{c^3 k_s} \ell I_{po} I_{so} e^{-2\varepsilon_o} \delta [\phi_{0-1}^{1111} + \phi_{01}^{1111} - 2\phi_{10}^{1111}]$$

$$I_3 = \frac{96\pi^2\omega_s^2}{2c^3 k_s} \ell I_{po} I_{so} e^{-2\varepsilon_o} \delta^2 (\psi_{1-1}^{1111} + \psi_{-11}^{1111})$$

$$I_4 = \frac{96\pi^2\omega_s^2}{2c^3 k_s} \ell I_{po} I_{so} e^{-2\varepsilon_o} \delta^2 (\phi_{1-1}^{1111} - \phi_{-11}^{1111})$$

$I_5(t)$ = terms proportional to ψ^2 and ϕ^2.

OHD RIKES

Those intensity components that are of interest in OHD RIKES are given in equation (A-22). Equation (B-5) is the equation for $\delta\tilde{E}_{sx}$. The term $\delta\tilde{E}_{sy}$ is also given by equation (B-5) but with ψ_{rs}^{1111} and ϕ_{rs}^{1111} replaced by ψ_{rs}^{2112} and ϕ_{rs}^{2112}, respectively. In this case, equation (A-22) becomes

$$\frac{c}{8\pi} \frac{E_{so}}{2} \theta \left[\frac{-12\pi\omega_s^2}{c^2 k_s} \ell E_{po}^2 E_{so} e^{-2\varepsilon_o} (\psi_{oo}^{1111} e^{-j\omega_s t} + \frac{\delta}{2}\psi_{01}^{1111} e^{-j(\omega_s - \omega_m)t} \right.$$

$$\left. - \frac{\delta}{2}\psi_{0-1}^{1111} e^{-j(\omega_s + \omega_m)t} + \frac{\delta}{2}\psi_{10}^{1111} e^{-j(\omega_s + \omega_m)t} + (\frac{\delta}{2})^2 \psi_{11}^{1111} e^{-j\omega_s t} \right.$$

$$-\left(\frac{\delta}{2}\right)^2\psi_{1-1}^{1111}e^{-j(\omega_s+2\omega_m)t}-\frac{\delta}{2}\psi_{-10}^{1111}e^{-j(\omega_s-\omega_m)t}-\left(\frac{\delta}{2}\right)^2\psi_{-11}^{1111}e^{-j(\omega_s-2\omega_m)t}$$

$$+\left(\frac{\delta}{2}\right)^2\psi_{-1-1}^{1111}e^{-j\omega_s t}\Big)e^{j\omega_s t}-\frac{j12\pi\ell\omega_s^2}{c^2k_s}E_{po}^2E_{so}e^{-2\varepsilon_o}\{\text{Same Terms as}$$

above but with ψ_{rs}^{1111} replaced by $\phi_{rs}^{1111}\}e^{j\omega_s t}$ +

$$\frac{12\pi\omega_s^2}{c^2k_s}\ell E_{po}^2E_{so}e^{-2\varepsilon_o}\{\text{Same terms as above, but with } \psi_{rs}^{1111}$$

replaced by $\psi_{rs}^{2112}\}e^{j\omega_s t}+j\frac{12\pi\omega_s^2}{c^2k_s}\ell E_{po}^2E_{so}e^{-2\varepsilon_o}\{\text{Same terms}$

terms as above but with ψ_{rs}^{1111} replaced by $\phi_{rs}^{2112}\}e^{j\omega_s t}\}+\text{c.c}$

Reducing the above yields

$$\text{d.c. terms} + \frac{48\pi^2\omega_s^2}{c^3k_s}\ell\theta I_{po}I_{so}e^{-2\varepsilon_o}[\delta(\psi_{0-1}^{1111}-\psi_{01}^{1111}+$$

$$+\psi_{-10}^{1111}-\psi_{10}^{1111}+\psi_{01}^{2112}-\psi_{0-1}^{2112}+\psi_{10}^{2112}-\psi_{-10}^{2112})\cos\omega_m t$$

$$+\frac{\delta^2}{2}(\psi_{1-1}^{1111}+\psi_{-11}^{1111}-\psi_{1-1}^{2112}-\psi_{-11}^{2112})\cos 2\omega_m t$$

$$+\delta(\phi_{0-1}^{1111}-\phi_{10}^{1111}+\phi_{01}^{1111}-\phi_{-10}^{1111}+\phi_{10}^{2112}-\phi_{01}^{2112}+\phi_{-10}^{2112}-\phi_{0-1}^{2112})\sin\omega_m t$$

$$+\frac{\delta^2}{2}(\phi_{1-1}^{1111}-\phi_{-11}^{1111}-\phi_{1-1}^{2112}+\phi_{-11}^{2112})\sin 2\omega_m t]$$

Again, $\psi_{-10} = \psi_{10}$ and $\phi_{-10} = \phi_{10}$. Hence, the total Stokes intensity becomes, after combining the above with the first and last term of equation (A-21),

$$I_s(z=\ell,t)=I_o+I_1 \cos \omega_m t + I_2 \sin \omega_m t + I_3 \cos 2\omega_m t$$

$$+ I_4 \sin 2\omega_m t + I_5(t)$$

where

I_o = d.c. terms

$$I_1 = \frac{48\pi^2\omega_s^2}{c^3 k_s} \ell I_{po} I_{so} \theta e^{-2\varepsilon_o} \delta [(\psi_{0-1}^{1111}-\psi_{01}^{1111})+(\psi_{01}^{2112}-\psi_{0-1}^{2112})]$$

$$I_2 = \frac{48\pi^2\omega_s^2}{c^3 k_s} \ell I_{po} I_{so} \theta e^{-2\varepsilon_o} \delta [(\phi_{0-1}^{1111}+\phi_{10}^{1111}-2\phi_{10}^{1111})$$

$$- (\phi_{01}^{2112}+\phi_{0-1}^{2112}-2\phi_{10}^{2112})]$$

$$I_3 = \frac{24\pi^2\omega_s^2}{c^3 k_s} \ell I_{po} I_{so} \theta e^{-2\varepsilon_o} \delta^2 [(\psi_{1-1}^{1111}+\psi_{-11}^{1111})-(\psi_{1-1}^{2112}+\psi_{-11}^{2112})]$$

$$I_4 = \frac{24\pi^2\omega_s^2}{c^3 k_s} \ell I_{po} I_{so} \theta e^{-2\varepsilon_o} \delta^2 [(\phi_{1-1}^{1111}-\phi_{-11}^{1111})+(\phi_{-11}^{2112}-\phi_{1-1}^{2112})]$$

$I_5(t)$ = terms proportional to $(\delta\psi)^2$ and $(\delta\phi)^2$.

Appendix C

Noise Spectra of Pump Dye Laser and Ar^+ Laser

Figure C-1 below shows the noise spectrum of the pump dye laser operated at 5954Å with an input Ar^+ pump power of 2.5 watts. Figure C-1 also shows the noise spectrum of the Ar^+ laser operated at 1 watt in the Light Control Mode. The spectrum analyzer settings were the same as that for the HeNe noise spectra in Figures 10 and 11. Hence, direct comparison may be made between the spectra.

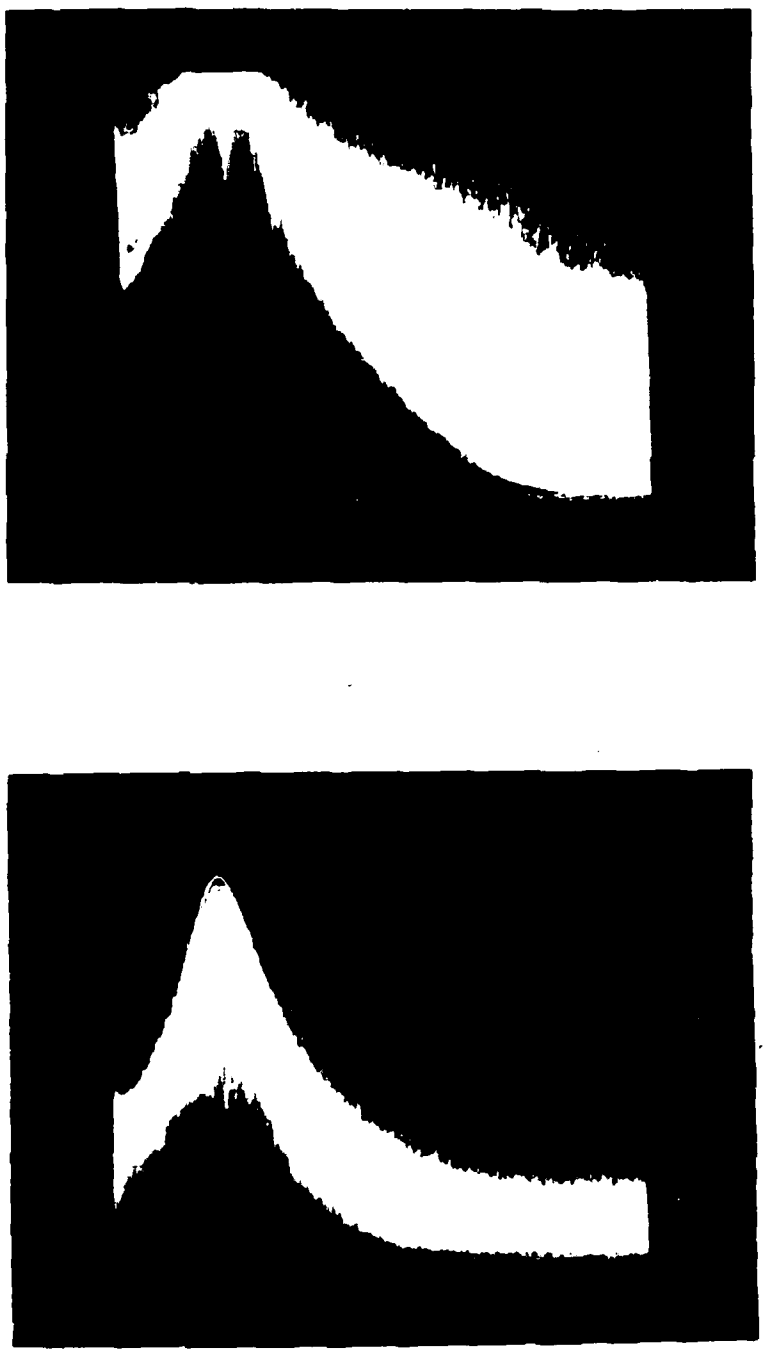

Figure C-1: Noise Spectra of Pump Dye Laser and Ar^+ Laser. Top, Spectrum of Pump Dye Laser. Bottom, Spectrum for Ar^+ Laser. Each Horizontal Division is 20 kHz.

Using equation (100) on page 86 the root-mean-squared fractional intensity deviations in the pump dye laser and the Ar^+ laser were found using the spectrum in Figure C-1. These values are given in Table C-I below.

TABLE C-1

Values of $\delta_p^{\frac{1}{2}}$ and $\delta_{Ar^+}^{\frac{1}{2}}$ vs Frequency

Frequency (kHz)	$\delta_p^{\frac{1}{2}}$ (dye laser) (x 10^{-8})	$\delta_{Ar^+}^{\frac{1}{2}}$ (Ar^+ laser) (x 10^{-8})
1	12600	2815
10	7070	1260
20	5620	255
40	2240	40
60	1120	13
80	707	7
100	400	5
120	140	5
140	125	5
160	125	5

Vita

David Charles Slater was born in Los Angeles, California on August 12, 1957 to the parents of Mr. and Mrs. Charles N. Slater, Jr. He attended the University of California at Los Angeles where he received his B.S. degree in Physics in June 1979. A graduate of AFROTC at UCLA he was commissioned as a second lieutenant in the United States Air Force also in June 1979. The next year and a half he spent as a student at the Air Force Institute of Technology in the Graduate Engineering Physics Department.

David Slater is a member of the Sigma Pi Sigma Society of Physics Students and the Tau Beta Pi national engineering honor society.

UNCLASSIFIED

SECURITY CLASSIFICATION OF THIS PAGE (When Data Entered)

REPORT DOCUMENTATION PAGE	READ INSTRUCTIONS BEFORE COMPLETING FORM
1. REPORT NUMBER: AFIT/GEP/PH/80-9 — 2. GOVT ACCESSION NO.: AD-A094 418	3. RECIPIENT'S CATALOG NUMBER
4. TITLE (and Subtitle): A THEORETICAL AND EXPERIMENTAL STUDY ON THE APPLICATION OF STIMULATED RAMAN SPECTROSCOPY	5. TYPE OF REPORT & PERIOD COVERED: MS THESIS
	6. PERFORMING ORG. REPORT NUMBER
7. AUTHOR(s): David C. Slater, 2nd Lt, USAF	8. CONTRACT OR GRANT NUMBER(s)
9. PERFORMING ORGANIZATION NAME AND ADDRESS: Air Force Institute of Technology (AFIT-EN) Wright-Patterson AFB, OH 45433	10. PROGRAM ELEMENT, PROJECT, TASK AREA & WORK UNIT NUMBERS
11. CONTROLLING OFFICE NAME AND ADDRESS: Air Force Institute of Technology (AFIT-EN) Wright-Patterson AFB, OH 45433	12. REPORT DATE: December 1980
	13. NUMBER OF PAGES: 126
14. MONITORING AGENCY NAME & ADDRESS(if different from Controlling Office)	15. SECURITY CLASS. (of this report): UNCLASSIFIED
	15a. DECLASSIFICATION DOWNGRADING SCHEDULE

16. DISTRIBUTION STATEMENT (of this Report)

Approved for public release; distribution unlimited

17. DISTRIBUTION STATEMENT (of the abstract entered in Block 20, if different from Report)

18. SUPPLEMENTARY NOTES

Approved for public release; IAW AFR 190-17

Frederick C. Lynch, Major, USAF
Director of Public Affairs

06 JAN 1981

19. KEY WORDS (Continue on reverse side if necessary and identify by block number)

Stimulated Raman Spectroscopy
Nonlinear Optics
RIKES
OHD RIKES

20. ABSTRACT (Continue on reverse side if necessary and identify by block number)

An analysis of the stimulated Raman scattering process has been carried out for three variational techniques of stimulated Raman spectroscopy (SRS) using low power CW lasers and synchronous detection techniques. The three variational techniques of SRS examined are direct SRS, Raman-Induced Kerr Effect (RIKES) and Optically Heterodyned RIKES (OHD RIKES). In this analysis the Raman scattered signals for all three variational techniques were derived using Maxwell's equations for both amplitude and phase

DD FORM 1 JAN 73 1473 EDITION OF 1 NOV 65 IS OBSOLETE

UNCLASSIFIED

SECURITY CLASSIFICATION OF THIS PAGE (When Data Entered)

modulation techniques. The noise contributions for each technique were also examined. It was found that the main source of noise for each technique was due to probe laser intensity fluctuations.

The results of this analysis were utilized on an experimental SRS system using low power CW lasers and synchronous detection which was built to record Raman spectra. This technique would provide the Air Force with a valuable diagnostic tool for potential use in many areas such as combustion research, chemical kinetics and solid state technology. This system failed to record Raman resonance of liquid benzene at 992 cm^{-1} and solid silicon at 520 cm^{-1}. This was due to poor signal-noise ratios of less than one caused primarily by probe laser intensity fluctuations. The results of the analysis on this system yielded the minimum necessary modulation frequencies for each variational technique in order to detect the Raman resonance in benzene.

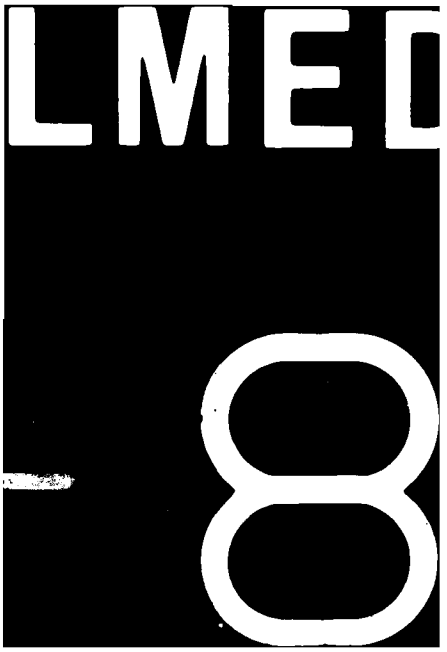
LMED
8